UNIVERSITÀ DEGLI STUDI FIRENZE

Da un secolo, oltre.

HR EXCELLENCE IN RESEARCH

PhD in Chemical Sciences

CYCLE XXXVIII

COORDINATOR Prof. ANNA MARIA PAPINI

Electrodeposition with modulated currents in optics of a Circular Economy

Academic Discipline (SSD) CHEM-01/A

Doctoral Candidate
Dr. Elena Mariani

Supervisor
Prof. Massimo Innocenti

Co-Supervisor 1
Prof. Pierandrea Lo Nostro

Co-Supervisor 2
Dr. Vincenzo Dell'Aquila

Coordinator
Prof. Anna Maria Papini

Table of Contents

PREFACE

Abstract

This doctoral thesis presents a comprehensive investigation into the application of pulsed current (PC) electrodeposition for metallic coatings used in decorative electroplating, with a particular focus on processes relevant to the fashion and luxury industry. The work originates from a close collaboration and continuous synergy established during the Ph.D. period with an industrial partner specialized in galvanic processes for decorative metal finishing. This collaboration provided direct access to real production environments, enabling the identification of technological gaps in industrial electroplating and the definition of scientifically grounded strategies for process optimization.

Although direct current (DC) electroplating still represents the industrial standard due to its simplicity and robustness, pulsed current techniques have long been recognized for their potential to improve deposit properties by offering better control over nucleation and growth mechanisms. However, their industrial adoption has been limited by the complexity of process control and the need for precise parameter tuning. This research therefore aimed to bridge the gap between empirical industrial practice and scientific understanding, exploring how current modulation can enhance coating performance and promote more sustainable use of materials.

The study focused on four metallic systems that are among the most widely used in decorative electroplating: alkaline copper, acid copper, palladium and gold. Each system was systematically investigated under both DC and PC conditions, with variations in waveform parameters such as frequency, amplitude and duty cycle. The study combined electrochemical techniques with advanced surface

characterization to establish correlations between electrical parameters, deposition mechanisms and the resulting morphological, structural and aesthetic properties of the coatings.

The results demonstrated that the use of pulsed current can significantly enhance deposit quality when properly optimized for each metal. For copper, in both alkaline and acidic baths, pulsed deposition resulted in smoother, less porous and more homogeneous coatings with lower internal stress.

Palladium layers exhibited reduced porosity, improved corrosion resistance, and greater uniformity, suggesting the potential to lower the amount of precious metal required without compromising performance.

Gold deposits, in turn, showed increased brightness, higher reflectivity and better mechanical stability under optimized pulsed current conditions, enabling the achievement of high decorative quality with thinner films.

Beyond the material improvements, the research emphasizes the relevance of pulsed current electroplating as a sustainable and efficient alternative to traditional DC methods. By reducing the consumption of precious metals, minimizing waste and enabling thinner yet more compact coatings, pulsed deposition aligns with the principles of green manufacturing and circular economy. The findings also highlight how a scientific and data-driven approach can transform decorative electroplating from an empirical craft into a controlled and reproducible process.

Overall, this thesis provides new insights into the electrochemical and material aspects of pulsed current electrodeposition, offering both a scientific framework and practical guidelines for industrial implementation. The outcomes demonstrate that, through the optimization of waveform parameters, it is possible to achieve coatings of superior aesthetic and functional performance while advancing toward more sustainable and resource-efficient galvanic production.

Scientific Production

- Mariani, E., Giurlani, W., Bonechi, M., Dell'Aquila, V. & Innocenti, M. A systematic study of pulse and pulse reverse plating on acid copper bath for decorative and functional applications. *Scientific Reports* 12, 18175 (**2022**). DOI: https://doi.org/10.1038/s41598-022-22650-x
- Mariani, E., Giurlani, W., Verrucchi, M., Dell'Aquila, V., Lo Nostro, P. & Innocenti, M. Pulse electroplating of Gold-Nickel alloys - morphological and aesthetic improvement compared to DC. *Journal of the Electrochemical Society* 171, 012504 (**2024**). DOI: https://doi.org/10.1149/1945-7111/ad1d97
- Giurlani, W., Pappaianni, G., Biffoli, F., Mariani, E., Bonechi, M., Giliberti, L., Tufarelli, M., Franzo, P., Cianfanelli, E. & Innocenti, M. What Is the Current State of Sustainability in the Decorative Electroplating Industry? A Close Look at New Practices and Advances. *Sustainability* 16, 5821 (**2024**). DOI: https://doi.org/10.3390/su16135821
- Verrucchi, M., Pelagatti, A., Biffoli, F., Mariani, E., Del Pace, I., Giurlani, W., Bazzicalupi, C., Innocenti, M. Impact of electrodeposition parameters on hydrogen absorption and α-β phases formation in palladium electroplating. *Journal of Electroanalytical Chemistry* 12, 119108 (**2025**). DOI: https://doi.org/10.1016/j.jelechem.2025.119108
- Mariani, E., Bitossi, S., Bonechi, M., Dell'Aquila, V., Giurlani, W., Lo Nostro, P., Pagliai, M. & Innocenti, M. Achieving multiple colors from a single gold electroplating bath for decorative applications using pulse current deposition. *Materials Today Communications* 47, 113037 (**2025**). DOI: https://doi.org/10.1016/j.mtcomm.2025.113037

List of Abbreviations

AFM	Atomic Force Microscopy
BSE	Backscattered Electron
CE	Counter Electrode
CFD	Computational Fluid Dynamics
CIE	Commission Internationale de l'Éclairage
CPE	Constant Phase Element
CV	Cyclic Voltammetry
DC	Direct Current
DFT	Density Functional Theory
DRS	Diffusive Reflectance Spectroscopy
EIS	Electrochemical Impedance Spectroscopy
EOL	End-of-Life
EDS	Energy Dispersive X-ray Spectroscopy
FEM	Finite Element Method
FP	Fundamental Parameters
HCS	Homogeneous Coating System
HER	Hydrogen Evolution Reaction
HPS	High Performance System
$\mathbf{i_c}$	Capacitive Current
ICDD	International Centre for Diffraction Data
$\mathbf{i_f}$	Faradic Current
IHP	Inner Helmholtz Plane
$\mathbf{i_p}$	Pulse Current
$\mathbf{J_a}$	Anode Peak Current Density
$\mathbf{J_{AV}}$	Average Current Density

J_c	Cathode Peak Current Density
J_p	Pulse Current Density
LSV	Linear Sweep Voltammetry
MCL	Maximum Contaminant Limit
MM	Molecular Mechanics
MMO	Mixed Metal Oxides
NSS	Neutral Salt Spray
OHP	Outer Helmholtz Plane
PC	Pulsed Current
PP-H	Polypropylene Homopolymer
PRC	Pulsed Reverse Current
QM	Quantum Mechanics
RAEP	Raddrizzatore Anti Effetto Punta
RDE	Rotating Disk Electrode
RE	Reference Electrode
Sa	Arithmetic Mean Roughness
SCE	Standard Calomel Electrode
SCE	Specular Component Excluded
SCI	Specular Component Included
SDG	Sustainable Development Goal
SEM	Scanning Electron Microscopy
L	Mean Square Roughness
t_a	Anode Pulse Duration
t_c	Cathode Pulse Duration
t_C	Charge Time
t_D	Discharge Time
t_{on}	Pulse Time
t_{off}	Relaxation Time

TP	Throwing Power
USEPA	United States Environmental Protection Agency
WE	Working Electrode
XRD	X-ray Diffraction Spectroscopy
XRF	X-ray Fluorescence Spectroscopy

1 Introduction

Electroplating represents one of the most widespread technologies for the functionalization and aesthetic enhancement of metallic surfaces. Its versatility and cost-effectiveness have made it a key process in numerous industrial sectors, from electronics and automotive to luxury goods, jewelry, and interior design. In particular, in the decorative industry - where visual appearance, brilliance, and color uniformity are of paramount importance - electrodeposition is not merely a surface treatment but a requirement for controlled material transformation [1].

Among the various electrodeposition techniques, direct current (DC) still represents the current industrial state of the art, especially in the decorative sector. Its widespread use is primarily due to its technical simplicity, ease of control and compatibility with large-scale production systems. However, despite its ubiquity, DC electroplating suffers from intrinsic limitations, such as non-uniform thickness distribution, porosity, and edge effects, that affect the quality and durability of the coatings [2].

Conversely, the use of pulsed current (PC) and pulsed reverse current (PRC) has long been recognized in the scientific literature as a powerful strategy to improve the microstructural and aesthetic properties of electrodeposited films. By modulating the current in time, these techniques enable a more precise control over nucleation and growth processes at the cathode, leading to finer grains, reduced porosity, improved brightness and enhanced leveling [3]. Nevertheless, their industrial adoption has remained limited. In recent years, however, advances in power electronics and process control have renewed interest in current modulation as a viable alternative to conventional DC plating. The increasing demand for improved performance, sustainability, and metal efficiency has driven research toward understanding how pulsed current

parameters can be optimized to enhance deposit properties while maintaining industrial feasibility.

In fashion and design sectors, where the final product's aesthetic quality directly defines its value, these features are not auxiliary but fundamental.

This doctoral thesis is based on a close collaboration and intense synergy developed during the doctoral period with a company (Eco-Tech Finish srl) specialized in galvanic processes for the fashion and luxury goods sector. Operating at the intersection of chemistry, materials science and design, this industrial environment provided a unique opportunity to observe the gaps between empirical industrial practices and the scientific understanding of pulsed electroplating processes. Although pulse and reverse-pulse plating have been industrially implemented for decades, especially for gold and palladium coatings, process parameters are often chosen empirically rather than based on quantitative models. The absence of standardized criteria for waveform optimization results in non-reproducible outcomes, excessive use of metals and limited control over film morphology and color.

The main objective of this thesis is therefore to perform a systematic investigation of pulsed current electrodeposition applied to metallic films relevant to the decorative sector, namely alkaline copper, acid copper, palladium and gold. These metals constitute the fundamental sequence of layers in modern galvanic processes: copper as a base for adhesion and leveling, palladium as a diffusion barrier and bright interlayer, and gold as the final noble and decorative coating. Each of these layers contributes distinct mechanical, chemical, and optical properties to the final article, and the fine-tuning of their deposition parameters determines both product quality and process sustainability.

From a scientific standpoint, pulsed electrodeposition enables the precise modulation of electrochemical kinetics by controlling pulse amplitude, frequency, duty cycle, and waveform. This modulation influences not only

nucleation rates and crystal growth dynamics but also mass transport phenomena, adsorption processes, and the evolution of the double electric layer [4], [5]. Consequently, PC and PRC techniques can yield metal films with tailored grain sizes, preferred orientations, and superior aesthetic and functional performances compared to those obtained under direct current conditions.

However, despite their established industrial relevance, pulsed current electrodeposition processes still suffer from limited theoretical modeling and scarce quantitative optimization, particularly in the decorative field. Most academic studies have focused on functional coatings or electronic applications - where deposition uniformity and mechanical performance are crucial - while the decorative sector, often dominated by traditional know-how, has received limited scientific attention. This thesis seeks to bridge that gap by integrating a research-driven approach within a real industrial context, combining electrochemical characterization, materials analysis and process engineering.

The experimental project was structured across several complementary levels. The first stage involved a theoretical and electrochemical analysis of the mechanisms governing electrodeposition and the influence of pulsed currents, with a focus on the role of the electrical double layer, mass transport and diffusion layers under modulated waveforms. These studies provided the framework for defining the operative limits of pulse time and pause time, as well as identifying the optimal ranges for nucleation and growth of metallic deposits [6], [7], [8].

Subsequent chapters are dedicated to the experimental investigation of the four selected metals: alkaline copper, acid copper, palladium, and gold. For each system, the effects of pulsed current parameters on deposition kinetics and coating characteristics were systematically studied and compared with those obtained by direct current deposition. Analytical techniques such as scanning electron microscopy (SEM), X-ray diffraction (XRD), X-ray fluorescence (XRF), colorimetric analysis and microhardness testing were employed to

evaluate morphology, crystallite size, composition, reflectivity and mechanical properties. These analyses enabled a direct correlation between pulse parameters (t_{on}, t_{off}, duty cycle, current amplitude) and the resulting chemical–physical properties of the coatings.

From an environmental perspective, the research aligns with the current drive toward sustainable electroplating. Traditional decorative coatings often rely on baths containing toxic compounds such as cyanides, as well as high concentrations of precious metals including gold, palladium and rhodium. In contrast, this work aims to demonstrate that by optimizing pulsed current parameters, it is possible to achieve equivalent or superior aesthetic results using thinner layers and less metal, without compromising corrosion resistance or brilliance. The adoption of cyanide-free baths and reduced-metal formulations contributes to lowering environmental impact, minimizing waste, and improving operator safety.

The final part of this thesis extends beyond the experimental results, addressing the integration of pulsed current technologies into sustainable industrial frameworks. It explores how process digitalization, predictive modeling and simulation can further refine deposition efficiency, paving the way for next-generation galvanic processes that combine scientific rigor with environmental responsibility.

In summary, this doctoral research aims to provide a comprehensive and interdisciplinary understanding of pulsed current electrodeposition, bridging the gap between academic electrochemistry and industrial practice. By correlating waveform parameters with film properties across different metallic systems, this work contributes both to the optimization of decorative electroplating processes and to the advancement of sustainable manufacturing in the fashion and design industries. Through this approach, the thesis aspires not only to deepen the knowledge of pulse-driven electrodeposition mechanisms but also to lay the

foundation for a new paradigm in decorative electroplating, one that is technologically advanced, economically efficient and environmentally conscious.

2 Theory and Methods

In this chapter, the theoretical background and methodological principles underlying this research are presented. The section is intended to provide a comprehensive yet concise overview of the fundamental electrochemical concepts and experimental techniques employed throughout the thesis. Particular emphasis is placed on those aspects directly related to the study of electrodeposition processes under direct and pulse current regimes.

The aim is not to offer an exhaustive description of all electrochemical phenomena but rather to outline the theoretical framework necessary to understand the experimental results discussed in the subsequent chapters. Therefore, well-established notions and classical theories that are considered common knowledge in the field are not treated in detail here. For all basic concepts, additional explanations or complementary information, the reader is referred to the relevant literature cited throughout the text.

Special attention is devoted to the mechanisms governing metal electrodeposition, the structure of the electrochemical double layer and the dynamics of mass transport, as these are key factors influencing the morphology and properties of the deposits obtained under pulsed current conditions.

2.1 Electrodeposition

2.1.1 Historical Background of Electroplating

The use of metals by humans dates back about 11’000 years, as evidenced by the discovery of the first gold and copper artifacts [9]. Since ancient times, metals have been exploited not only for decorative purposes but later also for broader applications. The desire to transform common materials into objects of greater value, brilliance, and nobility has its roots in ancient Egypt, more than 5,000 years ago, where thin metallic films were applied to statues to produce the first

gilding [1]. Remarkably, archaeological findings in Peru, attributable to the Moche civilization, suggest the use of electroless deposition of gold - a process that does not require an external current - centuries before its modern rediscovery [9].

The first artifacts obtained through electrochemical processes requiring electron flow are closely related to the discovery of electricity. In 1772, Giovanni Battista Beccaria (1716-1781) succeeded in depositing a metal from its components using a primitive capacitor [10]. A few years later, Luigi Galvani (1737-1798) observed that a frog's muscle contracted when touched simultaneously with copper and zinc wires, laying the foundations of bioelectricity. His disagreement with Alessandro Volta (1745-1827) ultimately led Volta to develop the first galvanic cell in 1800: the Voltaic pile, consisting of alternating zinc and copper disks separated by cloth soaked in brine or diluted sulfuric acid [11]. Shortly thereafter, William Nicholson (1753–1815) and Anthony Carlisle (1768–1840) used such a pile to decompose water into hydrogen and oxygen, thus discovering electrolysis [10].

Building on these developments, Luigi Valentino Brugnatelli (1761-1818) carried out in 1805 the first electrodeposition of gold from an Au^{3+} solution onto a silver substrate [9], [11], [12]. This milestone marked the true birth of electroplating. Subsequent decades witnessed significant progress: in 1837, Moritz Hermann von Jacobi introduced electroforming of copper; in the 1840s, the Elkington brothers filed the first patent for gold and silver electrodeposition from cyanide solutions [13]; and by 1876 Birmingham had become the first industrial electroplating center.

In 1946, Abner Brenner developed electroless deposition for metallizing non-conductive surfaces such as plastics [14]. Later, cataphoresis, electropolymerization [15], [16], [17], [18], and electrodeposition from ionic liquids [19], [20], [21] expanded the range of depositable materials to include

paints, polymers, and metals like aluminum, previously unattainable from aqueous solutions. From the 1950s onwards, industrial practices evolved toward alloy deposition and multilayer architectures [22], [23], [24], which offer several advantages compared to single-layer coatings, such as preventing electroless deposition by redox replacement, reducing stress from lattice mismatches, and limiting interdiffusion between metals over time.

Modern research in electrodeposition focuses on reducing the precious metal content of coatings (e.g., from 24 kt to 18 kt gold) while preserving corrosion resistance , eliminating toxic cyanide from baths, replacing harmful heavy metals like cadmium, nickel, and palladium, improving waste and wastewater management, developing alternative engineering processes [25], and synthesizing new alloys.

2.1.2 Fundamentals of Electrodeposition

Electrodeposition is an electrochemical process that enables the formation of a metallic coating on a conductive substrate [1]. It is based on the passage of direct or modulated current through an electrolyte containing salts of the metal (or metals) to be deposited, thereby promoting the electrochemical reduction of metal ions. In a classical electrodeposition process, the object to be coated is immersed in an electrolytic cell containing the metallic salt, a supporting electrolyte - whose role is to maintain constant ionic strength and minimize ohmic resistance - and electrodes connected to a power supply. The substrate to be coated acts as the cathode and is connected to the negative terminal, while the anodes are connected to the positive terminal. The anodes may either be composed of the same metal to be deposited - defined as *soluble anodes* - or of inert conductive materials (*insoluble anodes*) [1]. Soluble anodes dissolve upon oxidation under current passage, thereby replenishing the ions consumed at the

cathode and maintaining the concentration of the depositing metal in the electrolyte.

Two main experimental setups are employed in electrochemistry. The first is the three-electrode system (Figure 2.1), widely used in research and development: the cell configuration includes a working electrode (WE), a reference electrode (RE) and a counter electrode (CE), each performing a distinct and complementary function. The working electrode, in this case, is where the electrodeposition process takes place. Its potential is controlled during the experiment, and its material composition can vary depending on the specific application. At this interface, electron transfer reactions occur between the electrode surface and the electroactive species in solution.

The reference electrode provides a stable, well-defined potential against which the potential of the working electrode is measured. It does not conduct current, thus maintaining its potential throughout the experiment. Common reference electrodes include the standard calomel electrode (SCE), the silver/silver chloride (Ag/AgCl) electrode, and, less commonly, the hydrogen electrode. The presence of a stable RE allows for precise control of the potential applied to the working electrode while maintaining a constant and reproducible reference point.

The counter electrode completes the electrical circuit within the electrochemical cell. The CE balances the current generated at the working electrode, ensuring the current flows through the solution without participating in the electrochemical reactions being tested [1].

The entire setup operates under the control of a potentiostat, an electronic device that maintains the desired potential difference between the working and reference electrodes and measures the corresponding current flowing between the working and counter electrodes.

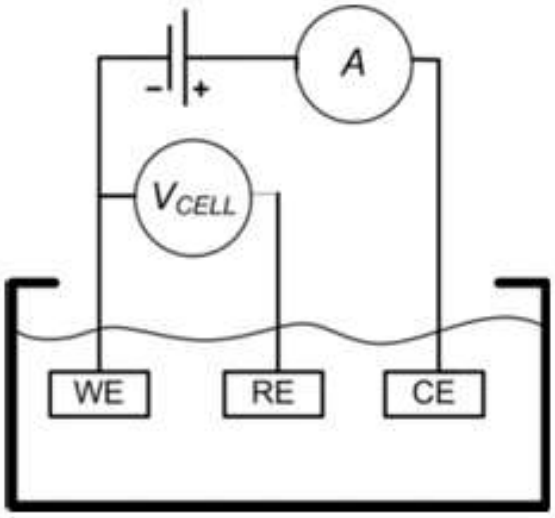

Figure 2.1: Scheme of an electrochemical cell. WE: working electrode; RE: reference electrode; CE: counter electrode

This configuration provides valuable mechanistic insights but is rarely applicable to industrial scales, as maintaining RE stability in large vessels is challenging. The second configuration is the two-electrode system, or *galvanic cell*, which is typically employed in industrial electrodeposition processes. This arrangement includes only a cathode and an anode. In both systems, the process is driven by an external power source, operating under either current or potential control. The selection of the appropriate operational mode depends on the specific experimental requirements: for instance, sharp current variations can be effectively managed under potentiostatic conditions, whereas other experimental circumstances may favor galvanostatic operation.

In industrial electroplating, the substrate is rarely coated with a single metallic layer; instead, multilayer deposition strategies are typically employed (Figure 2.2). This approach is preferred because the direct electrodeposition of the final decorative alloy onto the substrate often leads to adhesion failures, primarily caused by internal stress accumulation within the coating, which can result in peeling or delamination.

In the metal finishing industry, numerous galvanic processes are available [26], [27], yet for traditional base metals such as brass, bronze and ZAMAK, the process generally begins with the deposition of a relatively thick intermediate layer (5–20 μm) of nickel or copper. This interlayer serves a dual function: it enhances surface leveling and produces a smooth, lustrous base suitable for subsequent decorative coatings.

However, these initial metallic films are seldom the final finish. Instead, additional electroplated layers are sequentially applied until the desired color tone and surface characteristics are achieved. A critical aspect to consider in multilayer systems is the interdiffusion of metals between adjacent layers, which can progressively alter the chemical and aesthetic properties of the coating stack over time.

This diffusion phenomenon is particularly relevant in gold-on-gold systems [28], where intermixing may lead to reddening and purity degradation of the precious metal finish. To mitigate this effect, barrier layers are routinely introduced between gold deposits. Historically, a nickel barrier (1–5 μm) was the standard choice; however, due to allergenic risks and environmental concerns, it has been progressively replaced by bronze interlayers (2–5 μm), sometimes followed by a thin palladium coating (0.5–1 μm) to further enhance diffusion resistance.

For aluminum substrates, the same multilayer deposition approach is adopted. Nevertheless, prior to electroplating, an electroless zinc pre-coating is required to ensure proper adhesion, as it prevents the detrimental effects of the native oxide passivation layer naturally forming on aluminum surfaces.

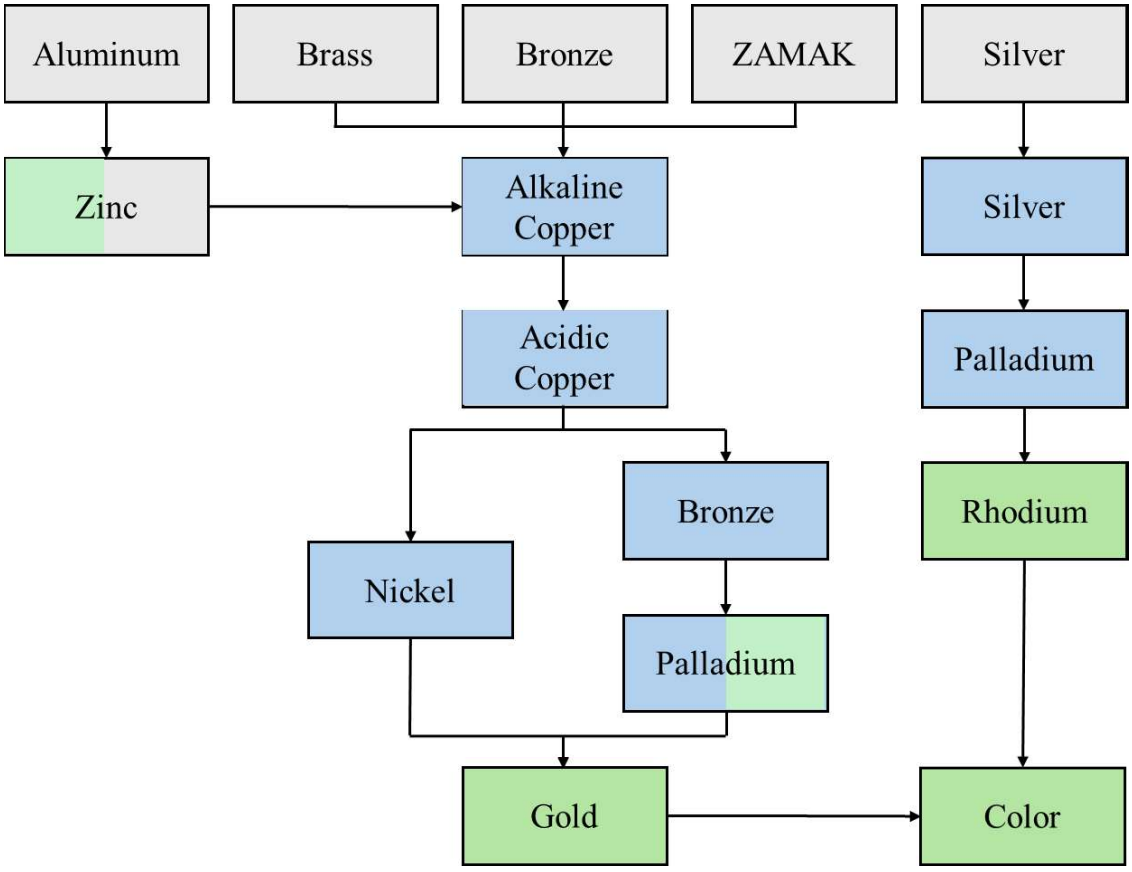

Figure 2.2: General scheme of the most common industrial electroplating processes. The boxes' color differentiates between the base metals (grey), intermediate depositions (blue) and the finishing layers (green)

From a quantitative standpoint, the deposition rate and coating thickness are governed by Faraday's laws. The total charge passed determines the deposited mass (Equation 2.1), where M is the mass of the coating, A_{mol} is the molar mass of the metal, Q is the charge, z is the number of electrons exchanged, and F is the Faraday constant, corresponding ti the charge of one mole of electrons (F = 96,485 C/mol = 26.8 A·h/mol):

$$M = \frac{A_{mol} Q}{zF} \tag{2.1}$$

This relationship can be adapted to estimate coating thickness, via Equation 2.2:

$$D = \frac{A_{mol} j t}{z F \rho} \tag{2.2}$$

Where D is the film thickness, j is the current density, t is the deposition time, and ρ is the film density (which may differ from bulk density due to voids or defects). It should be noted that these expressions are valid under the assumption that no parasitic reactions occur.

At equilibrium, the electrode potential is described by the Nernst equation (Equation 2.3), reflecting the balance between metal ion reduction and dissolution.

$$E_{eq} = E° + \frac{RT}{zF} \ln (C_{Me^{z+}}) \tag{2.3}$$

Where E° is the equilibrium potential under standard conditions, R is the gas constant, T is the absolute temperature, ln stands for the natural logarithm and $C_{Me^{z+}}$ is the concentration of the metal ions in moles per liter.

For electrodeposition to occur, the applied potential must be more negative than E_{eq}, thus favoring reduction over dissolution. The driving force for metal deposition is the overvoltage, defined as the difference between the applied potential (V_{app}) and E_{eq} (Equation 2.4).

$$\eta = V_{app} - E_{eq} \tag{2.4}$$

2.1.3 Diffusive Layer and Compact Layer

In an electrochemical system, when a potential difference is applied, a double electric layer is generated at each electrode, a structure that originates at the solid-liquid interface, where an electric charge transfer takes place accompanied by redox half-reactions. In an electrochemical cell, the solid phase is represented by

the electrode, while the liquid phase is represented by the electrolyte. As the reaction proceeds, the electric field generated causes the migration of ions present in solution, determined by the interaction between their charge and that accumulated on the electrode surface. Moving away from equilibrium conditions, as in the case of current flow, it is necessary to use a model that describes the interface as a transition region between two massive systems, the electrode and the solution, with different thermodynamic properties.

The first attempt to model this interface can be attributed to Helmholtz. In his model, the interface is imagined as a parallel plane capacitor, consisting of a layer of positive or negative charges on the metal and a layer of opposite sign in solution, located at the minimum possible distance from the electrode: a separation of charges and therefore a potential difference is established [4]. The concept of two layers of opposite charge is the origin of the term "double layer." This simple model is able to explain the existence of capacitive effects at the interface, but it fails to describe two fundamental aspects: the variation of capacitance with potential and its actual measured value at each potential.

An alternative approach, developed independently by Guoy and Chapman in 1913, considers that, although the charge of the metal is necessarily confined to the surface of the electrode, the same is not true for the charge on the solution side, which can instead extend into the bulk of the solution following a statistical distribution. This introduces the concept of a diffuse layer. This model, based on the Poisson-Boltzmann equation shown below, neglects the finite size of the ion, which inevitably cannot approach the electrode at a distance less than its ionic radius [29].

$$C_i(x) = C_i^0 e^{\frac{-z_i F \Phi(x)}{kT}} \tag{2.5}$$

Equation 2.5 describes the variation in concentration as the position along the deposition axis changes. The term $C_i(x)$ represents the concentration of the i-th species at distance x, C_i^0 the concentration of the species in solution, z_i the charge of the species, k the Boltzmann constant, while $\Phi(x)$ is a position-dependent potential function [22].

The two models of Helmholtz and Guoy-Chapman were combined by Stern in 1926, with the introduction of a plane of maximum approach. The potential variation is linear between the metal and the plane of maximum approach, while it is exponential from the latter towards the bulk of the solution. A distinction is thus made between a compact part and a diffuse part of the double layer in which the potential variations are linear and exponential, respectively [4].

The current description of the electrode-solution interface is based on Grahame's triple layer model, which introduces greater structural complexity than previous models. In this interpretation, the interface consists of three distinct zones. The first, known as the Inner Helmholtz Plan (IHP), is defined by the center of gravity of the ions adsorbed on the surface, which have the same charge as the electrode and are partially or completely desolvated. The second zone, known as the Outer Helmholtz Plan (OHP), is identified by the center of gravity of the solvated ions with a charge opposite to that of the electrode. Finally, at a greater distance, here is the diffusion layer or Guoy-Chapman layer.

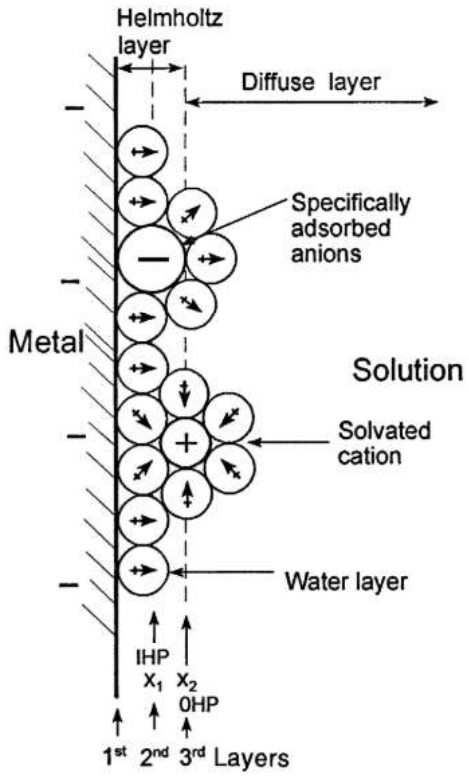

Figure 2.3: Schematic representation of Grahame's triple layer

2.2 Pulsed Currents

In the electroplating industry, direct current (DC) is currently used almost exclusively for the electrodeposition of most metals and alloys. This type of current is characterized by a linear waveform and requires only one parameter to be applied: current density [1]. Although direct current is the most widely used form of current due to its relative ease of implementation, it has a number of critical issues: firstly, it provides a constant flow of electrons that tends to favor preferential growth on the most protruding points of the substrate (edge effect), leading to the formation of non-uniform deposits [5]; furthermore, it promotes the formation of porosity in the deposit, with consequent deterioration of the properties of the metal film, including decreased conductivity, greater mechanical fragility, and lower corrosion resistance [2].

Despite these limitations, the use of pulsed current (PC) and pulsed reverse current (PRC) in industry has long remained restricted to specific applications, particularly in electronics and printed circuit boards [30]. Initially, modulated current systems were limited by the lack of sufficiently performing rectifiers and their high cost, which hindered industrial adoption [3], [31]. However, with technological advancements and the advent of modern electronics and microprocessor control, it became possible to precisely regulate the waveform of the applied current, adjusting amplitude and pulse duration to control the deposit morphology and thickness with atomic precision [1], [3], [32], [33], [34].

Electroplating with modulated currents has since become increasingly important, not only in electronics but also in alloy [35], composite materials [36] and semiconductor [37], [38]. Although only DC is still used in the decorative field [52], several studies suggest that PC and PRC could be successfully extended to this sector, reducing the use of organic brighteners and improving deposit uniformity with both environmental and economic benefits [39], [40].

The waveforms used in electrodeposition can be divided into two main groups, shown in Figure 2.4: unipolar pulses, in which all pulses are oriented in one direction (in this case, the current is called pulsed current, or PC), and bipolar pulses, in which both anodic and cathodic pulses are present (in this case, it is called reverse pulsed current, or PRC) [5].

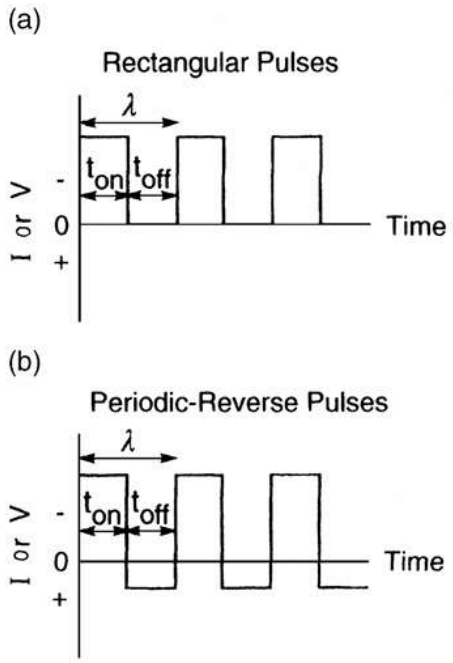

Figure 2.4: Examples of waveforms: (a) pulsed currents; (b) reverse pulsed currents

In the conventional DC plating there is only one parameter, called the current density, which can be varied. In pulse electroplating, there are at least three parameters, including pulse height (current amplitude), relaxation time (t_{off}) and pulse time (t_{on}) whose values can be effectively optimized. Each pulse consists of an on-time during which the potential or the current is applied, and an off-time during which the zero current is applied (Figure 2.4, (a)). In pulse reverse current, four parameters are required: cathode peak current density of the pulse, j_c, the duration of the cathode pulse, t_c, anode peak current density of the pulse, j_a, and the duration of the cathode pulse, t_a (Figure 2.4, (b)).

In the current pulse, the duty cycle (γ) corresponds to the percentage of the total time of a cycle and is given by:

$$\%\gamma = \frac{t_{on}}{t_{on} + t_{off}} x\ 100 \qquad (2.6)$$

J_{AV} (average current density) is calculated from:

$$J_{AV} = \frac{J_P t_{on}}{t_{on} + t_{off}} \quad (2.7)$$

Where, J_P is the pulsed current density. Based on the above, J_P can be derived as:

$$J_P = J_{AV}(P + 1) \quad (2.8)$$

Where P represents the ratio of the off-time to the on-time ($P = t_{off}/t_{on}$) [2], [41]. The limits of t_{on} and t_{off} are governed by two main phenomena: (i) the capacitive effects of the electrical double layer, which define the minimum feasible duration of each phase, and (ii) mass transport by diffusion of electroactive ions, which determines the maximum useful t_{on}.

The great advantage of modulated currents lies in their ability to influence electrocrystallization mechanisms and, consequently, the structural and mechanical properties of the deposits [31], [42], [43].

Since the nucleation rate is proportional to the applied current density, the application of pulsed currents to electrodeposition processes, which allow significantly higher current densities to be achieved than with direct currents, promotes faster nucleation thanks to the high cathodic overvoltage of the pulse [31]. This leads to the formation of deposits with a finer grain size and, generally, greater homogeneity [44], [45].

At the end of each cathodic pulse, the combination of several phenomena allows these results to be achieved. It is now known that the population of metal ions tends to decrease constantly near the cathode during deposition, particularly in areas of the surface where the electric field is greater; with direct current, it is not possible to replenish the deposited ions; on the contrary, the use of a pulsed current allows the metal ions to repopulate the area near the cathode during the off phase, promoting nucleation and greater concentration homogeneity, which translates into greater uniformity of the metal surface [1]. Furthermore, in the

absence of current, deposited impurities and additives can diffuse outward, avoiding inclusion within the metal deposit and consequently reducing porosity [46].

At the same time, the alternation of pulses allows the discharge of the electrostatic diffusion layer that forms near the cathode during DC deposition, enhancing ion transport and promoting more uniform growth [47], [48]. As a result, deposits obtained under pulsed current show improved compactness, higher density, and better electrical and mechanical performance [35], [49], [50], [51].

In reverse pulsed current electrodeposition, the anodic pulse induces a selective redissolution of the metal at protruding points, where the local current density is higher. This process has a self-levelling effect, smoothing the surface and reducing thickness inhomogeneities [5], [30], [52]. The result is a significant reduction in the "*edge effect*" and improved uniformity of the deposited layer.

Moreover, the alternation between cathodic and anodic pulses facilitates the detachment of hydrogen bubbles generated during the cathodic phase, leading to smoother and less porous deposits [53]. This mechanism also enhances the overall ductility and conductivity of noble metal deposits, particularly gold and its alloys, allowing thinner yet high-quality coatings that pass porosity tests - an important economic advantage in electronics [3].

From an environmental perspective, the advantages of modulated current techniques are equally significant. PC deposition can reduce additive consumption by 50–60%, while PRC can nearly eliminate the need for such agents [2], [54]. This not only improves bath stability and process efficiency but also reduces the generation of hazardous waste, contributing to more sustainable electroplating operations [55].

Today, pulse and reverse-pulse plating are widely used in advanced applications such as composite coatings, amorphous alloys, and anodizing [55]. With the

availability of efficient and programmable rectifiers, the technique has evolved into a mature and versatile technology, enabling precise control over the microstructure and performance of electrodeposited materials.

2.2.1 Double Electric Layer

When a potential difference is applied between the working electrode and the counter electrode, a double electric layer forms near the electrode-solution interface. In the simplest case, the working system can be likened to an electrical circuit consisting of a resistor and a parallel plane capacitor [56].

In this approximation, each element of the circuit corresponds to an element or phenomenon associated with our working system. The resistor is attributable to the solution, which opposes the passage of current, while the capacitor is attributable to the formation of the double electric layer. This phenomenon involves a separation of charges at the electrode-solution interface comparable to two plates of a parallel-plate capacitor [4]. The capacitance of the hypothetical capacitor can be determined using Equation 2.6:

$$C = \frac{\varepsilon A}{d} \tag{2.6}$$

Where ε represents the absolute dielectric constant of the medium between the two plates, A represents the surface area of the capacitor faces, and d represents the distance between the plates.

Since the distance between the charges in the double layer is on the order of Ångström, it is necessary not to neglect the value of the capacitance.

When a current is passed through the hypothetical circuit, part of the current is consumed to charge the capacitor up to a maximum defined by the capacitance and the potential difference between the plates, and the time required to charge the capacitor is defined as the “charging time.” Once the current between the

electrodes has been applied, the capacitor will undergo a discharge process, generating a current for a time known as the “discharge time” [7].

At the beginning of a pulse, therefore, the total current applied by the generator is composed of two components, a “capacitive” current (which charges the double layer) and a “faradic” current (which corresponds to the deposition rate), according to the formula [7]:

$$i_P = i_c + i_f \tag{2.7}$$

Where i_p represents the applied current, i_c the capacitive current, and i_f the faradic current.

Figure 2.5 shows some current pulse profiles that illustrate the distortion of the faradic current pulse due to capacitive effects. In profile (a), the t_{on} is much longer than the charging time of the double layer and, as a result, the total current is almost exclusively faradic. In profile (d), on the other hand, the charging time is much greater than t_{on}, a factor that causes a marked flattening of the faradic current, which approaches a direct current considerably. Profiles (b) and (c) represent intermediate situations [8].

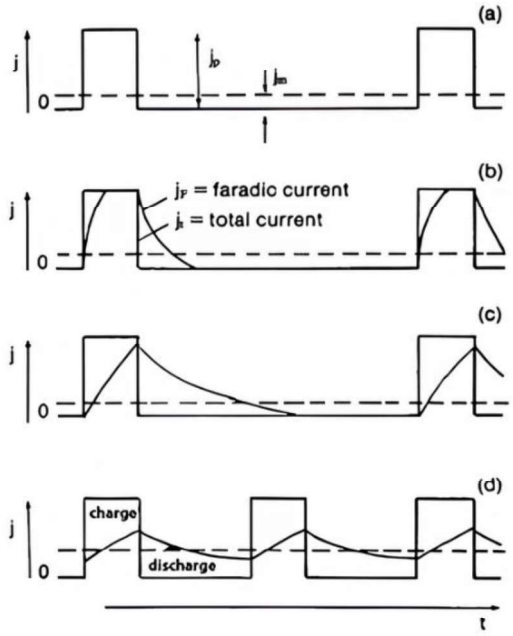

Figure 2.5: Current pulse profiles showing the distortion of the faradic current due to capacitive effects

It is therefore necessary to use tones greater than the charging time (t_C) of the capacitor, otherwise the system would only exploit the capacitive current without causing any redox reaction, as the capacitor would not have been charged and the current would not flow to the working electrode. It is equally important to maintain a t_{off} greater than the discharge time (t_D) so as to allow the system to return to equilibrium and promote all those desirable phenomena associated with the use of PC. Although it is essential to use an adequate minimum t_{off}, it is necessary to consider that there is no physical upper limit to the interval between two pulses, as the greater the t_{off}, the better the deposits obtained [8]. A real limit is given by the lengthening of deposition times with a consequent increase in production costs. It is therefore important to balance the benefit/cost ratio.

Knowing the charging and discharging times of the capacitor, it is possible to determine the lower limits for t_{on} and t_{off}. The Equations used are 2.8 for t_{on} and 2.9 for t_{off}, respectively [8].

$$t_{on}^{min} = 5t_C \tag{2.8}$$

$$t_{off}^{min} = 7t_C \tag{2.9}$$

The capacitor charging time can be calculated using the following Equation [7]:

$$t_C = \frac{C\eta}{J_p} \tag{2.10}$$

Where C represents the capacitor capacity, η the overpotential, and J_p the pulse current density.

2.2.2 Mass Transport

To correctly evaluate the upper limit of the t_{on}, it is necessary to introduce a fundamental concept in metal electrodeposition: mass transport. This is mainly because the use of a pulsed waveform is closely linked to the variation in mass transport conditions on the electrode surface [57].

The term mass transport refers to the set of phenomena that cause the movement of a chemical species within a solution. Generally, there are three mechanisms that contribute to the transport of electrolyte in solution [58]:

- Diffusion, the spontaneous movement of chemical species due to a concentration gradient;
- Convection, the transport of chemical species due to the movement of the solution (which can be caused by mechanical or air agitation, a difference in temperature, or a difference in density);
- Migration, the movement of electroactive ionic species under the action of the electric field generated between the two electrodes.

Mass transport plays a fundamental role during electrodeposition operations, both in direct current and pulsed current, as it limits the deposition rate and influences the structure and properties of the deposit [58].

When a direct current is applied to a galvanic system at equilibrium, there is a decrease in ionic species near the electrode surface, with a consequent variation in concentration as the distance from the electrode increases. In other words, at a greater distance, the concentration of the chemical species will remain unchanged (in the bulk of the solution), while as it approaches the electrode surface, the concentration will tend to decrease (Figure 2.6). A diffusion layer will therefore be established near the electrode, in which mass transport depends mainly on diffusion phenomena [58].

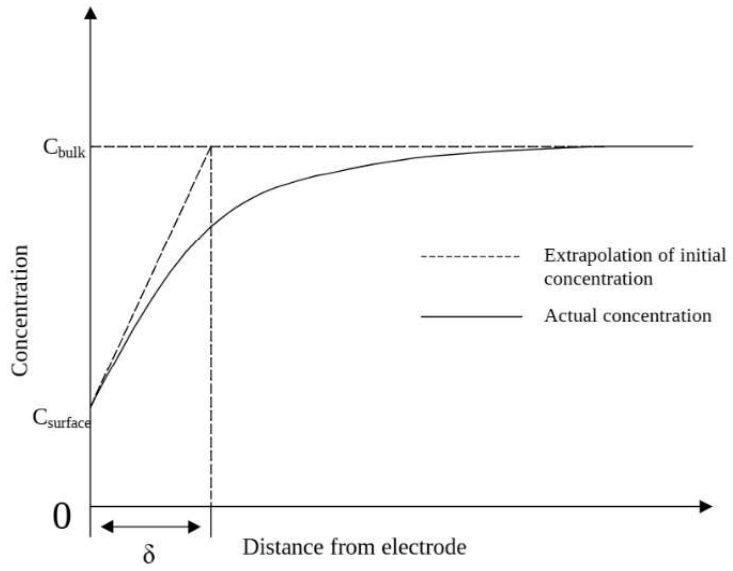

Figure 2.6: Concentration profile of the species of interest as a function of distance from the electrode

Beyond the diffusion layer (δ) is the bulk of the solution, where mass transport returns to being controlled primarily by convection phenomena.

Using a modulated current, it is possible to describe what happens on the electrode surface using a model that involves a double diffusion layer: a first internal diffusion layer (δ_p), close to the cathode, and a second external diffusion layer (δ), which precedes the bulk of the solution [5], [35], [59]. In this model, linear concentration profiles are assumed in the diffusion layer, as shown schematically in Figure 2.7.

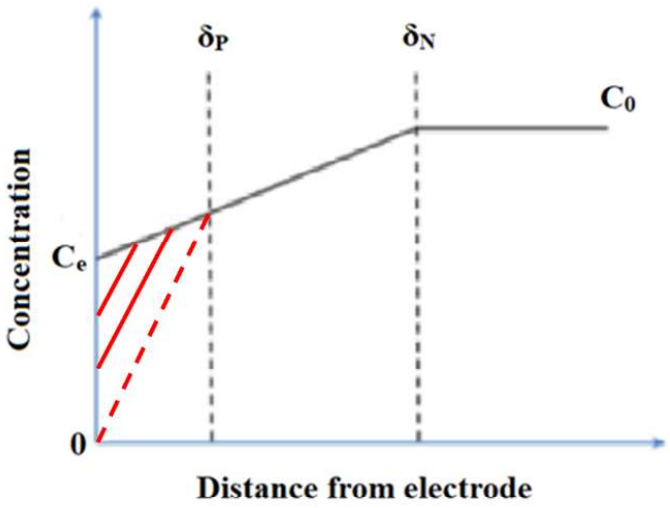

Figure 2.7: Schematic representation of the double diffusion layer formed near the electrode surface. The black line represents the concentration profile just at the start of the cathodic pulse. Solid red lines show the evolution of the concentration gradient during the pulse period. The dashed red line corresponds to the achievement of the transition time

The double diffusion layer therefore exhibits a particular behavior: during the t_{on}, the internal diffusion layer will be depleted of the electroactive species, consequently developing a strong concentration gradient. During the t_{off}, the external diffusion layer will supply the internal diffusion layer with species, so that the concentration gradient generated during the pulse will tend to relax. This implies that the inner layer has a concentration profile that pulses with time constants similar to those of the applied pulse [57]. Similarly, the outer diffusion layer is fed by the bulk of the solution.

Considering that the inner diffusion layer expands as the pulse duration increases (t_{on}), it is essential to evaluate the upper limit of the latter. In fact, if the t_{on} is too large, the diffusion layer would expand to the bulk of the solution, an area where mass transport is mainly influenced by convective and non-diffusive phenomena. If the pulse duration is particularly long, the electroactive species in the diffusion layer may be depleted, resulting in the need to apply a higher potential to replenish the inner layer [58]. The time during the pulse beyond which the

electrolyte concentration in the inner diffusion layer becomes zero is defined as the transition time (τ). For this reason, we can assume τ as the maximum time (t_{on}^{max}) for a deposition to be considered a pulse deposition. Unlike t_{on}, the off time does not have an upper limit due to the absence of mass transport constraints. The transition time is typically calculated using the following equation [59]:

$$\tau = t_{on}^{max} = \frac{\pi D (C_0 nF)^2}{4{J_P}^2} \tag{2.11}$$

Where D is the diffusion coefficient of the electrolyte, C_0 represents the bulk concentration of the electroactive species, n is the number of electrons transferred and F is the Faraday constant.

The diffusion coefficient D can be determinated by applying Fick's law for steady-state current conditions [60], specifically when $t >> r^2/D$, where r is the radius of the circular electrode. Under these conditions, the relationship between current and diffusion coefficient is established as follows:

$$i_{(t)} = 4nFC_0Dr \tag{2.12}$$

3 Copper

Copper electrodeposition is a process widely used in the electroplating industry; its applications can range from the production of thin layers to improve adhesion and reduce crystal stresses in subsequent layers, to the deposition of thin films on printed circuits for electronics [1]. The use of copper for the formation of metal substrates has been widespread for more than 50 years and is one of the fundamental operations within the electroplating industry [26]. Copper coatings can easily correct pre-existing defects on substrates such as holes, protuberances, and scratches while maintaining high cathodic efficiency, high penetrating power, and low cost.

Copper electrodeposition processes are widely used but present a number of critical issues that should not be underestimated, among which environmental impact stands out. Conventional formulations for copper baths present hazards related to the use of toxic cyanide-based chemicals and the consequent production of waste that must be treated as hazardous waste.

Consequently, the significant toxicity of the substances used in electroplating processes requires companies in the sector to invest in reagent control and management systems, as well as in the training of qualified personnel capable of operating safely and ensuring compliance with environmental and occupational safety regulations.

The most common electrolytic baths for copper plating can be classified into two categories [26]:

- Alkaline baths, typically characterized by the presence of a series of cuprocyanide complexes obtained by adding copper or copper salts, also cyanide-based, to concentrated cyanide solutions;
- Acid baths, generally consisting of copper sulfate ($CuSO_4$) and sulfuric acid (H_2SO_4).

The choice of baths is closely linked to the type of work and the nature of the substrate [26]. Acid copper baths are extremely popular due to their ease of preparation and management, the low cost of chemicals, and current yields close to theoretical values. However, this type of bath has one drawback: it is not possible to deposit acid copper directly on most metal substrates (brass, zamak, aluminum) due to the phenomenon of cementation. Cementation is a spontaneous electrochemical process in which a less noble metal (i.e., with a lower reduction potential) oxidizes, allowing the reduction of the more noble metal (with a higher reduction potential). The main disadvantage is that the deposited copper does not adhere to the substrate and appears in a spongy form, rendering the coating unusable.

To avoid the phenomenon of cementation, therefore, a preventive deposition of copper is carried out using an alkaline copper bath. In alkaline baths, copper is generally present in solution in the form of very stable cyanide-based complexes, making the copper less reactive and less available for spontaneous reduction, thus reducing the risk of cementation. However, this type of bath does not allow for high thickness to be achieved, beyond which the deposit becomes fragile and poorly adherent. Consequently, copper plating of a certain thickness requires two steps: first, deposition in an alkaline bath for protection, and then thick copper plating in an acid bath.

3.1 Alkaline Copper

3.1.1 Introduction

In large industrial cycles of electrodeposition on metal substrates, copper plating plays an important role. Although it does not provide a protective coating, it forms an essential intermediate layer that improves the adhesion properties of subsequent deposits, ensuring the quality of the final coating. Copper is generally electrodeposited from solutions in which it is present in a bivalent state and from solutions in which it is monovalent. In the first case, sulfate baths are usually used; in the second case, cyanide baths are used [26].

Although extremely effective in obtaining high-quality coatings, cyanide-alkaline copper plating baths present numerous problems regarding plant safety, environmental impact, and wastewater and waste management. The main problem concerns the toxicity of cyanide, which poses a danger to human health, the environment, and ecosystems. The management of cyanide baths therefore requires careful monitoring and a team of certified operators capable of preventing spills or accidental exposure. Galvanotechnicians exposed to cyanide must wear personal protective equipment and follow strict safety protocols to ensure their own safety and that of others.

Waste disposal is equally problematic, as it requires industries to comply with the European Waste Code (CER 06 03 11), which dictates the rules for handling and disposing of solutions containing cyanides. According to European regulations, this waste must be managed in a specific manner due to its hazardous nature. Generally, wastewater from cyanide-containing baths involves the oxidation of cyanide to cyanate, which is much less toxic, through the addition of sodium hypochlorite, according to the following reaction:

$$CN^- + ClO^- \rightarrow CNO^- + Cl^- \quad (3.1)$$

The process is carried out at a pH of 9-10 in order to prevent the accidental formation of extremely toxic hydrogen cyanide. Destruction can be pushed beyond the cyanate stage by using an excess of oxidant:

$$2CNO^- + 3ClO^- + 2H^+ \rightarrow 2CO_2 + N_2 + H_2O + 3Cl^- \quad (3.2)$$

Concerns related to health and safety at work, high waste treatment costs, and significant environmental impact have prompted research into new non-cyanide plating technologies.

There are a considerable number of studies in the literature on cyanide-free alkaline copper baths [61], [62], [63], however, most of these electrodeposition processes have been conducted using direct current, which does not allow for deposit characteristics comparable to those obtainable with traditional cyanide-alkaline baths. This limitation represents a significant obstacle to the industrial replacement of the alkaline copper plating process. The application of pulsed currents to low environmental impact copper baths, on the other hand, has not been adequately explored. As already mentioned, pulsed current requires the optimization of multiple parameters, but on the other hand offers greater flexibility in the production of metal deposits.

In light of all these considerations, the objective of this work is to conduct a preliminary study on the application of pulsed currents to copper electrodeposition, using low environmental impact alkaline copper plating baths. The aim is to obtain copper deposits with properties comparable to, if not superior to, those obtainable through classic electrochemical direct current processes in cyanide-containing baths. In particular, the aim is to verify the quality of the deposit, adhesion, and corrosion resistance, with the goal of improving coatings in an environmentally friendly context.

3.1.2 Experimental

The tests were conducted on a commercial cyanide-free alkaline copper bath (KEMTECH 430, Kemia), with a copper concentration of 9 g/L and an optimal current density, as specified in the technical data sheet, of 2 A/dm2.

For the electrochemical study, a circular platinum electrode (RDE) with a radius of 1.5 mm was used as the working electrode, a platinum wire as the counter electrode, and a saturated Ag/AgCl/KCl electrode as the reference electrode, whose potential measured against a calomel electrode (SCE) is -43.7 mV. Unless otherwise noted, all electrochemical analyses were performed in a beaker, using a solution volume of 100 mL and a controlled temperature of 50 ± 1 °C.A commercial basic degreaser (owned by ITALFIMET) was used for the preliminary preparation of the samples.

The thickness of the deposits was measured by XRF analysis [64], [65], [66], [67], performed with a Bowman B Series XRF spectrometer (Schaumburg, IL, USA) using an acquisition time of 60 s, 50 kV tube voltage, 0.8 mA tube current, and a collimator of 0.6 mm in diameter.

Scanning electron microscopy (SEM) images and microanalysis were obtained with variable pressure Hitachi SU3800 (Hitachi High-Tech, Tokyo, Japan) equipped with an Oxford Instruments NanoAnalysis Ultim Max 40 silicon drift EDS detector. The analyses were performed using an accelerating voltage of 5 kV.

Quantitative color comparisons were obtained using the portable spectrophotometer CM-700d (Konica Minolta, Tokyo, Japan) equipped with an integrating sphere controlled by SpectraMagicNX software (Konica Minolta, Tokyo, Japan). Color coordinates were expressed in the CIE-Lab color space: L* = light vs. dark, a* = red vs. green, and b* = yellow vs. blue. In the CIE-Lab color space, the a and b coordinates define the hue (color) and the chroma (vividness/dullness), while the degree of lightness is represented by the L*

values. The measurement was obtained from diffuse reflectance spectra according to the CIE's recommendations [68] using a D65 illuminant, an observer at 10°, and maximum aperture with an angle of incidence θ = 8°. The specular component was included (SCI). The measurements were performed using a 11 mm in diameter circular masks (MAV11). The gloss (8°) estimation, the function of luminous directional reflectance of a specimen responsible for its shiny or lustrous appearance, was obtained measuring both the reflectance spectrum of the samples including and excluding the specular component (SCI method and SCE method, respectively) [69], [70]. For both colorimetric and gloss assessment, the results reported are the average of five repeated measurements for each sample.

X-ray diffraction (XRD) analyses were performed using a Brucker (Billerica, MA, USA) New D8 Da Vinci diffractometer, employing Cu Kα radiation (λ = 1.54056 Å), operating at 40 kV and 40 mA. The X-ray diffractometer was equipped with a θ-2θ geometry, an Euler cradle, and a Brucker LYNXEYEXE detector. The acquisitions were performed in the range 2θ = 40°-100°, using a step of 0.03° and an integration time of 0.3 s per step.

3.1.3 Results

A preliminary electrochemical study was carried out, using the commercial alkaline copper electroplating bath, to investigate the parameters to be varied for the pulse electrodeposition. The purpose of these experiments is to obtain ranges useful in choosing the appropriate settings for pulse plating, taking into consideration the electrochemical limiting factors.

The capacitance value was derived through electrochemical impedance spectroscopy [71], resulting in a value of C = 2.77 mF/cm^2. The equivalent circuit used to fit the Bode diagram, corresponding to our working system, allowed us to assimilate the non-faradic process into a constant phase element (CPE), which

was then converted into its equivalent capacitor, using the following formula [71]:

$$C_{eff} = \frac{(Y_0 R_p)^{1/n}}{R_p} \sin\left(\frac{n\pi}{2}\right) \quad (3.3)$$

Where C_{eff} is the effective capacitance, Y_0 and n are the characteristics parameters of the CPE and R_p is a resistor.

The commercial copper plating bath has an optimal current density, as specified in the data sheet, of 2 A/dm^2, which was therefore used as the average current density for all DC and PC tests.

Overpotential is defined as the difference between the equilibrium potential for a given reaction (also called the thermodynamic potential) and the potential at which the electrochemical reaction operates at a specific current under specific conditions [72].

Through chronopotentiometries performed with different current densities (related to each value of P), we calculated the overpotential and through Equation 2.10 the value of t_C. Using Equations 2.8 and 2.9 we obtained respectively the lower limits of t_{on}^{min} and t_{off}^{min}, as shown in Table 3.1.

Table 3.1: overpotential values and charging time obtained for different P values

P	**η (V)**	**t_C (ms)**
0	-1.0992	15.25
1	1.2226	8.48
2	-1.2199	5.64
3	-1.2787	4.43
4	-1.3342	3.70
5	-1.3999	3.23

The transition time τ was then estimated by performing chronoamperometric measurements and using Equation 2.11. These results, together with the lower limits for pause and pulse times, are shown in Table 3.2.

Table 3.2: Lower operating limit for pulse time and pause time obtained from the experimental value of η and t_C and upper operating limit for pulse time corresponding to t_C, for the chosen P values

P	t_{on}^{min} (ms)	t_{off}^{min} (ms)	t_{on}^{max} (ms)
0	76.3	107	14279
1	42.4	59.4	3417
2	28.2	39.5	1638
3	22.1	31.0	900
4	18.5	25.9	567
5	15.1	22.7	385

Once lower and upper limits have been established, we chose parameterizations within these operational ranges, which are considered optimal, for different values of pulse current density.

Table 3.3: Selected experiments and parameterizations of sample obtained

Sample	P	t_{on} (ms)	t_{off} (ms)	J_p (A/dm^2)
A	DC	/	/	2
B	1	60	60	4
C	1	100	100	4
D	2	50	100	6
E	2	100	200	6
F	3	50	150	8
G	3	100	300	8
H	4	20	80	10

I	4	100	400	10
J	5	20	100	12
K	5	50	250	12
CN	DC	/	/	1

All samples were prepared from circular brass plates (diameter 39 mm) that had been suitably degreased using cathodic degreasing. Once electrodeposition was complete, the samples were suitably washed with milliQ water, dried, and characterized.

Samples A-K were prepared using a cyanide-free alkaline copper bath, while sample CN was prepared using an alkaline copper bath containing cyanides. In this section, characterization analyses will be used to compare the samples obtained using direct and pulsed current with the sample obtained from the cyanide-alkaline bath.

SEM analysis

The samples were analyzed using scanning electron microscopy in order to evaluate the morphology and particle size of the copper deposit obtained.

The analyses were conducted in the central area of each sample in order to ensure greater representativeness of the results. The SEM images obtained are shown below.

Sample A

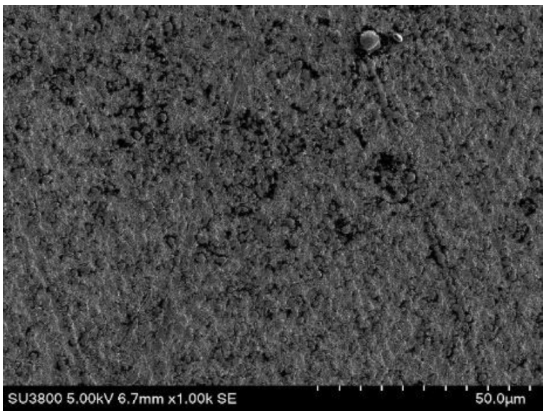

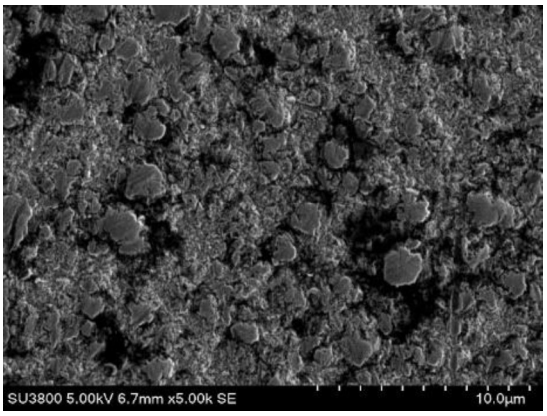

Sample B

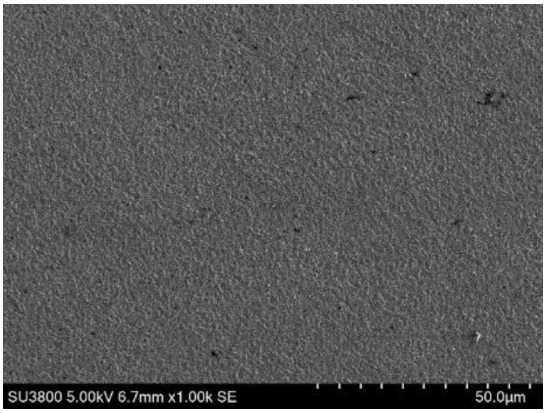

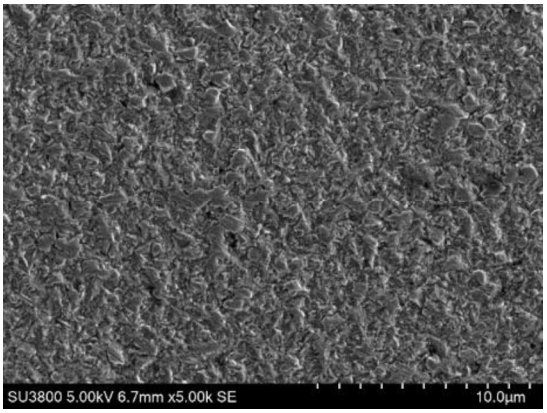

Sample C

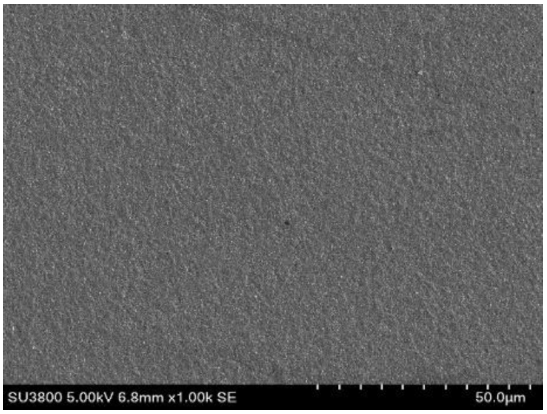

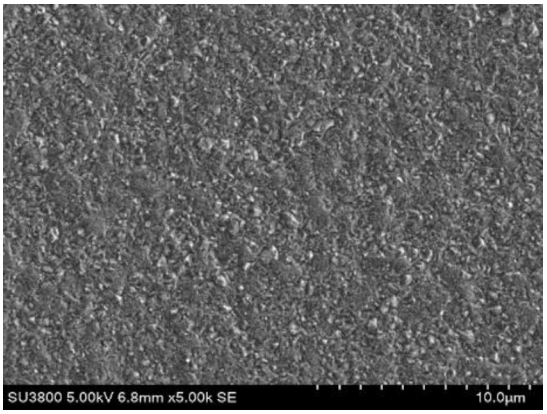

Sample D

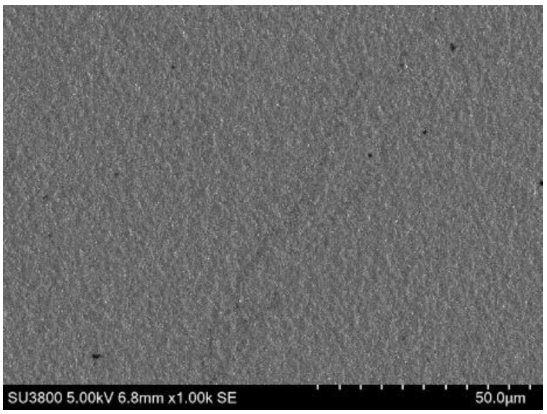

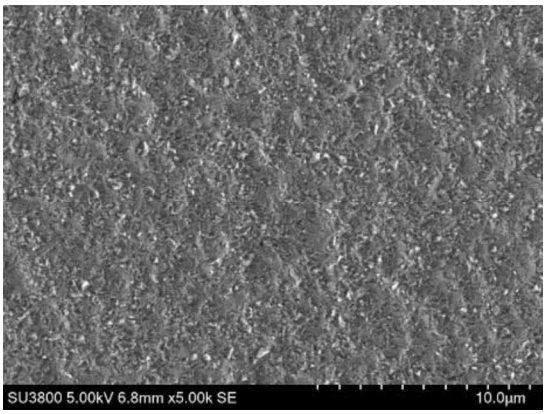

Sample E

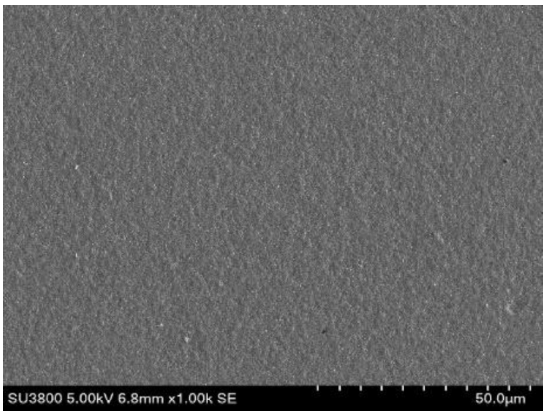

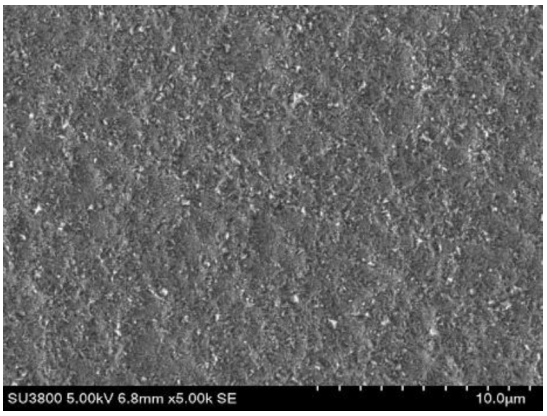

Sample F

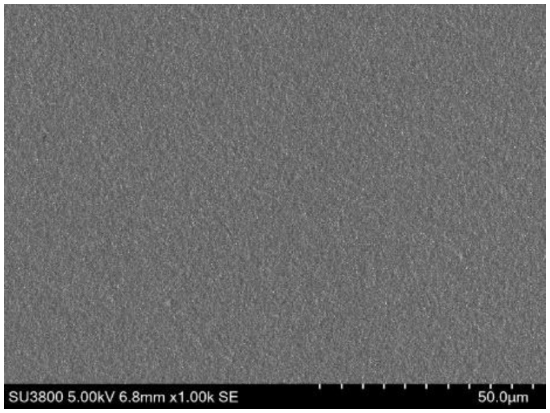

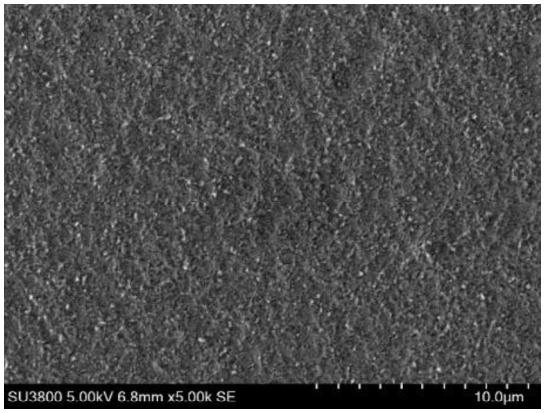

Sample G

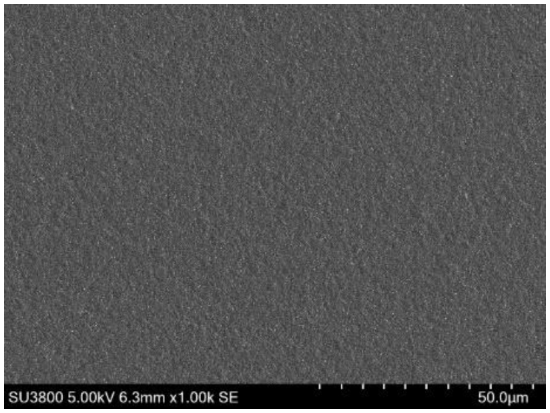

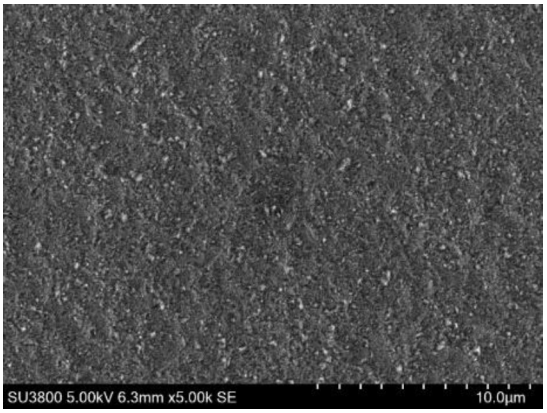

Sample H

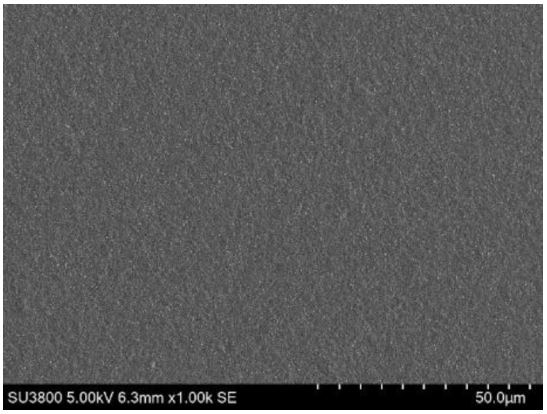

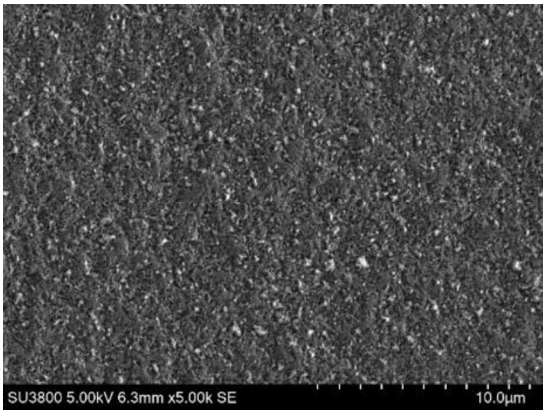

Sample I

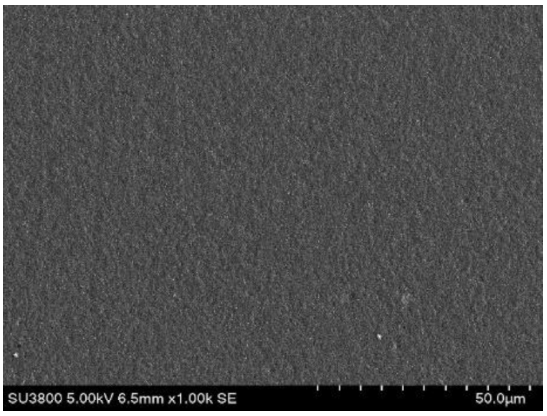

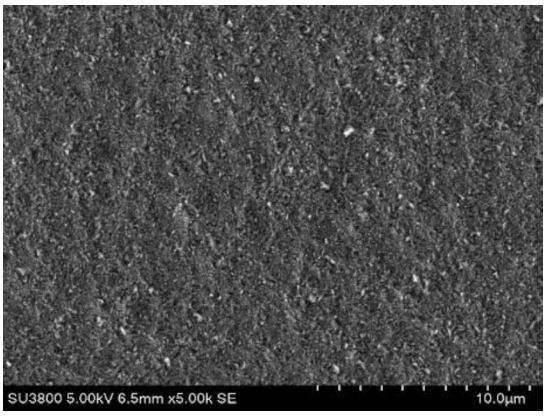

Sample J

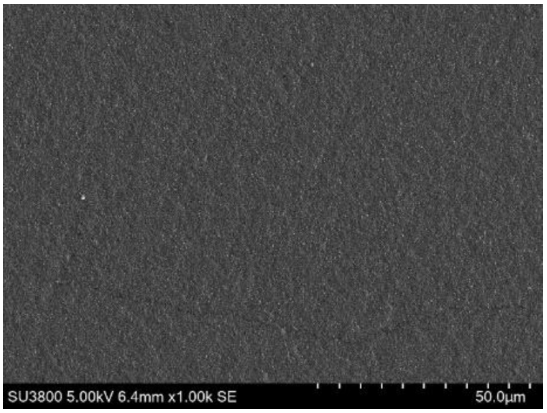

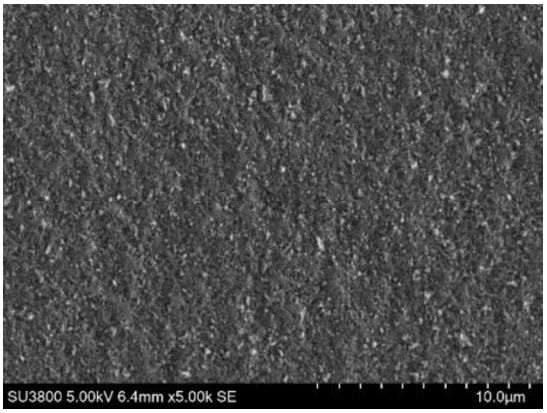

Sample K

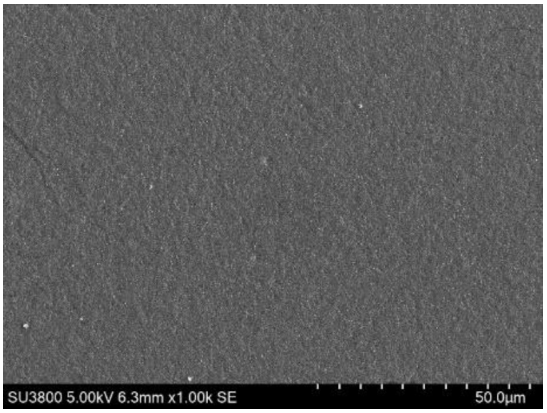

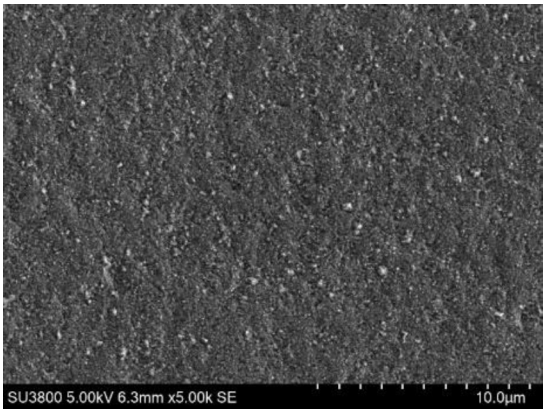

Sample CN

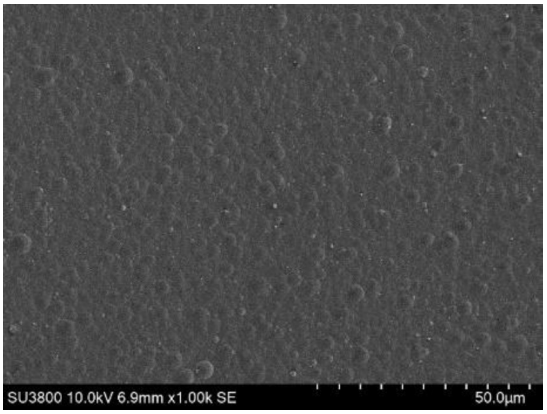

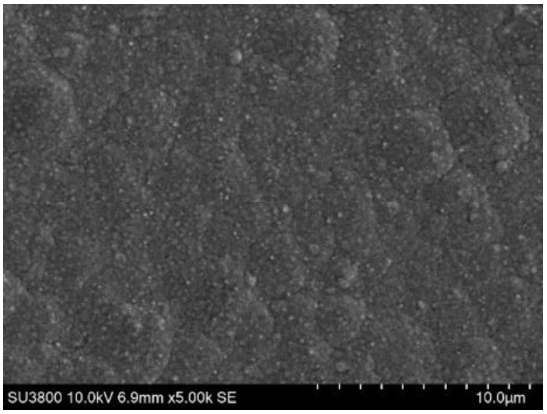

Figure 3.1: SEM images of the various samples at two different magnifications, 1k and 5k

Some qualitative observations can be drawn from the images collected. In particular, it can be noted that sample A, obtained by direct current electrodeposition, has an uneven surface, characterized by an irregular morphology with numerous pores and reliefs. On the contrary, the samples obtained in pulsed current show, albeit with some distinctions, a significantly more homogeneous surface, which is free of appreciable irregularities. Finally, comparing the results obtained with pulsed current with the sample produced using an alkaline copper bath containing cyanides, it can be seen that the samples obtained with pulsed current have a more homogeneous grain and a morphology free of the reliefs that characterize the CN sample.

Granulometric analysis

To complete the morphological characterization of the samples at the SEM, a granulometric analysis was performed on the SEM images acquired at 5k magnification using ImageJ software. Due to the small size of the grains and the nature of the deposit, especially in the samples produced in pulsed current, where the smaller grains are fused together, it was not possible to quantitatively determine the average grain size.

To calculate the dimensions, each SEM image was divided into six equal sections and, in each section, the dimensions of the largest grains were measured. The estimated grain dimensions, obtained by averaging the results determined from the various measurements, are shown in Table 3.4.

Table 3.4: estimated grain size for each sample

Sample	Grain size (µm)
A	0.88 ± 0.30

B	0.62 ± 0.14
C	0.44 ± 0.11
D	0.34 ± 0.07
E	0.28 ± 0.07
F	0.23 ± 0.04
G	0.32 ± 0.07
H	0.35 ± 0.10
I	0.27 ± 0.06
J	0.33 ± 0.06
K	0.29 ± 0.07
CN	0.46 ± 0.15

Looking at the results, it can be seen that the samples obtained with direct current (A and CN) have the largest grain size of all the samples analyzed, providing experimental evidence of the ability of pulsed currents to produce finer and more homogeneous deposits.

Throwing Power (TP)

In the electrodeposition process, the distribution of primary current on the cathode is determined by the shape of the galvanic tank and the configuration and position of the electrodes inside it. Under ideal conditions, with constant electrode polarization and 100% cathodic efficiency, the thickness of the deposit is directly proportional to the current density. However, in industrial baths, it is extremely difficult to achieve uniform current distribution; recessed or shielded areas tend to receive lower current densities, resulting in a reduction in deposit thickness.

In this context, throwing power (TP) is a measure of the ability of the electroplating bath to compensate for uneven current distribution, ensuring the

production of a more uniform deposit. Good penetrating power is essential in all electrodeposition processes, but it plays a greater role in cases where the coating has protective purposes, such as corrosion protection, considering that the first areas to be affected by corrosive processes are precisely those where the deposit is thinner [73]. The quantitative evaluation of penetrating power can be carried out on different configurations of galvanic baths, provided that it is possible to determine or estimate the current density distribution; it is important to remember that the results obtained will only be valid for the experimental configuration studied. Among the various experimental approaches developed for the evaluation of penetration power, the most used is that based on the Haring-Blum cell [74]. However, the approach used in this thesis is different: penetration power is measured using a Hull cell and is expressed as a function of the thickness of the deposit, measured at different points arranged horizontally along the cathode.

For the TP evaluation, a series of Hull plates were prepared using the same operating parameters used for the electrodeposition of the copper samples. The electrodeposition process was carried out in a Hull cell, using brass plates, for 5 minutes. In order to reproduce the working conditions of an industrial galvanic bath as faithfully as possible, air agitation was used, as required by the Technical Data Sheet.

Using XRF analysis, 50 points were sampled along the entire length of the Hull plates, at a height of 2.5 cm from the lower edge. Each point was sampled for 20 seconds.

Once the thicknesses on the Hull plates had been determined, it was possible to proceed with the calculation of the penetrating power of the galvanic bath. Figure 3.2 shows the thickness profiles of the various plates; from an initial qualitative analysis,it is possible to note some “peaks” at almost regular intervals, probably due to the air agitation of the cell.

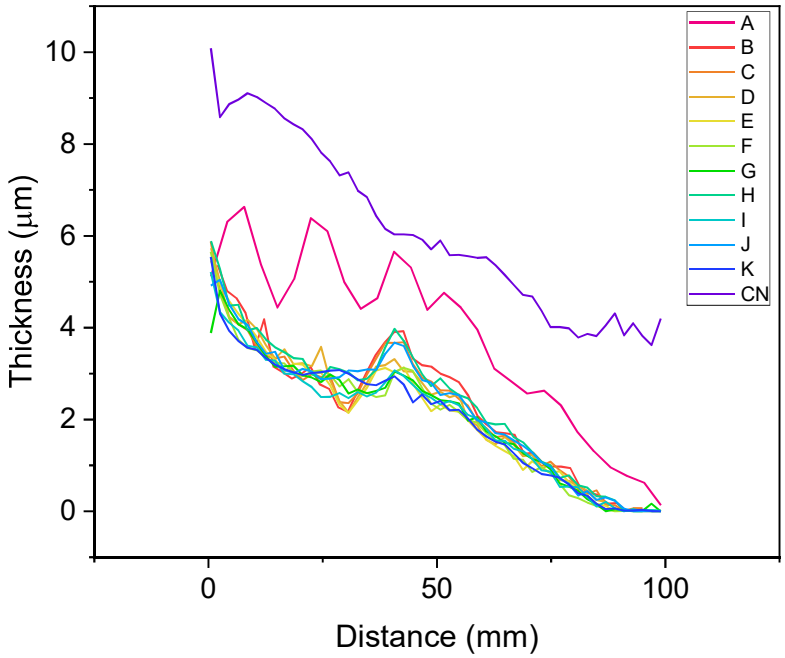

Figure 3.2: Profiles of measured thicknesses as a function of distance on the Hull plate

It can be seen that samples prepared in pulsed current show lower thicknesses but with a more homogeneous distribution than the samples in direct current.

Thanks to the measured copper thicknesses and Equation 3.4 [73], it was possible to calculate the throwing power of the bath, obtaining the results shown in Table 3.5.

$$TP(\%) = \frac{P - M}{P + M - 2} \tag{3.4}$$

$$P = \frac{J_a}{J_b} \tag{3.5}$$

$$M = \frac{S_a}{S_b} \tag{3.6}$$

$$J = i(5.1 - 5.24\log(d)) \tag{3.7}$$

Where J_a, J_b represents the primary current density and S_a, S_b represents the measured thickness. The primary current density within a Hull cell is calculated using Equation 3.7 (DIN 50 957), where J (A/dm²) represents the current density,

i (A) represents the current intensity, and d represents the distance (cm), measured along the cathode of a standard hull cell, from the high current density end.

Table 3.5: Penetrating power values determined by XRF analysis for each sample

Sample	TP (%)
A	71.8 ± 0.1
B	62.3 ± 0.1
C	50.8 ± 0.1
D	39.4 ± 0.1
E	38.8 ± 0.1
F	11.9 ± 0.1
G	32.4 ± 0.1
H	47.4 ± 0.1
I	34.5 ± 0.1
J	37.9 ± 0.1
K	39.0 ± 0.1
CN	80.1 ± 0.1

Looking at the data, it can be seen that the TP of the cyanide-free bath, operated in pulsed current, cannot reach the TP of the cyanide-alkaline bath, except in cases where continuous currents are used. However, an interesting result is that by modifying the operating parameters of the pulsed current, it is possible to modify the TP.

XRD analysis

The results of the diffractometric analysis are obtained as spectra; an example relating to sample J is provided in Figure 3.3.

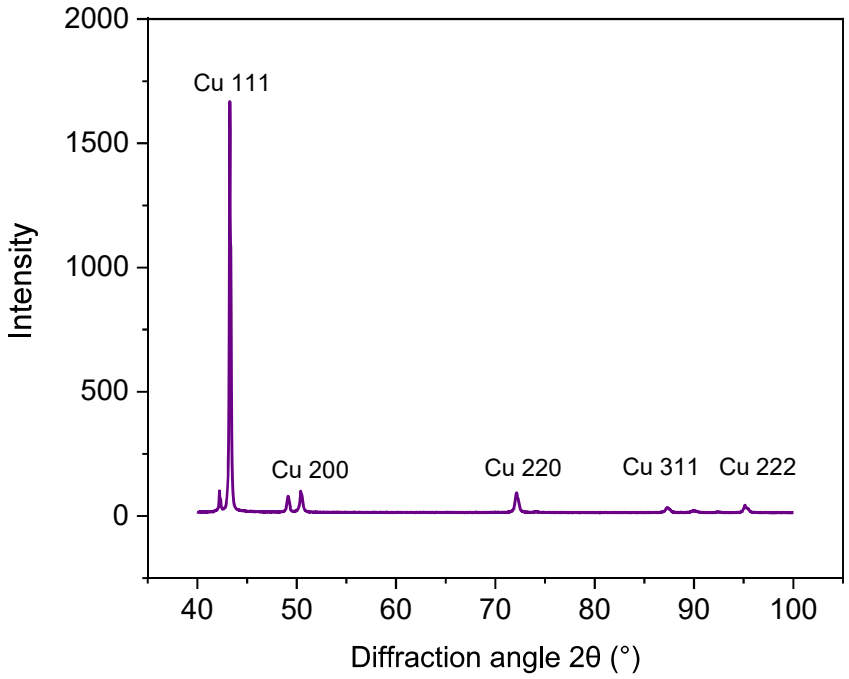

Figure 3.3: Diffractogram for sample J

Using DIFFRAC.TOPAS software and the Pawley method, it was possible to determine the crystallites size, which are shown for each sample in Table 3.6 [75].

Table 3.6: Crystallite size extrapolated from XRD analyses

Sample	Crystallite (nm)
A	73.2 ± 1.2
B	78.1 ± 1.0
C	128.7 ± 1.8
D	131.8 ± 1.3
E	121.7 ± 1.1
F	118.1 ± 1.9
G	116.7 ± 1.4
H	106.8 ± 1.2
I	131.5 ± 1.2
J	112.5 ± 1.2

K	136.2 ± 1.3
CN	60.1 ± 1.2

Looking at the results collected, although the crystallite sizes are larger in the pulsed current samples, their sizes are close to those of the grains (Table 3.4). It can be concluded that, as a first approximation, the grains of the deposits obtained by pulsed currents consist mainly of a single type of crystallite.

Colorimetric analysis and gloss evaluation

The last characterization analysis conducted on the samples is colorimetric analysis, together with gloss evaluation. The SCI/SCE measurements were repeated five times for each sample, and the results were then average. Table below shows the CIE L*a*b* parameters for the SCI measurements and the gloss values determined for each sample.

Table 3.7: Summary table of results obtained from colorimetric analysis and gloss evaluation

Sample	L* (D65)	a* (D65)	b* (D65)	Gloss 8°	Pseudo-Color
A	71.21 ± 0.01	17.36 ± 0.01	18.99 ± 0.01	171 ± 1	
B	72.92 ± 0.01	18.90 ± 0.01	20.59 ± 0.01	316 ± 1	
C	80.15 ± 0.01	17.62 ± 0.01	19.23 ± 0.01	827 ± 3	
D	80.64 ± 0.01	17.06 ± 0.01	19.18 ± 0.01	820 ± 3	
E	81.89 ± 0.01	16.59 ± 0.01	19.23 ± 0.01	989 ± 4	
F	83.19 ± 0.01	16.10 ± 0.01	18.70 ± 0.01	1138 ± 5	
G	81.43 ± 0.01	16.66 ± 0.01	19.94 ± 0.01	1060 ± 4	
H	81.67 ± 0.01	16.31 ± 0.01	18.62 ± 0.01	1049 ± 4	
I	82.45 ± 0.01	16.26 ± 0.01	19.54 ± 0.01	1151 ± 5	
J	78.33 ± 0.01	18.65 ± 0.01	22.35 ± 0.01	940 ± 4	

K	77.48 ± 0.01	19.02 ± 0.01	24.06 ± 0.01	884 ± 4
CN	79.69 ± 0.01	16.64 ± 0.01	19.94 ± 0.01	580 ± 2

Looking at the results obtained, we can affirm that, also in this case, by varying the operating parameters in pulsed current, it is possible to vary the colorimetric coordinates of each sample and, consequently, the gloss values. In particular, the samples obtained using pulsed currents, except for sample B, have gloss values significantly higher than those obtained using direct current, both from a cyanide-free alkaline copper bath and from an alkaline copper bath containing cyanides.

3.1.4 Discussion and Conclusions

This study carried out an electrochemical investigation of a cyanide-free alkaline copper electrodeposition bath, with the aim of verifying the potential of using modulated currents in electrodeposition processes. Almost all galvanic processes, in fact, use direct currents, which are extremely widespread due to the technical and instrumental limitations of pulsed currents, which have historically prevented their widespread use.

Despite the environmental and toxicological risks, alkaline cyanide-containing copper plating baths are the main technology used in galvanic processes, thanks to their high efficiency and the quality of the coatings produced. However, national and international environmental regulations are increasingly requiring the replacement of these baths due to their high toxicity for operators and the critical management of the waste produced.

Once the preliminary study was completed, a series of copper coatings on brass substrates were prepared in order to study their chemical-physical characteristics. For easier visualization of the results, all the quality parameters investigated in the various characterizations can be reported in a table. For all the results obtained, the CN sample (highlighted in yellow) is taken as the reference sample. This sample was obtained through a direct current electrodeposition process

starting from a cyanide-alkaline copper plating bath, which currently represents the state of the art. For each characterization, when the results obtained showed an improvement compared to the reference sample, they were highlighted in green. On the other hand, the results highlighted in red are those that show a relative deterioration compared to the CN sample. If, on the other hand, the parameters can be considered comparable to those of the CN sample, they are highlighted in orange. The results obtained from the XRD analysis of the samples, which are difficult to compare with the CN sample, are highlighted in white.

Table 3.8: Summary table of all characterizations performed on the samples

Sample	Grain (µm)	TP %	Crystallite (nm)	Gloss 8°
CN	0.46 ± 0.15	80.1 ± 0.1	60.1 ± 1.2	580 ± 2
A	0.88 ± 0.30	71.8 ± 0.1	73.2 ± 1.2	171 ± 1
B	0.62 ± 0.14	62.3 ± 0.1	78.1 ± 1.0	316 ± 1
C	0.44 ± 0.11	50.8 ± 0.1	128.7 ± 1.8	827 ± 3
D	0.34 ± 0.07	39.4 ± 0.1	131.8 ± 1.3	820 ± 3
E	0.28 ± 0.07	38.8 ± 0.1	121.7 ± 1.1	989 ± 4
F	0.23 ± 0.04	11.9 ± 0.1	118.1 ± 1.9	1138 ± 5
G	0.32 ± 0.07	32.4 ± 0.1	116.7 ± 1.4	1060 ± 4
H	0.35 ± 0.10	47.4 ± 0.1	106.8 ± 1.2	1049 ± 4
I	0.27 ± 0.06	34.5 ± 0.1	131.5 ± 1.2	1151 ± 5
J	0.33 ± 0.06	37.9 ± 0.1	112.5 ± 1.2	940 ± 4
K	0.29 ± 0.07	39.0 ± 0.1	136.2 ± 1.3	884 ± 4

Looking at the results presented in Table 3.8, the samples produced using pulsed currents, except for sample B (P = 1, t_{on} = 60 ms), have characteristics that are comparable to, if not better than, the CN sample in terms of grain size and gloss. In particular, samples F (P = 3, t_{on} = 50 ms) and I (P = 4, t_{on} = 100 ms) show an

extremely fine grain size with higher gloss values than all the other samples analyzed. The results relating to the evaluation of throwing power, on the other hand, appear to have worsened. Among the pulsed current samples, those with higher TP values are samples C (P = 1, t_{on} = 100 ms), D (P = 2, t_{on} = 50 ms), and H (P = 4, t_{on} = 20 ms), which, however, fail to reach the throwing power value of the CN sample.

Regardless of the improvement or deterioration of the deposit characteristics, pulsed currents represent a promising strategy, allowing finer control of the characteristics of the electrodeposition process, enabling control of the morphology and particle size of the deposit, throwing power, and gloss. However, some critical issues remain unresolved, particularly those related to the optimization of TP.

In conclusion, in this preliminary study on modulated current electrodeposition, it was not possible to obtain copper deposits that simultaneously showed improvements in all the qualities investigated. However, some combinations of operating parameters were identified that offer a compromise between surface morphology, gloss, bath penetrating power, and environmental sustainability. In this context, the prospects appear interesting since, by modulating the experimental parameters, it is possible to vary the characteristics of the deposit, allowing for greater flexibility in the industrial process. After all, this thesis work has only superficially investigated the optimization of parameters and how they influence the coating produced. A more in-depth study of the relationship between cathodic pulse parameters and the chemical-physical characteristics of the deposit, perhaps linked to an optimization of the bath additives, could make the use of pulsed currents on a cyanide-free alkaline copper plating bath the new technological frontier of copper electrodeposition in the electroplating industry.

3.2 Acidic Copper

3.2.1 Introduction

Electroplating of copper is one of the most used plating processes for both functional and decorative applications [76], [77]. Pulsed (PC) and pulsed-reverse current (PRC) plating is widely used in electronics for printed circuit boards [30], but also for the deposition of alloys [35], composite materials [36] and semiconductors [37], [38]. On the contrary, only direct current (DC) is used in the decorative field [77].

While there is a considerable amount of empirical information in the literature on how pulse plating variables affect the structure of the deposit, only a few systematic investigations have been carried out and the effects of current modulation on the microstructure of electrodeposited surfaces are still not well understood [78]. As a result of all these considerations, we decided to launch a preliminary study on everything related to the parameterisation of each deposition technique.

In this work we focussed on the acid copper bath because it is a ubiquitous solution in many industrial processes and has a quite simple composition. This type of bath has a stable and straightforward formulation that lends itself well to systematic analysis for new deposition techniques. In addition, industries use acid copper plating as an intermediate step in most electroplating processes [26], [79]. Acid copper plating can improve subsequent electroplated layers adhesion and achieve a glossy finish [77]. Therefore, improvements in the copper deposition would have applications in many industrial processes. This study will be used as a first step for the application of pulsed current in the decorative field to more complex baths of precious metals and alloys. Once we chose the most promising parameters, samples were prepared and coated using both direct current and pulsed (PC) and reverse pulsed currents (PRC). The deposits obtained were

characterised by estimating the metal surface's deposition yield, homogeneity, hardness, and reflectivity.

3.2.2 Experimental

We used a commercial acid copper electroplating bath (BLUCLAD 250 MUP) to replicate the industrial conditions as closely as possible. The solution consists in a full operative bath: 217.2 g/L $CuSO_4 \cdot 5\ H_2O$ (0.87 M) as metal precursor, 66.1 g/L H_2SO_4 98 % (0.66 M) as electrolyte and all the necessary proprietary additives (brightening, levelling and complexing agent). This commercial acid copper plating bath has a working range between 3 and 5 A/dm^2, we chose to use it within the upper limit of its characteristics to highlight any differences. Therefore, regardless of the type of current used, the average current density remains constant at 5 A/dm^2, all tests were conducted without stirring.

The cell used has dimensions 10 x 5 x 9 cm^3 and was made of Moplen, an isotactic polypropylene thermoplastic material (PP-H), allowing us to drill a hole in one of its faces to create a housing for the cathode (cylinder of the chosen metal), so that the latter would face the surface to be coated inside the galvanic cell, but would still have one end outside that could be connected, via a clamp, to our electrical circuit. The anode was anchored to the face opposite the one presenting the hole for the cathode, so as to keep the distance between the two electrodes constant and reproducible throughout the experimental phases.

We used Pt electrode as a working electrode (diameter of 0.6 mm) when the electrochemical tests required an inert metal under the Cu deposit. Otherwise, we used Nickel electrodes with a diameter of 10 mm. Copper plate is always used as a counter electrode. A simple copper wire was chosen as a reference electrode because the solution used contains a very high and constant amount of copper ions. The value of this working electrode was compared with a commercial SCE

electrode, obtaining a potential of 52 mV. Each test was carried out under controlled temperature conditions of 25 ± 1 °C.

XRF measurements were performed with a Bowman B Series XRF spectrometer (Schaumburg, IL, USA) using an acquisition time of 60 s, 50 kV tube voltage, 0.8 mA tube current, and a collimator of 0.6 mm in diameter. We used the spectra to obtain the thickness information with the FP method with one empirical point correction [64], [65], [66], [67].

Hardness was investigated through the Vickers Microhardness Meter (Microhardness Tester HX-1000) using a load of 10 g, the diamond tip was kept on the sample for a time of 15 s. The diagonals of the imprinted footprints give the hardness value in Vickers Pyramid Number **(**HV) [80].

A DRS (Diffuse Reflectance Spectroscopy) spectrophotometer, Agilent Cary 300, was used to estimate the reflectance of each sample as a function of the wavelength of incident radiation. The high-resolution spectrophotometer used has an 8°/d geometry, with adaptive sample positioning and 7 mm diameter spots. Measurements were made between 380 nm and 780 nm with 5 nm steps.

Atomic force microscopy (AFM) measurements were performed in contact mode (0.5 V force set point) with a non-conductive Si_3N_4 triangular cantilever (Veeco, NP-S10, 0.12 N/m force constant) on a Molecular Imaging PicoSPM (10 μm × 10 μm, 512 px × 512 px, 1 lines/s speed) to evaluate the morphology and roughness of the samples.

Scanning electron microscopy (SEM-EDS) images were acquired using a Variable Pressure Hitachi SU3800 using an accelerating voltage of 5 kV.

3.2.3 Results

Pulsed current study

It is well known that good metal deposits are obtained in the frequency range from 10 to 500 Hz. It is also known that the range of valuable frequencies is

limited by the capacitive effect of the double electric state at high frequencies and by mass transfer effects at low-frequency values. At high frequencies, the faradic current decreases approaching a state similar to that achieved in DC [81]. Similarly, we reach conditions close to DC at very low frequencies.

The quantitative criterion that mainly affects the best frequency range is the average potential, which increases both with the distortion of the faradic current wave at high frequencies and in the case of mass transfer limitations [31], [82]. Hence the assumption that the minimum value of the average potential recorded indicates the frequency range for optimum deposition.

When working with pulsed current, we set the cathode current value, the cathode pulse time and the anode pulse duration, and the total electrodeposition period for each deposition. Equation 3.8 connects the three variables.

$$J_P = J_{AV}(P + 1) \tag{3.8}$$

Where J_P is the cathodic pulse current density; J_{AV} is the average current density; P is the pause/pulse ratio. We used the same average current density (5 A/dm^2) for both pulsed and direct current deposition; for the value of P, we took measurements for t_{off}/t_{on} ratios ranging from 1 to 5. The average current density value of the cathode pulse for each P are: P = 1, J_P = 10 (A/dm^2); P = 2, J_P = 15 (A/dm^2); P = 3, J_P = 20 (A/dm^2); P = 4, J_P = 25 (A/dm^2); P = 5, J_P = 30 (A/dm^2). For each value of P, we repeat the measurement with the following t_{on} times: 10^{-4}; 10^{-3}; 10^{-2}; 10^{-1}; 1; 10 s and the average potential value is recorded as reported in Figure 1.

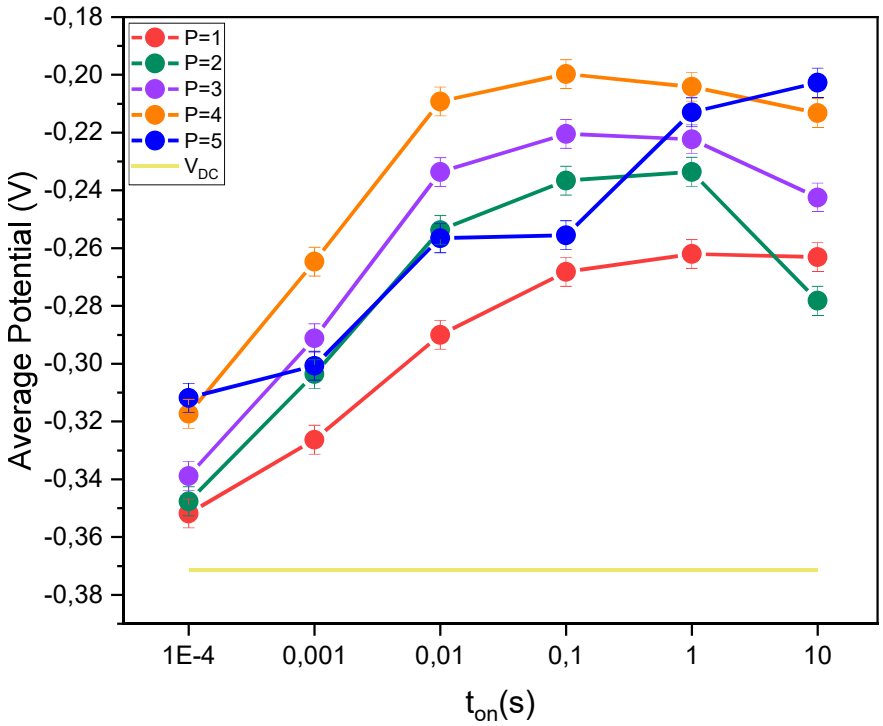

Figure 3.4: Average potential versus pulse time (t_{on}), measured for each value of P at different pulse times (t_{on}= 10^{-4}; 10^{-3}; 10^{-2}; 10^{-1}; 1; 10 s) and for DC deposition

Since the literature defines, in some cases, $J_{AV} < J_{DC}^{L}$ and $J_p < J_p^{L}$ as the necessary operational limit, in others $J_p < J_{DC}^{L}$ and $J_p < J_p^{L}$ (where J_{DC}^{L} is the limiting current density under steady-state conditions and J_p^{L} is pulse limit current density) [2], [83] we decide to calculate the values of J_{DC}^{L} and J_P^{L}. The limiting current density value, J_{DC}^{L}, was obtained experimentally through potentiostatic measurements by performing a procedure of deposition and stripping in sequence, and the experimentally derived value is $J_{DC}^{L} = 17.5\ \frac{A}{dm^2}$.

Pulse limit current was derived through the Equation 3.9:

$$J_P^L = J^L \left(\frac{\delta^P}{\delta} (1 - \theta) + \theta \right)^{-1} \tag{3.9}$$

Where δ^P is the pulsing diffusion layer, δ is Nernst diffusion layer and θ is the duty cycle (θ = 1/(P+1)). All parameters respect the condition $J_p < J_p^{L}$, but only

samples with a value of P = 1; 2 satisfy the operating limit $J_p < J_{DC}^{L}$. Based on these considerations, we decide to carry out two samples for each operational limit, for a total of four samples, whose parameters (pause/pulse ratio, cathode pulse, pause and cathode current value) are given below:

- P = 1; t_{on} = 0.01 s; t_{off} = 0.01 s; i_p = -0.0785
- P = 1; t_{on} = 0.1 s; t_{off} = 0.1 s; i_p = -0.0785
- P = 4; t_{on} = 0.01 s; t_{off} = 0.04 s; i_p = -0.1963
- P = 4; t_{on} = 0.1 s; t_{off} = 0.4 s; i_p = -0.1963

The first two are more similar to those used in the literature and meet the conditions of both articles on limiting currents; the second two, on the other hand, are the best candidates according to Popov's treatment [84], [85], [86], [87] and only meet the conditions of the first article on current limits.

Reverse pulsed current

As far as reverse pulsed current is concerned, we proceed along two distinct paths: relying on the literature and on what are considered to be the optimal parameters for deposits with the characteristics we seek, but also starting from the criteria considered to be fundamental for reverse pulsed current electrodepositions and refining the setting based on the preliminary results we have obtained.

For the electrodeposition of copper, by sulphate and sulphuric acid solutions, without stirring, at room temperature, Vene and Nikolayeva [88] claim that, irrespective of the overall current density and the period of the PRC wave, the best results were obtained with:

$t_a/t_c = 1/7;\ 3\ t_0 < T < 16\ t_0;\ J_a/J_c = 1$

In solutions containing additives [76], the optimum criteria for high penetration power are as follows:

$t_c/t_a = 20$; $1 \leq J_a/J_c \leq 3.5$ (with the best value $J_a/J_c = 2$); $q_a/q_c < 0.2$

Using the data considered ideal in the literature, we derive the parameters through theoretical considerations and practical results. Knowing the values of δ and D, we estimate t_0 through the Equation 3.10:

$$t_0 = \frac{\delta^2}{\pi^2 D} = \frac{(5.8 \cdot 10^{-3} cm)^2}{\pi^2 \cdot 6.17 \cdot 10^{-6} \frac{cm^2}{s}} = 0.55\ s \tag{3.10}$$

The best depositions should occur for $3\ t_0 \leq T \leq 16\ t_0$. Furthermore the Equation 3.11 correlate the $\frac{t_a}{t_c}$ ratio with t_0 and T.

$$\frac{t_a}{t_c} = \left(\frac{4t_0}{T}\ln\left(\frac{2}{1+exp\left(-\frac{T}{4t_0}\right)}\right)\right)\left(1-\frac{4t_0}{T}\ln\left(\frac{2}{1+exp\left(-\frac{T}{4t_0}\right)}\right)\right)^{-1} \tag{3.11}$$

Combining the two expressions we obtain that $1.4 \leq \frac{t_c}{t_a} \leq 4.9$

We set an intermediate value to this range as a parameter for our electrochemical tests, namely:

$t_c/t_a = 3$; $J_a/J_c = 1$

The anodic and cathodic current values are calculated using the same average current density as for the DC and PC tests, i.e. $J_{AV} = 5$ A/dm^2.

Knowing the ratios between t_c/t_a and J_a/J_c, the individual currents can be calculated using the Equation 3.12:

$$J_{AV} = \frac{q_c - q_a}{t_c + t_a} = \frac{J_c t_c - J_a t_a}{t_c + t_a} \tag{3.12}$$

We therefore have three different sets of variables concerning reverse pulsed current electrodeposition, which are reported below:

$t_a/t_c = 3$; $J_a/J_c = 1$; $i_c = -0.0771$ A; $i_a = 0.0771$ A; $q_a/q_c = 0.33$

$t_a/t_c = 7$; $J_a/J_c = 1$; $i_c = -0.0524$A; $i_a = 0.0524$ A; $q_a/q_c = 0.14$

$t_a/t_c = 20$; $J_a/J_c = 2$; $i_c = -0.0458$ A; $i_a = 0.0916$ A; $q_a/q_c = 0.10$

Based on the previously established deposition parameters, we evaluate the best cathodic and anodic pulse time to obtain homogeneous and brilliant deposits. Even if the working conditions are different, we decide to proceed as we did for the pulse current. The potentiometric operating sequence is the same as that used for the pulsed current tests, with the only difference that for these samples, for each t_c/t_a ratio of we have worked in sequence over the whole range of pulses. For each deposition, we extrapolated the average potential value, as reported in Figure 3.5.

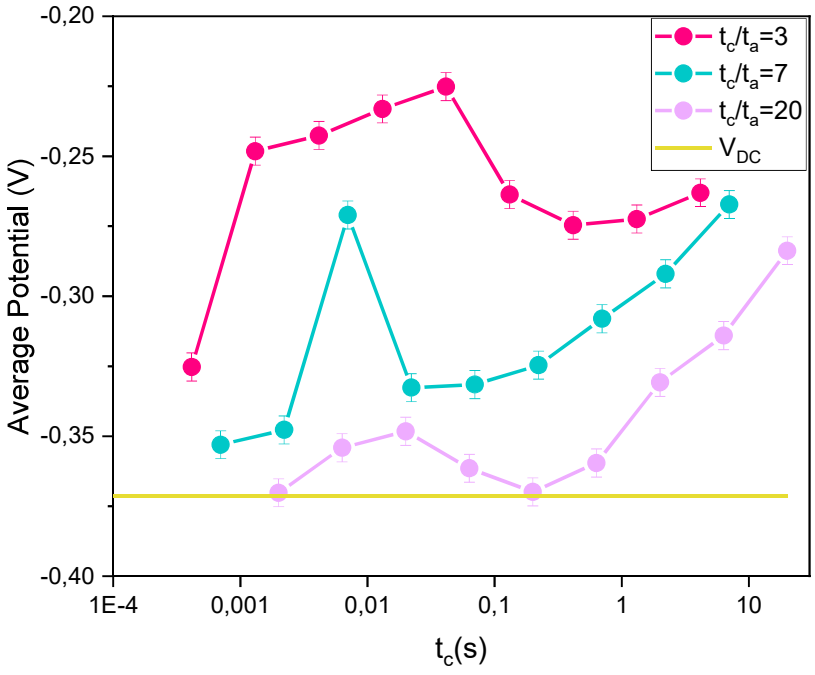

Figure 3.5: Average potential versus pulse time (t_{on}), estimated for each t_c/t_a ratio (t_c/t_a = 3; 7; 20) at different cathode pulse times

Based on the experimental values, we declare the following variables to be the best:

- $t_c/t_a = 3$; $J_a/J_c = 1$; $t_c = 0.013123$ s; $t_a = 0.004269$ s

- $t_c/t_a = 3$; $J_a/J_c = 1$; $t_c = 4.15$ s; $t_a = 1.35$ s
- $t_c/t_a = 7$; $J_a/J_c = 1$; $t_c = 0.007$ s; $t_a = 0.001$ s

All prepared samples and their operating parameters are shown in Table 3.9.

Table 3.9: Totality of samples prepared and their operating parameters (tipe of deposition current, cathode pulse duration, anode pulse duration, cathode and anode current values)

Name	Current	t_c (s)	t_a (s)	i_c (A)	i_a (A)	F (Hz)
A	**DC**	600	-	-0.0392	-	-
B	**PC**	0.1	0.4	-0.1963	0	2
C	**PC**	0.01	0.04	-0.1963	0	20
D	**PC**	0.01	0.01	-0.0785	0	50
E	**PC**	0.1	0.1	-0.0785	0	5
F	**PRC**	7	1	-0.0524	0.0524	0.125
G	**PRC**	0.02	0.001	-0.0458	0.0916	48
H	**PRC**	4.15	1.35	-0.0771	0.0771	0.182
I	**PRC**	0.013123	0.004269	-0.0771	0.0771	57.498
L	**PRC**	0.007	0.001	-0.0524	0.0524	125

Hardness

Hardness was investigated through the Vickers Microhardness Meter using a load of 10 g, the diamond tip was kept on the sample for a time of 15 s. The measurement was repeated on ten different random spots for each sample. For sample H, it was not possible to use the above parameters because the tip made no impression on the surface of the sample. Possible explanation derives from the surface morphology of the deposit, which is highly irregular, with clusters of deposition cores extending at least a few μm in height, hindering the penetration of the pyramidal diamond placed on the tip of the microdurometer. We report the average hardness and its standard deviation in Figure 3.6.

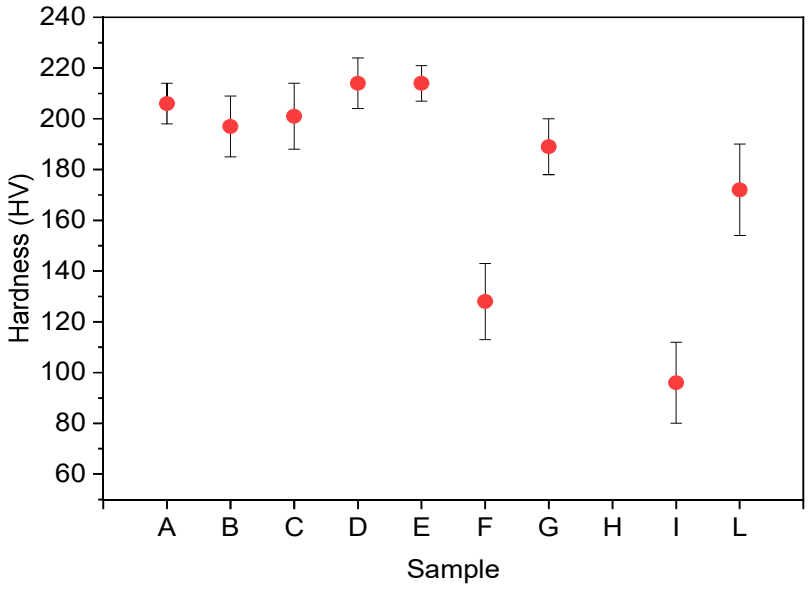

Figure 3.6: Hardness graph for each sample with relative standard deviations (excluding sample h for which measurement was not possible)

The variation in the hardness of the film may be justified considering that modulated currents can change the compactness of the metal during electrodeposition processes; a further explanation may be that pulsed currents are able to influence the crystal structure of Cu in the nucleation and lattice growth phases [89], [90], [91].

Brightness

A colour characterisation is carried out: for each sample was estimated the reflectance value using a UV-Vis spectrophotometer. We decide to evaluate as a parameter the relative reflectance of each sample, compared to sample A obtained in DC, since the latter is the technique considered as the state of the art in electroplating. The reflectance values obtained using the UV-Vis spectrophotometer are first normalised against the reflectance of black and white using the Equation 3.13:

$$R_C^N = \frac{R_C - R_N}{R_B - R_N} \tag{3.13}$$

And then compared to sample A with the equation 3.14:

$$R\% = \frac{R_C^N - R_A^N}{R_A^N} \cdot 100 \tag{3.14}$$

The results obtained are reported in Figure 3.7.

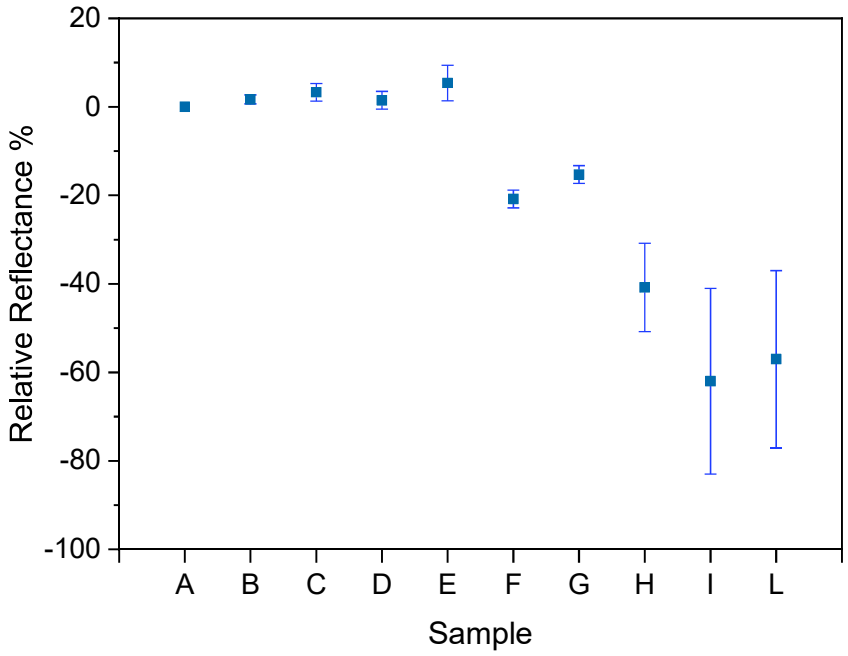

Figure 3.7: Relative reflectance of each sample to A estimated by UV-Vis spectrophotometry

Since reflectance values are closely related to the surface morphology of the samples, we performed SEM measurements to observe the metal films at microscopic scale, the images of which are shown in Figure 3.8.

Sample A

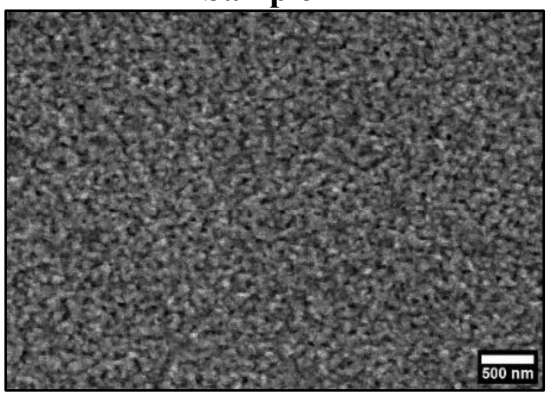

Sample B

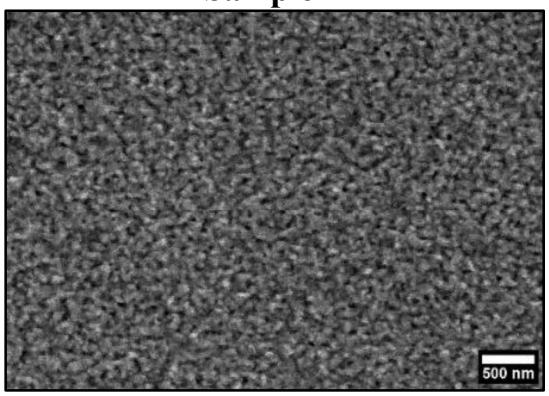

Sample C

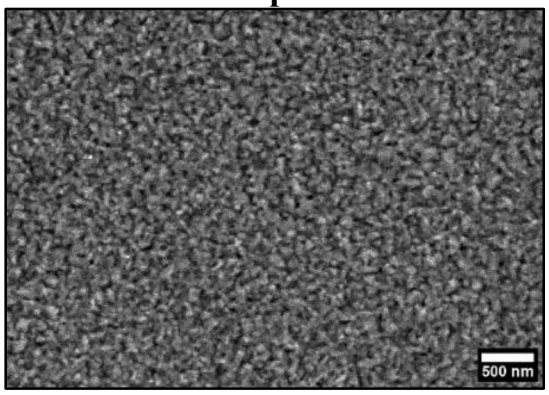

Sample D

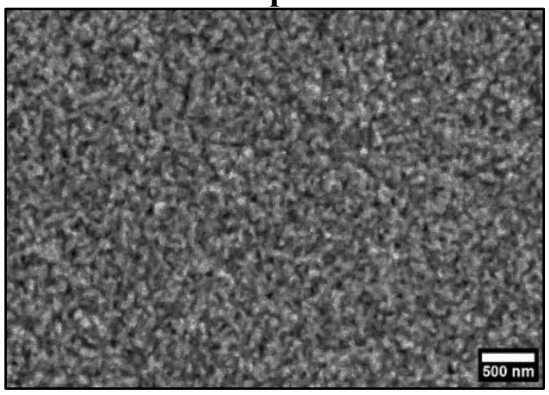

Sample E

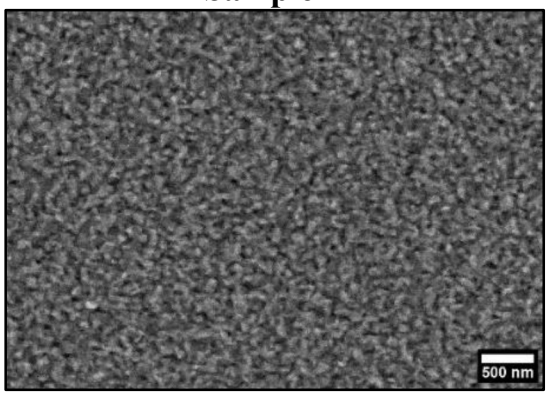

Sample F

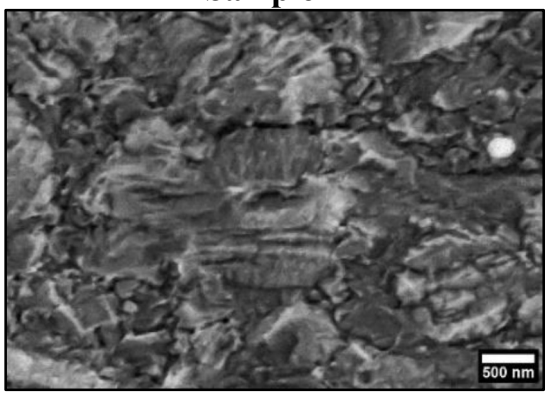

Sample G

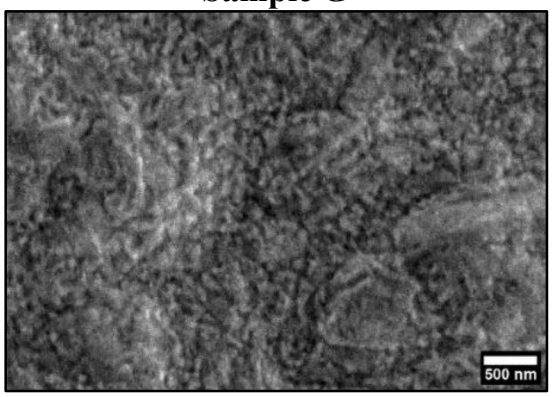

Sample H

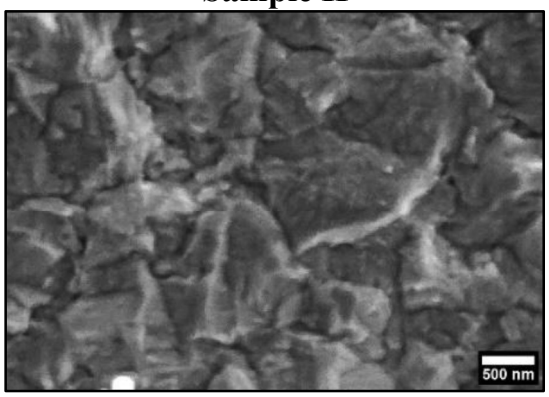

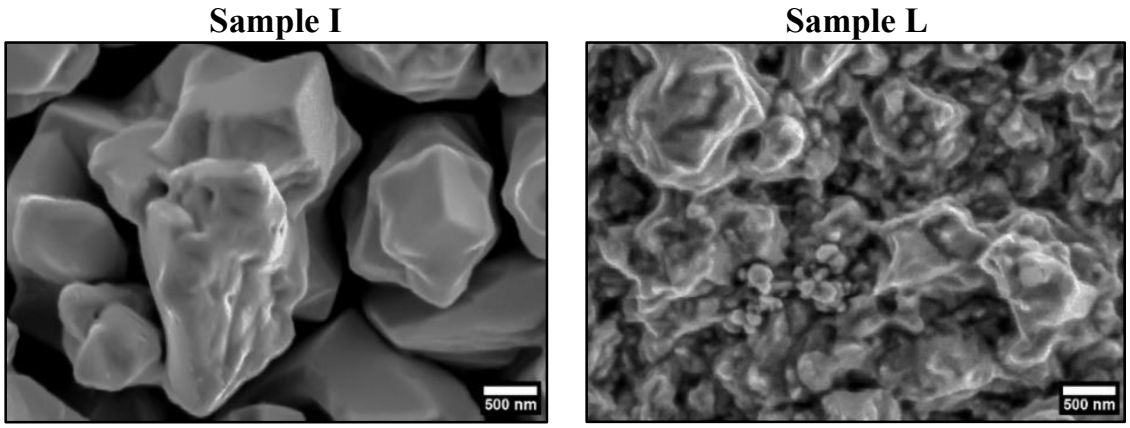

Figure 3.8: SEM images of the electrodeposited Cu surface of each sample

From the results it is evident that samples from A to E (DC and pulse current samples) present very small crystals, leading to an extremely smooth and compact surface. To emphasise the morphology of these samples the contrast of the images was maximised, inevitably losing quality.

To appreciate the surface of the samples in even greater detail, AFM analysis was performed on the sample that showed a higher reflectance value (sample E) compared to the sample produced using direct current (sample A): the sample produced using pulsed current (E) showed lower roughness value (Sq = 7.4 ± 0.2 nm) than the reference sample A (Sq = 13.7 ± 0.4 nm).

Bath efficiency

The efficiency of the electroplating bath is estimated by gravimetric analysis and the actual thickness of the metal film was obtained from the empirical mass; the results obtained are reported in Table 3.10.

Table 3.10: Percentage efficiency of each electroplating bath estimated by gravimetric analysis

Sample	Bath efficiency (%)
A	95.4 ± 0.3

B	97.9 ± 0.3
C	99.0 ± 0.3
D	99.3 ± 0.3
E	98.2 ± 0.3
F	95.3 ± 0.3
G	98.5 ± 0.3
H	92.3 ± 0.3
I	98.9 ± 0.3
L	86.8 ± 0.3

Inhomogeneity

Through X-ray fluorescence spectroscopy, we probe the thickness of the sample. We created a mapping grid to estimate the thickness of the deposit by measuring 21 points arranged in a radial geometry with respect to the centre of the sample, of which a graphic representation of the thicknesses by colour scale is shown in Figure 3.9.

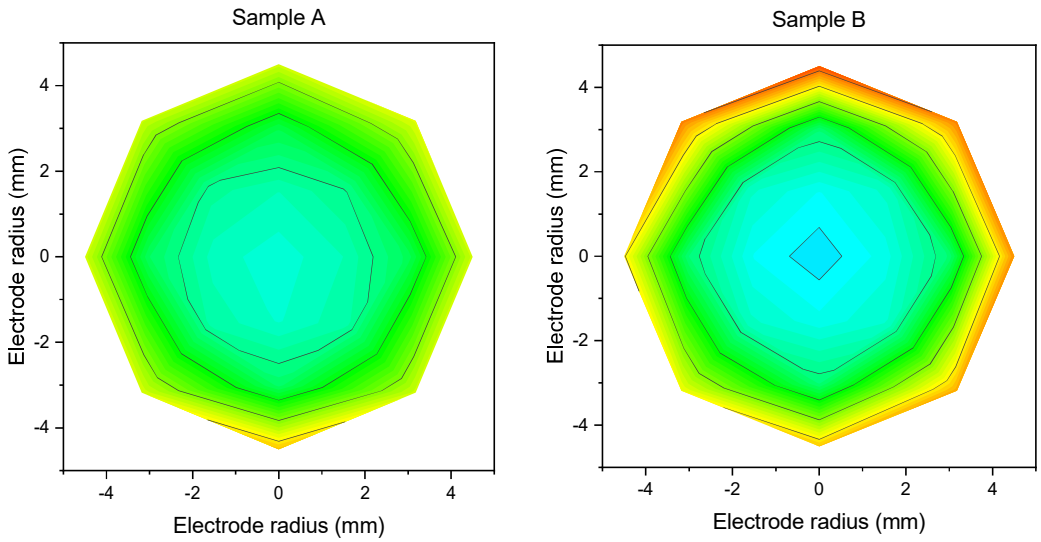

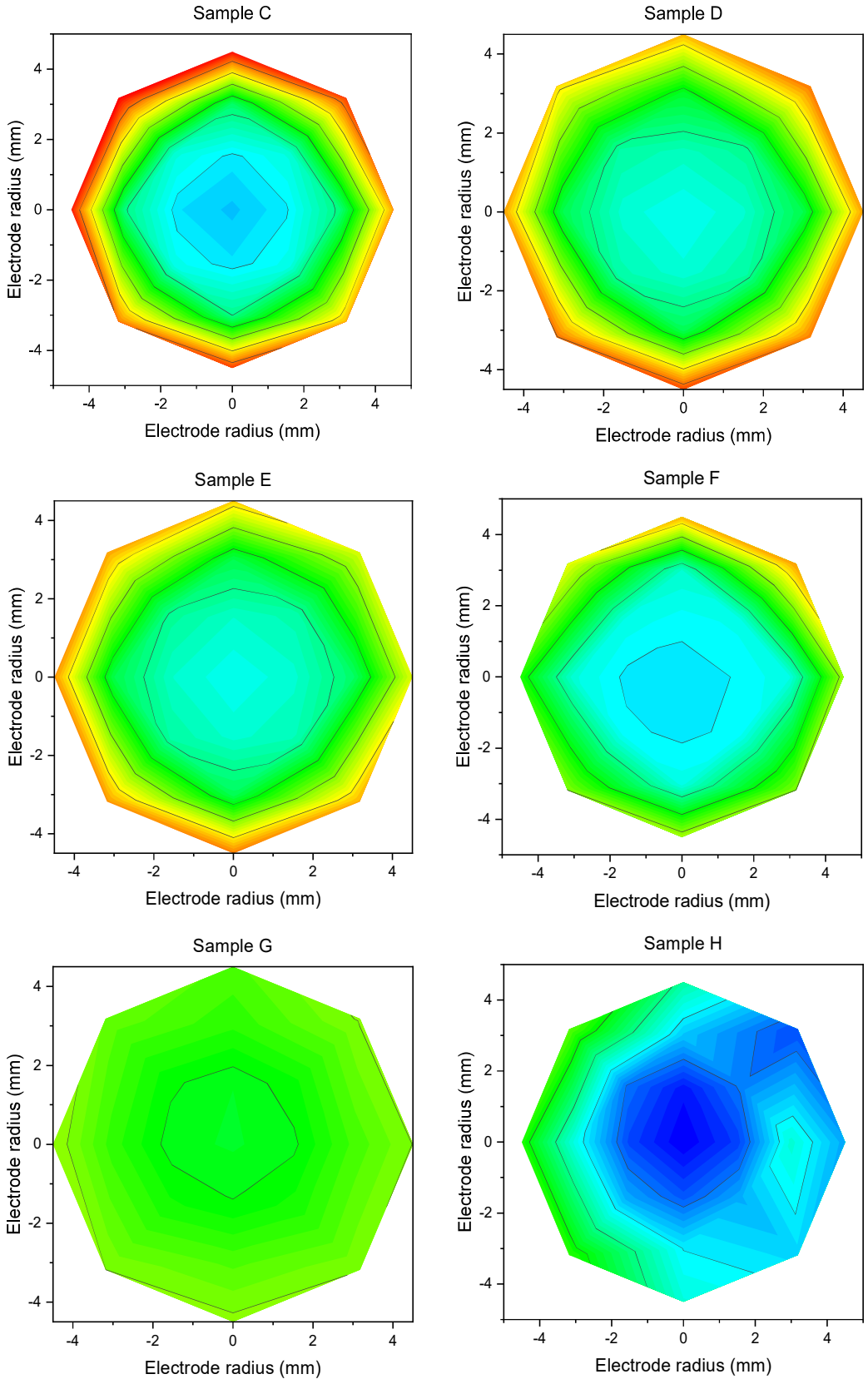
Sample C
Sample D
Sample E
Sample F
Sample G
Sample H
Electrode radius (mm)
Electrode radius (mm)
4
2
0
-2
-4

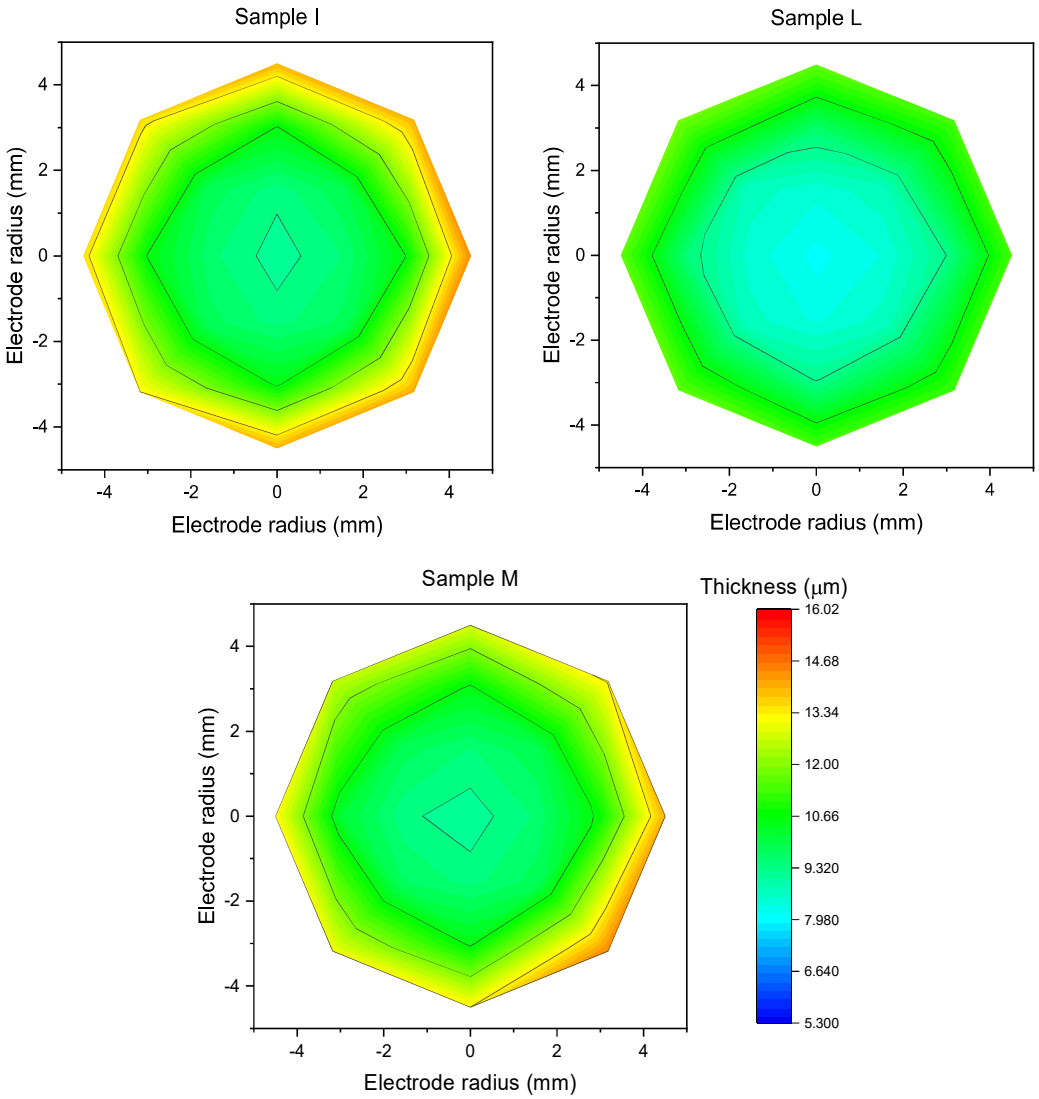

Figure 3.9: Graphic representation of the thicknesses by colour scale of each sample

The average thickness of the Cu deposit, measured at the centre of the samples, is 8.11 ± 0.41 µm; the sample that showing the lowest thickness is H with a deposit height of 5.30 ± 0.27 µm, while G is the sample with the highest thickness (10.40 ± 0.52 µm).

The measured metal film heights for each sample are fitted using an exponential function having the Equation 3.15:

$$y = a + b\left(e^{x/c} + e^{-x/c}\right) \tag{3.15}$$

In this case, we do not consider the standard deviation (reported in Equation 3.16) as the statistical error on thickness but as an estimator of deposition uniformity. A higher value of standard deviation corresponds to a less uniform deposit; the results are reported in Table 3.11.

$$\sigma = \sqrt{\frac{\int_0^r 2\pi r\left(f(r) - \bar{h}\right)^2 dr}{A}} \tag{3.16}$$

Table 3.11: Standard deviation, considered as an estimator of deposit uniformity, relative to each sample

Sample	Non-uniformity (µm)
A	1.84
B	2.69
C	3.30
D	2.59
E	2.37
F	2.58
G	0.53
H	1.14
I	1.31
L	1.71

3.2.4 Discussion and Conclusions

We can summarise the results obtained, through the various characterisations, concerning the quality and performance parameters investigated, for each sample, in Table 3.12.

Table 3.12: Summary of characterisations and results obtained (in yellow the reference values obtained for the DC sample; in red the results showing a worsening compared to those obtained in DC and in green the improved ones)

Sample	Bath efficiency %	Relative reflectance %	Hardness (HV)	Non-uniformity σ (µm)
A	95.4 ± 0.3	0	206 ± 8	1.84
B	97.9 ± 0.3	2 ± 1	197 ± 12	2.69
C	99.0 ± 0.3	3 ± 2	201 ± 13	3.30
D	99.3 ± 0.3	2 ± 2	214 ± 10	2.59
E	98.2 ± 0.3	5 ± 4	214 ± 7	2.37
F	95.7 ± 0.3	-21 ± 2	128 ± 15	2.58
G	98.5 ± 0.3	-15 ± 2	189 ± 11	0.53
H	92.3 ± 0.3	-41 ± 10	--	1.14
I	98.9 ± 0.3	-62 ± 21	96 ± 16	1.31
L	86.8 ± 0.3	-57± 20	172 ± 18	1.71

For all the results obtained, relative to each parameter investigated, the reference value is that estimated for sample A, the result of a direct current electrochemical process, which is, to date, the most widely developed and used technique in the industrial field for the most varied electroplating processes. Therefore, the parameters to be equalled and, if necessary, exceeded in performance are highlighted in yellow. The better values compared to those achieved with the DC sample are highlighted in green; in red are those for which there is a worsening; in white are the parameters that can be considered comparable (considering the error) to those of A, for which there is no significant difference in quality compared to DC.

It is evident that all the samples produced using pulsed current show comparable characteristics, if not superior, to those of the A deposit, in almost all the characterisations carried out, except for homogeneity, which appears to have deteriorated. The parameterisation that proves to be most effective in producing

a fine-grained, homogeneous and compact deposit using pulsed current is the one for which the ratio between the pause time and the pulse time is equal to 1, with pulse duration ranging from 0.01 (sample D) to 0.1 s (sample E); under these conditions, the efficiency of the bath also proves to be optimal. Both samples with P = 1 were also those that met the most stringent conditions regarding the pulse current density, i.e. $J_p < \mathrm{J}_{DC}^{\mathrm{L}}$ and $J_p < \mathrm{J}_p^{\mathrm{L}}$.

The only negative deviation, although not high, is with the average thickness, which is not uniformly distributed but affected by the edge effect; for sample E, however, this aspect is minimal compared to the others.

Concerning the deposits obtained in reverse pulsed current, no particular improvement in the quality of the metal film obtained can be seen, other than that of a highly homogeneous surface, thanks to the intrinsic characteristics of the deposit in bipolar current, which has a levelling effect thanks to the anodic pulses. This is true for all the samples, except for one, sample F, which has $\mathrm{t_c}/\mathrm{t_a}$ = 7 and $\mathrm{t_c}$ = 7 s; probably the pulse times (especially the cathodic one) are too long, so much so that they tend to a stationary condition as if at an electrochemical level two direct currents were alternately used and no longer a reverse pulsed current. We can make a similar consideration for the other sample (H) obtained with pulses in the second's range, i.e. $\mathrm{t_c}/\mathrm{t_a}$ = 3 and $\mathrm{t_c}$ = 4.15 s, which is worse than A in all characterisations except for the homogeneity of the deposit. The other sample (L) with a ratio of cathodic to anodic pulse times equal to 7 also shows unsatisfactory results, leading us to believe that precisely the parameterisation of the reverse current is not optimal, at least for this acid coppering bath. The best setting, among the various parameterisations of the bipolar pulses, appears to be the one used for sample G, i.e. $\mathrm{t_c}/\mathrm{t_a}$ = 20 and $\mathrm{t_c}$ = 0.02 s. Although the results are not comparable to those obtained with direct current or even pulsed current, it may be preferred in technical applications for which the homogeneity of the deposit is more important than its aesthetic appearance.

In conclusions, in this preliminary study on modulated current electrodeposition, we did not succeed in obtaining a copper deposit that presents improvements on all the qualities investigated.

Samples produced with pulsed current show improved characteristics compared to those obtained with direct current. This is especially true for the finishing of the piece, as the deposits are more compact and finer-grained. In almost all samples the metal films are shinier and more mirror-like.

The samples obtained using pulsed reverse currents, on the other hand, show a particular uniformity of deposit. Although the finish of the metal films is not brilliant, the thickness of the deposits is extremely homogeneous over the entire surface.

In conclusion, the optimal parameters were identified to obtain a compromise between the specific characteristics according to those desired for the industrial processing that the plated object will undergo. Based on the results obtained, pulsed currents will be preferred in electroplating applications where an optimum finish of the plated item is required. The process can be applied in fashion, furniture and all those sectors involving multilayer depositions, where the acid copper coating is used to obtain a good levelling, smooth and shiny surface. Reverse pulsed currents are recommended for applications where aesthetics is negligible but is required a good homogeneity of metal thickness. Thanks to the negative current transient, the deposit undergoes a process of self-levelling caused by the preferential redissolution of the metal film in the parts with higher surface energy; this feature could be useful in all those electroplating contexts where printed circuit boards are produced.

4 Palladium

4.1 Introduction

Palladium electrodeposition has been used for many years in the electroplating industry because of the technical and aesthetic properties this metal offers. Its use for decorative applications has become widespread since the 1980s as a step in the nickel-free processes and it is now exploited both as a final coating and as an intermediate layer to improve corrosion resistance and as a diffusion barrier layer [92], [93], [94]. However, palladium electrodeposition has been limited by some disadvantages, especially in the decorative field, such as dull appearance, high porosity and low ductility. For these reasons, it is generally deposited alloyed with other metals which minimize these drawbacks [95], [96], [97]. The electrodeposition of PdNi alloy (~80-20% w/w), for example, has made it possible to reduce the use of gold in the electronics industry and, because of the silvery white appearance, avoid the use of rhodium for decorative applications [95]. Given the allergology of nickel, the use of PdFe deposits (with Fe > 5% w/w) has also become widespread, especially for wearables [77]. Alloying of palladium with other metals has also been used to reduce hydrogen embrittlement due to the evolution of large quantities of hydrogen during the metal reduction and its consequent co-deposition [96], [98]. Indeed, palladium is able not only to absorb hydrogen in atomic form but also to dissolve it to give two bulk hydride phases known as α-PdH_x ($x \sim 0.02$) and β-PdH_x ($x \sim 0.67$) which have long been studied [99], [100], [101], [102], [103], [104], [105]. The preferential deposition of either phase depends on the conditions of temperature, pH, and agitation, as well as the specific composition of the electroplating bath used. Microfractures result from hydrogen desorption associated with the lattice contraction that occurs in the transition from the β-PdH_x to the thermodynamically more stable

α-PdH_x phase at standard ambient temperature and pressure (STP) [106], [107]. Indeed, the volume of the β phase is 11% larger than the α phase [108]. In the α phase, the face-centered cubic lattice of Pd does not undergo substantial changes and any further hydrogen desorption does not cause fractures. These fractures facilitate the entry of atmospheric agents which lead to corrosion of the substrate; furthermore, if palladium is not the finishing layer, the desorption of hydrogen forms pockets which lead to the detachment of the upper layers.

Based on our experience, palladium deposits appear to exhibit different brightness depending on the co-deposited hydrogen content. This problem mainly concerns decorative applications, but although the variations are, in some cases, visible to the naked eye, the authors are not aware of any systematic studies conducted previously.

Finally, the complete transition from the β phase to the α phase can take up to a few days, making it difficult to predict the behavior of the deposit in the finished product [107].

Despite the disadvantages for the electroplating industry of obtaining a palladium deposit with high hydrogen content, the β-PdH_x phase is of great interest for several applications [109], [110], [111], [112], [113], especially by exploiting it as an hydrogen solid storage matrix [114], [115], [116], that would mitigate the safety problems associated to compressed gas storage [117]. Moreover, the electrochemical method can represent an economical and straightforward alternative to the physical application of high hydrogen pressures [99]. However, the difficulty of incorporating considerable amounts of hydrogen and understanding the relationship between the applied current and the hydrogen concentration obtained makes this route still unattractive.

In this work, we mainly focused on the two parameters that we verified have a great influence in incorporating and retaining hydrogen during and after the electrodeposition of Pd: the deposition parameters (e.g. current density and

waveform) and thickness. The investigated current densities ranged from 0.25 to 4.00 A/dm^2, while the deposit thickness ranged from 0.25 to 1.00 μm. These parameters were chosen based on the decorative electroplating industry common practice. The samples were analyzed by X-ray diffractometry (XRD) that allows the two phases to be easily identified thanks to the diagnostic peaks associated with α-PdH_x and β-PdH_x at, 40.10° and 38.34° of 2θ, respectively [114]. Within the study of palladium hydrides by XRD analysis, other authors have employed electroplating as synthesis route to deposit the metal [118] or to incorporate hydrogen [114]. Abbondanza *et al*. studied the structural evolution of Pd nanowires made electrochemically *in situ* by grazing-incidence transmission small- and wide-angle x-ray scattering (GTSAXS and GTWAXS) [117], while Felici *et al.* performed in situ energy dispersive X-ray diffraction (ED-XRD) to evaluate the deuterium incorporation in Pd during an electrolysis [119]. To assess the desorption trend over time (in STP conditions) XRD analyses were carried out after 10, 90, 180 minutes, and, in some cases, 24 hours from the end of the deposition. We also evaluate the color variation by analyzing the samples just after the deposition and after 24 hours.

Furthermore, we performed 0.5 μm-thick depositions using pulsed currents (PC) and reverse pulsed currents (PRC) to observe any differences in behavior compared to the samples made in direct current (DC). Indeed, the introduction of non-continuous currents is expected to result in an alteration of the cathodic efficiency with a consequent influence in the hydrogen content incorporated in the deposit. Moreover, PC is known to be able to tune and produce significant changes in the morphology of the deposits [120] with possible consequences on the kinetics of hydrogen desorption. Thus, the morphology of deposits was investigated with both scanning electron microscopy (SEM) and atomic force microscopy (AFM).

All the analyzed samples were electrodeposited using a commercial palladium-iron (PdFe), which thanks to its low Fe content (< 1% w/w) retains the Pd crystallographic phase, forming a substitutional alloy. For these reasons, it is considered pure Pd by an industrial point-of-view, to be distinguished by standard PdFe alloys with high Fe content [121]. All of this was done with the aim of identifying the conditions necessary to avoid microfracturing of deposits and, more generally, to preferentially obtain one or the other phase, onto substrates commonly used in the electroplating industry.

4.2 Experimental

The palladium electroplating bath PALMETECO was prepared with the formulation provided by Valmet Plating s.r.l (Calenzano, Italy) using 3 g/L $Pd(NH_3)_2(NO_2)_2$. The formulation contains a variety of proprietary additives: 50 mg/L PalmetF (source of iron); 200 mg/L Palmet BR3; 5.5 g/L EcoX; 250 mg/L BR1; 120 mg/L BR2. The solution was adjusted to a pH of 7.15 ± 0.15 with H_2SO_4 96% w/w or NH_3 30% w/w (Carlo Erba, Milano, Italy). The initial electrochemical characterization was performed with a three electrodes set-up by using a commercial Ag/AgCl (3M KCl) reference electrode (RE), a gold rod counter electrode (CE) and a gold rotating disc electrode (RDE) with a diameter of 3 mm working electrode (WE). The RDE cleaning procedure consists of: (i) mechanical polishing on P4000 SiC abrasive paper; (ii) mechanical polishing on 0.5 μm diamond paste; (iii) electrochemical activation by performing 10 cyclic voltammetries (CVs) sweeping from 1.4 V to -0.3 V in H_2SO_4 0.5 M with a scan rate of 0.05 V/s. The Electrochemical Impedance Spectroscopy (EIS) measurements were performed in a galvanostatic mode at current densities of 1, 2 and 4 A/dm^2 and a mean amplitude of 0.25 mA_{RMS}. The spectra were acquired in the frequencies range: $10^5 – 10^{-2}$ Hz after 30 s of deposition. CV measurement of the electroplating bath was conducted between 0.75 V and -1.0 V, with scan

rate 0.05 V/s. All the experiments were performed at a 50 °C in a double wallet cell by using a μAutolab3 (Metrohm) equipped with FRA2 module and processed with NOVA 2.1 software.

The thickness of the deposits was measured by X-ray Fluorescence (XRF) analysis with the FP (Fundamental Parameters) method [64], [65], [66], [67]. The analyses were performed with a Browman BA-100 XRF spectrometer (Schaumburg, IL, USA), 50 kV tube voltage, 0.8 mA tube current, with an acquisition time of 30 s, and a collimator of 0.6 mm in diameter.

To identify the two different palladium hydrides, the samples were analyzed by XRD with a Bruker New D8 Da Vinci diffractometer (Cu-Kα radiation = 1.54056 Å, 40 kV x 40 mA), equipped with an Euler cradle for massive samples and a Bruker LYNXEYE-XE detector. Scans were performed in a range of 2θ = 35° - 45° with a 2θ increment of 0.03° and 0.8 second of integration step. For preliminary analysis the acquisition range was extended to 90°. The ICDD (International Centre for Diffraction Data) PDF-5+2024 database [122] was used for the attribution of the reflections. The XRD data were processed using Fityk [123] software (pseudoVoigt function, imposing the same shape for all the peaks) and DIFFRAC.TOPAS software to confirm the results.

The samples were also characterized by colorimetric measurements performed with a Konica Minolta (Tokyo, Japan) CM-700d portable spectrophotometer, 10° observer, D65 standard illuminant. The measurements were performed using both the specular component included (SCI) and excluded (SCE) mode, averaging the value of three measurements acquired in the center of the sample. Analyses were conducted both just after and 24 hours past the end of deposition to assess any color changes that can be attributed to hydrogen desorption. The determination of the spectral gloss is obtained by subtracting the entire visible spectrum: from 400 to 800 nm (every 10 nm) acquired in SCI mode from that acquired in SCE mode and normalizing the results. The 8° gloss value is obtained

by averaging the normalized spectral gloss values compared to those of a standard white.

Scanning electron microscopy (SEM) images were obtained with Hitachi SU3800 (Hitachi High-Tech, Tokyo, Japan) using an acceleration voltage of 15 kV. Then, secondary electron images were analyzed through ImageJ [124] to achieve the grain dimension thanks to the linear intercept method [125].

Atomic force microscopy (AFM) measurements were performed in contact mode (0.5 V force set point) with a non – conductive Si_3N_4 triangular cantilever (Veeco, NP-S10, 0.12 N/m force constant) on a Molecular Imaging PicoSPM (10 μm × 10 μm, 512 px × 512 px, 0.5 lines/s speed) to evaluate the morphology and the roughness of the deposits.

4.3 Results

Preliminary electrochemical measurements were conducted to characterize the solution and to select the right parameters for pulsed current electrodepositions. A Cyclic Voltammetry of the galvanic bath was performed between -1 V and 0.75 V (with respect to Ag/AgCl), recording a reduction and an oxidation peak of Pd(II) at -0.9 V and +0.6 V respectively.

The electrodepositions were made onto 5x7 cm^2 brass plates by Ossian Lagerqvist AB (Jarfalla, Sweden) in a glass cell with the parallel sides to hold the substrate in a fixed and reproducible position, at the temperature of 50 ± 1 °C, pH: 7.15 ± 0.15 and under stirring condition (300 rpm). The samples were placed in the cell after switching on the rectifier and immersing them for a total area of 21.5 cm^2. Moreover, the back of the plates was covered with an insulating tape to make the applied current density effective. A two-electrode configuration was used for the deposition with mixed oxide anode. For DC samples five different current densities (0.25; 0.50; 1.0; 2.0; 4.0 A/dm^2) and three different thicknesses (0.25, 0.50, 1.0 μm) were tested for a total of 15 samples (A-Q, Table 4.1).

Table 4.1: DC samples

Sample	J (A/dm^2)	Theoretical thickness (μm)
A	0.25	0.25
B	0.25	0.50
C	0.25	1.00
D	0.50	0.25
E	0.50	0.50
F	0.50	1.00
G	1.00	0.25
H	1.00	0.50
I	1.00	1.00
L	2.00	0.25
M	2.00	0.50
N	2.00	1.00
O	4.00	0.25
P	4.00	0.50
Q	4.00	1.00

To perform pulsed current electrodepositions, the lower and upper operating limits for each chosen peak current density (J_p) were calculated [126], [127] based on previously developed methods (Equations 2.8, 2.9, 2.10 and 2.11).

Table 4.2: Lower and upper operated limits for each current density value

J_p (A/dm^2)	η (V)	t_C (ms)	t_{on}^{min} (ms)	t_{off}^{min} (ms)	t_{on}^{max} (s)
1	0.94	4.7	23.4	32.8	5.3
2	0.97	1.4	7.1	9.9	2.6
4	1.01	0.8	4.0	5.6	1.5

PC and PRC samples were made testing, respectively, three and two different waveforms and maintaining the constant thickness of 0.5 μm (R-V, Table 4.3 and Table 4.4). An Aim-TTi (Huntingdon, United Kingdom) EX752M and an RCV s.r.l. (Altavilla Vicentina, Italy) R.S.A.T.I.O. power supply was used for the direct and the pulsed current depositions, respectively. Before each electrodeposition, the surface of the substrates was degreased in a commercial alkaline degreasing solution (Atmet 200 by Valmet Plating s.r.l.), rinsed in deionized water, rinsed in 5% sulfuric acid, and rinsed again with deionized water.

Table 4.3: PC samples

Sample	**t_{on} (ms)**	**t_{off} (ms)**	**J_p (A/dm^2)**	**J_{AV} (A/dm^2)**	**Theoretical thickness (μm)**
R	100	100	1	0.5	0.50
S	100	100	2	1	0.50
T	100	100	4	2	0.50

Table 4.4: PRC samples

Sample	**t_c (ms)**	**t_a (ms)**	**J_c (A/dm^2)**	**J_a (A/dm^2)**	**J_{AV} (A/dm^2)**	**Theoretical thickness (μm)**
U	100	10	2	4	1.45	0.50
V	100	30	2	2	1.08	0.50

The actual thickness of the palladium deposits was measured with XRF and it was verified that it was coherent with the desired one (Table 4.5).

Table 4.5: Comparison between expected and experimental thickness of Pd deposits measured with XRF

Expected thickness (μm)	**Measured thickness (μm)**
0.25	0.24 ± 0.02

0.50	0.52 ± 0.03
0.50 (PC and PRC samples)	0.52 ± 0.04
1.00	1.04 ± 0.05

XRD analysis

XRD measurements were performed on the bare brass substrate and on a palladium coated sample in the 25°-90° wide range to assess the position and intensity of the peaks. The diffractograms of the samples at pre-established times were acquired in the narrower of 35°-45° interval to keep the measurement time short. In this range it was possible to record the (111) reflection which is the most intense, of both palladium phases.

Figure 4.1 shows, as an example, the trend recorded for sample Q: over time there is a gradual shift of the palladium peak toward higher values of 2θ, corresponding to a lower lattice parameter, due to hydrogen desorption. Brass peak was used as internal standard for calibration, centering the (111) peak of the $Cu_{0.64}Zn_{0.36}$ cubic alloy at 42.319° [128].

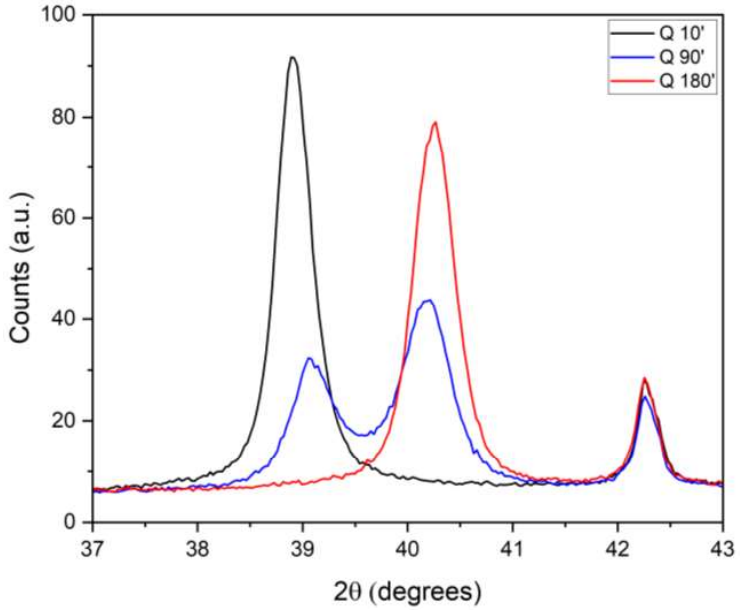

Figure 4.1: Diffractograms of the Q sample after 10, 90 and 180 minutes from the end of the deposition

Although lattice constants reported in literature for the H-Pd system are 3.895 Å for the α phase (PdH_x, x = 0.02) and 4.025 Å for the β phase (PdH_x, x = 0.58) [106], it is important to underline as the lattice constant is not a fixed value for each phase but varies within a range depending on the hydrogen concentration. Moreover, both phases coexist between 0.02 < x < 0.61 [112]. Hence, the lattice constants were calculated using Bragg's law as reported in Equation 4.1:

$$a = \sqrt{(h^2 + k^2 + l^2)(\lambda/2sin\theta)^2} \tag{4.1}$$

Where a is the lattice constant, h, k, l are the Miller indices referring, in this case, to the (111) phase of the fcc lattice, λ is the source wavelength (Cu-Kα) and θ is the angle the scattered beam forms with the normal coming out of the plan. All lattice constants found ranged from 3.895 Å to 4.025 Å. To discriminate the two phases, a threshold value was identified using the equation reported by Benck *et al*. [114] that correlates the lattice constants of the β-phase samples with the H/Pd ratio at 25 °C and 1 atm (Equation 4.2), imposing H/Pd = 0.02 corresponding to the maximum value for the α phase. Considering the error on the x-axis the lattice constant threshold is 3.935 $\pm$ 0.0034 Å.

$$\text{a (Å)} = 3.932 + 0.1719 * \text{H/Pd} \tag{4.2}$$

Therefore, we defined belonging to α-PdH_x those reflections with a < 3.932 Å and β-PdH_x those with a > 3.939 Å (Figure 4.2). The area of the peaks was used to obtain the β-PdH_x phase percentages. The results are reported as color maps in Figure 4.3 for DC samples (a, b, c). Figure 4.4 shows the results obtained for PC and PRC samples compared with DC samples of similar thickness and J_{AV}.

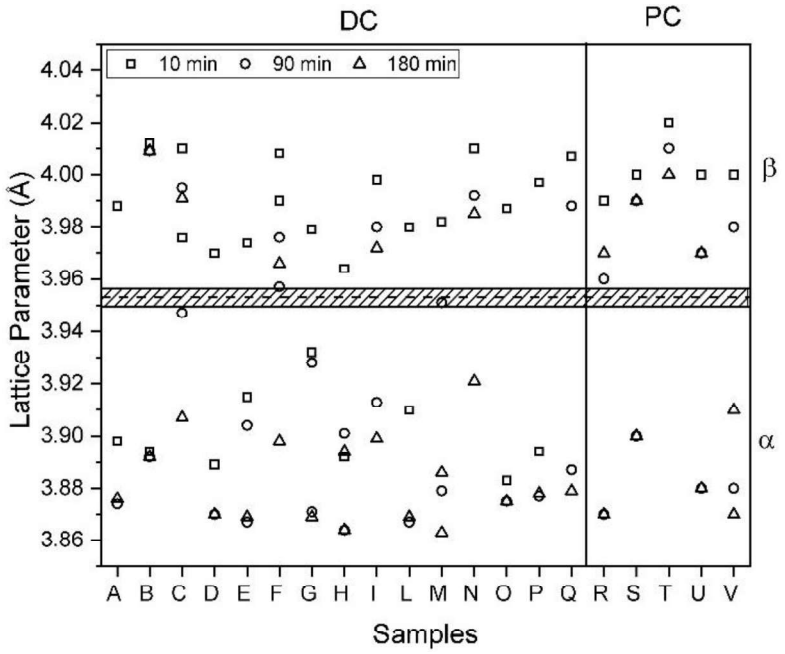

Figure 4.2: Lattice constants obtained for DC, PC (R, S, T) and PRC (U,V) samples. The dashed area corresponds to the threshold value: 3.935 ± 0.003 Å

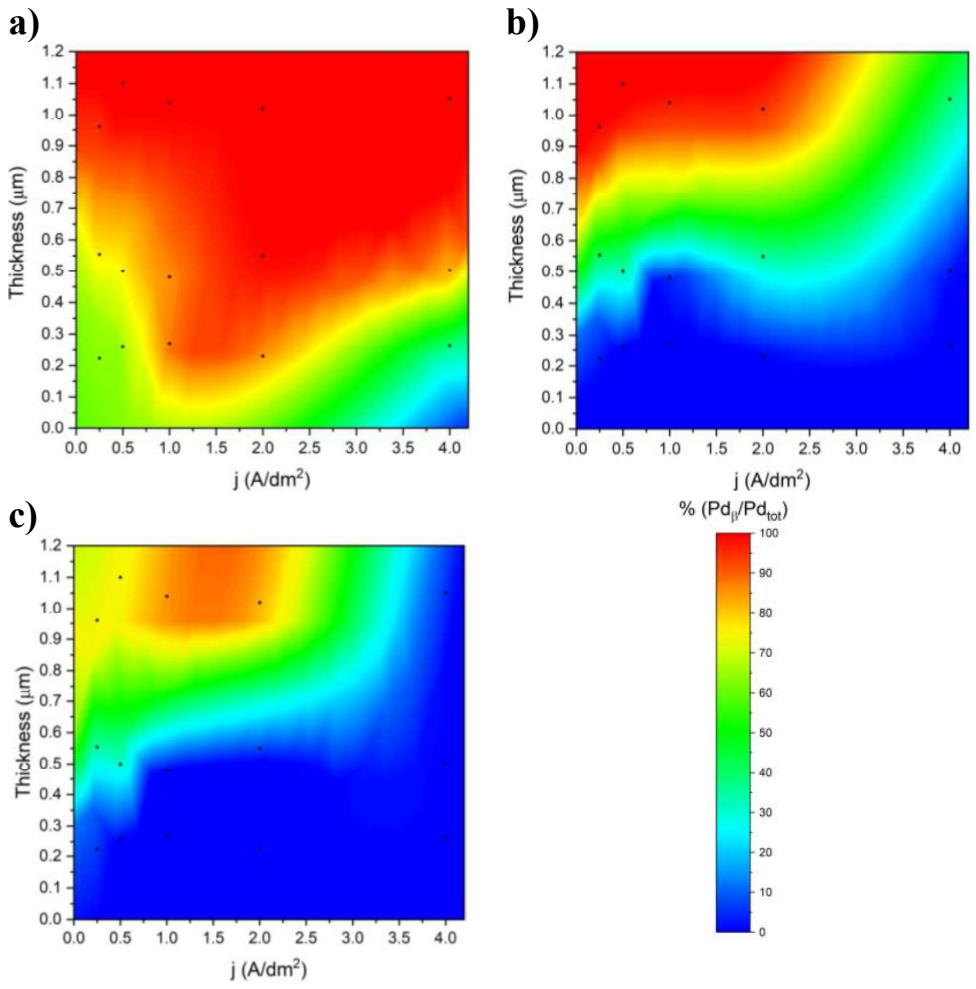

Figure 4.3: β-PdH_x percentages obtained on DC samples after 10 (a), 90 (b) and 180 (c) minutes after the end of deposition. The black dots represent the samples

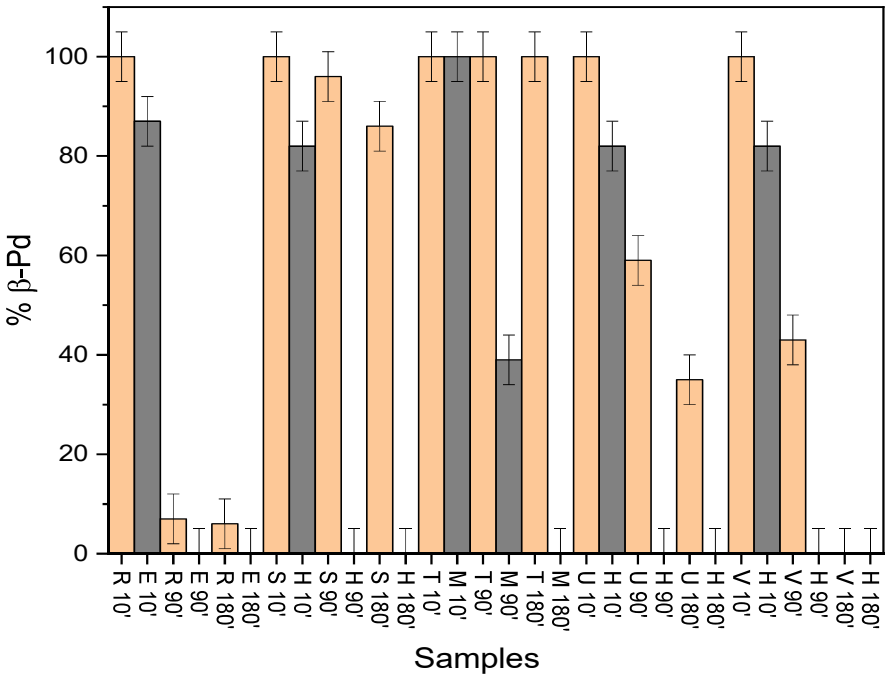

Figure 4.4: β-PdH_x percentages obtained on PC and PRC (orange) samples after 10, 90 and 180 minutes compared with DC samples (grey) realized with similar thickness and current density

The Scherrer equation (Equation 4.3) was used to estimate the crystallite size, where D is the crystallite size (nm), K is the shape factor (imposed as 0.94) and β is the full width at half maximum of peaks.

$$D = K \cdot \lambda / \beta cos\theta \tag{4.3}$$

The literature states that for sizes smaller than 4 nm the transition $\beta \rightarrow \alpha$ is inhibited [118], [129]. Moreover, Akiba et al., found that the difference in the lattice constant between the α and β phases becomes smaller as the particle size decrease [108].

As already observed [130], samples made with the lowest and highest value of current density (0.25 and 4 A/dm^2) show crystallites with the largest size (Figure 4.5), but in no case a value less than 5 nm was obtained.

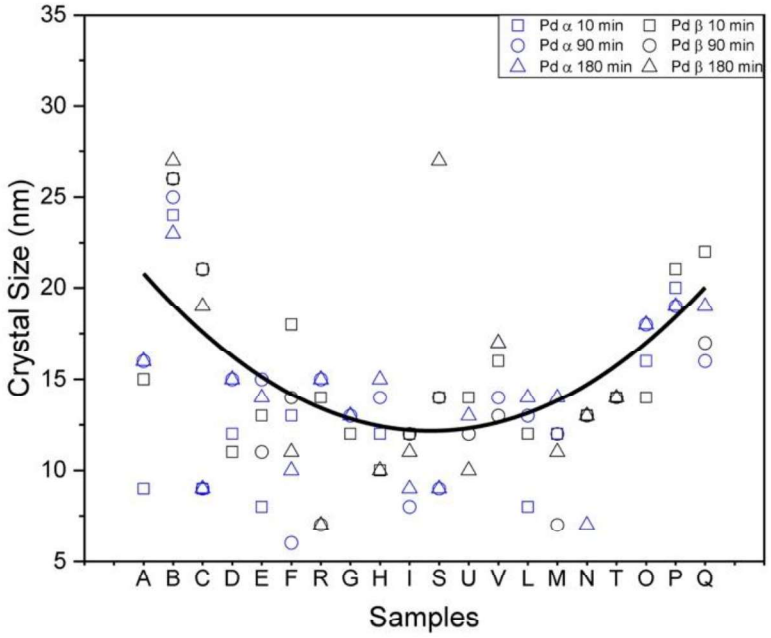

Figure 4.5: Pd-α and Pd-β crystallite size. Samples are listed in ascending order of j or j_{AV}. The black line represents the trend in crystallite size as a function of current density: the largest sizes occur for very high or very low current densities

To speed up the desorption process, some treatments have been tested which involve heating the sample in hot water or in oven. The experiments were conducted on sample H (0.5 μm, 1 A/dm^2) days after it was made. It should be emphasized that the cathodic degreasing procedure, which involves the hydrogen evolution reaction (HER) at the cathode, is able to restore the β-phase in the sample: 95% of the total palladium in the XRD analysis conducted after 10 minutes. However, 5 minutes in an oven at 100 °C is sufficient to decrease the percentage of β-PdH_x from 95% to 73%, and after 10 minutes the desorption process appears to be complete (Figure 4.6). Treating the samples with hot water at 70 °C yields similar results but in a longer time.

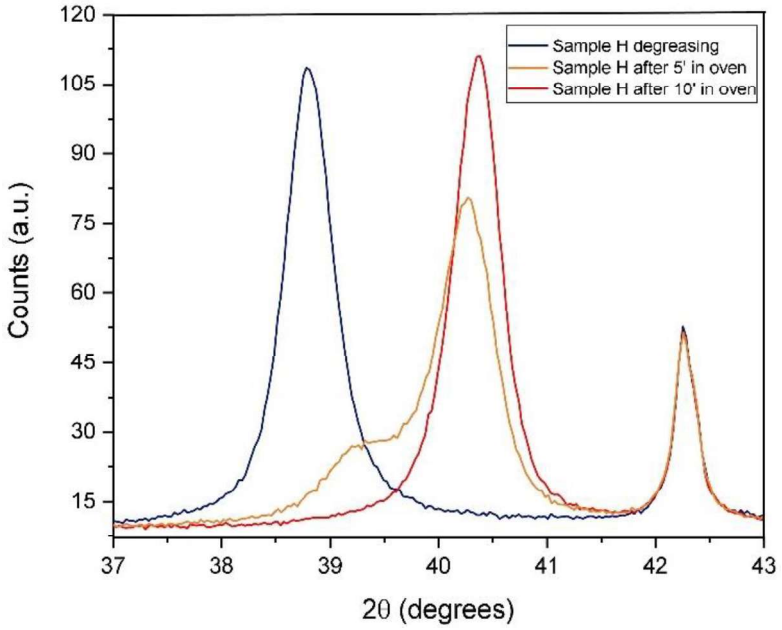

Figure 4.6: Diffractograms of sample H before and after (5 and 10 minutes) the treatment in oven at 100 °C

SEM analysis

Morphological analyses were conducted on samples H, S, T, U, and V. Samples H, S, U, and V were chosen to investigate the effect of the waveform used for the deposition, given the same thickness (0.5 μm ca.) and current density (1 or 1.45 A/dm^2). Sample T (0.5 μm, 2 A/dm^2) was analyzed for its high β-PdH_x content still present after 24 hours. SE images (Figure 4.7) have also been used to estimate grain size by the linear intercept method [125]. The results listed in Table 4.6 are averaged over five measurements.

a) H **b) S**

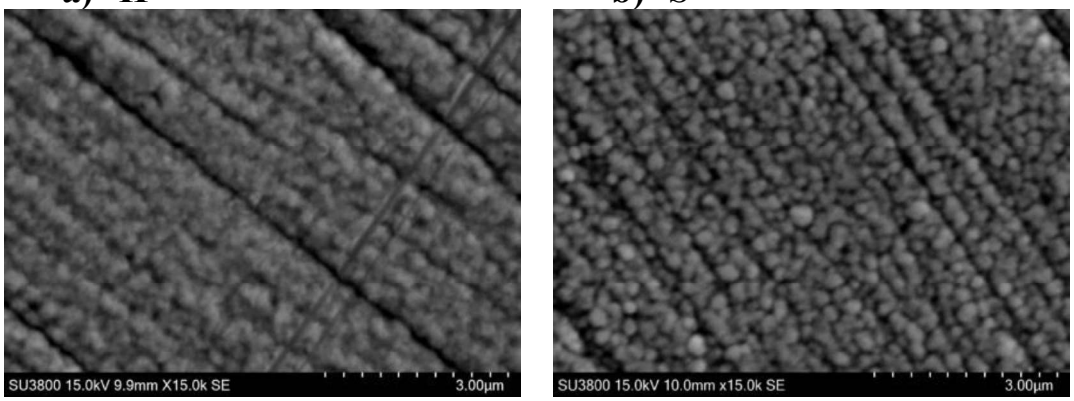

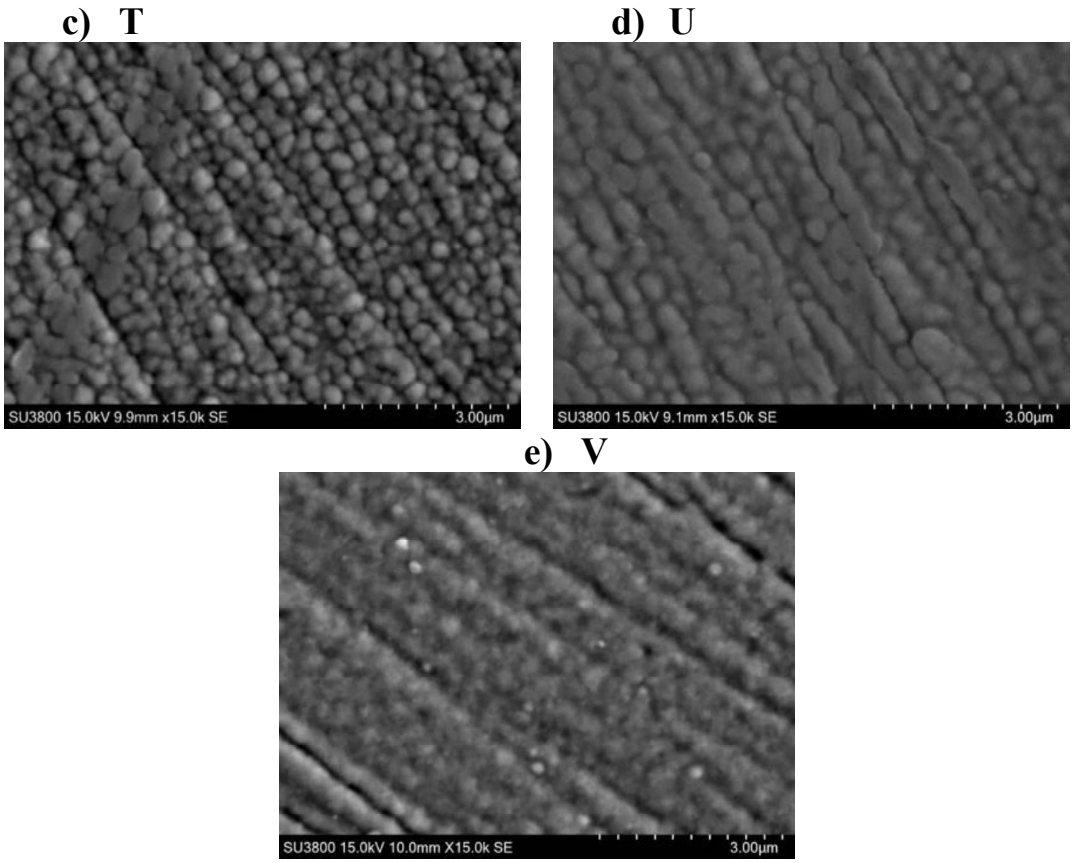

Figure 4.7: SE images evidencing the morphology of the samples: a) H, b) S, c) T, d) U, e) V

Table 4.6: Grain size determined by SE imaging of samples H, S, T, U and V

Sample	Grain size (µm)
H	0.21 ± 0.01
S	0.26 ± 0.03
T	0.36 ± 0.10
U	0.34 ± 0.05
V	0.23 ± 0.02

AFM analysis

To evaluate the surface roughness, samples H, S, T, U, and V were also analyzed by AFM. Figure 4.8 shows the 3D images obtained, and Table 4.7 lists the superficial roughness values in terms of Sq (mean square roughness), which represents the mean square deviation of the profiles from the mean line.

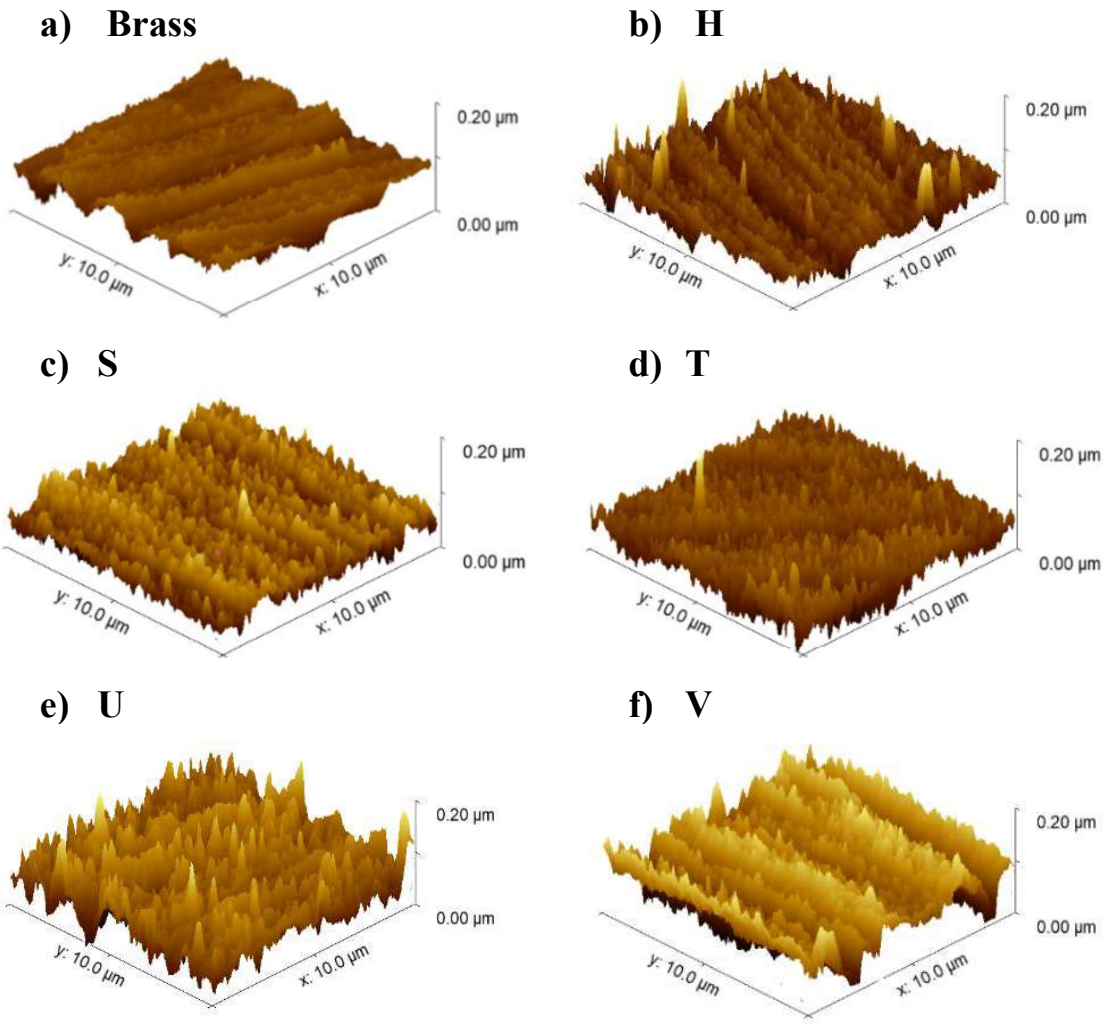

Figure 4.8: Three-dimensional AFM images of the substrate (a), brass) and samples: b) H, c) S, d) T, e) U, f) V

Table 4.7: Roughness values, obtained by AFM, expressed as Sq of Brass and samples H, S, T, U and V

Sample	Sq (nm)
Brass	9.5 ± 0.3
H	11.2 ± 0.3
S	12.7 ± 0.4
T	11.9 ± 0.4
U	21.6 ± 0.6
V	23.1 ± 0.7

Colorimetric analysis

Figure 4.9 shows the results of the colorimetric analysis as a function of the Gloss 8° parameter.

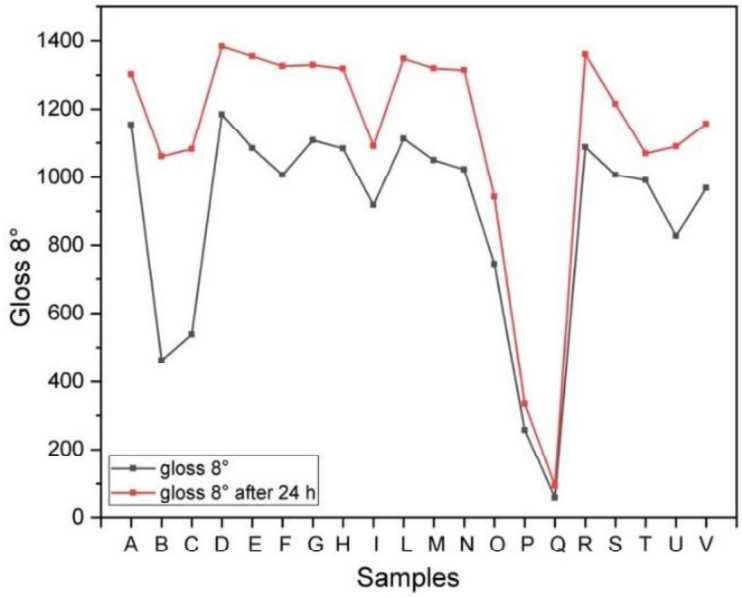

Figure 4.9: Gloss 8° values obtained for each sample immediately after (black line) and 24 h after (red line) the end of deposition

4.4 Discussion and Conclusions

In most samples, the transition from β to α phase is completed within 180 minutes, with the 10-minute measurement showing only the β peak. When considering DC samples, the thickness appears to be the primary factor influencing the kinetics of hydrogen desorption. Thinner samples, with a thickness of 0.25 μm, exhibit the fastest phase transition, typically occurring within 90 minutes, regardless of the applied current density (Figure 4.3Figure *4.3*). No linear relationship was observed between current density and either hydrogen content or hydrogen desorption rate. Still, from the color maps reported in the previous section a trend is observable: β phase seems to form prevalently at lower current densities. This could be a hint to the hydride formation process as formation of molecular hydrogen by the hydrogen evolution reaction (HER)

is favored by higher current densities, thus, it possible to speculate that the hydride formation occurs through a mechanism of co-deposition and the active species is not molecular hydrogen but a reduced form of atomic hydrogen.

SEM and AFM analyses reveal significant variations in sample morphology as a function of the waveform applied during deposition, even at the same J_{AV} (Figure 4.7, Figure 4.8). The parameters used for the pulsed deposition of sample T were particularly effective in producing deposits with a high hydrogen content and a low desorption rate. The β phase is still present after 180 minutes in other samples mainly because of the high thickness but only in sample T does it account for 100% of the palladium deposited even after 24 h (Figure 4.4). The 3D maps obtained by AFM show distinct structural differences between samples T and H, with a greater number of conical structures observed in the latter. Unlike the other samples, sample T exhibits significant variability in grain size (SD values in Table 4.6), which may suggest higher compactness of the deposit and a reduced presence of interstitial spaces, potentially limiting gas escape pathways. It is also safe to assume that the retention ability of hydrogen inside the deposit depends on its initial content. In sample H, for instance, the β → α transition is complete within 90 minutes, but the initial β-phase content was 22%, in contrast to the 0% observed in the rougher samples: S, U, V (Figure 4.10).

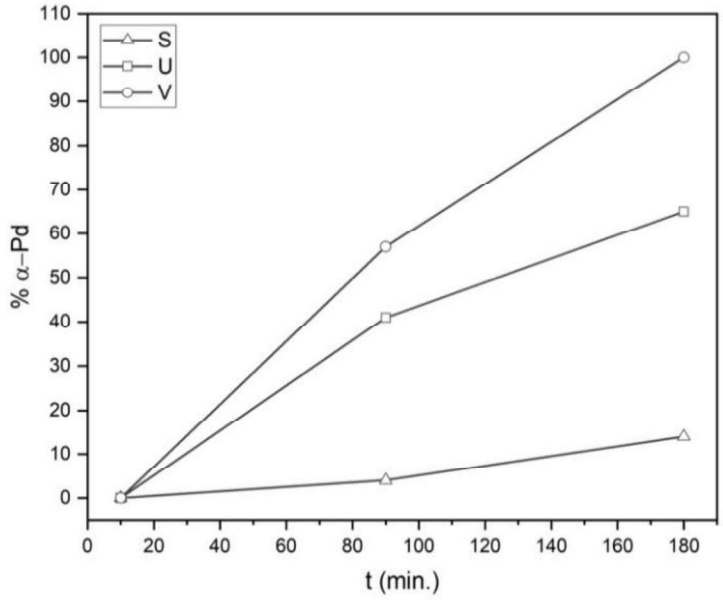

Figure 4.10: Hydrogen desorption rate for samples S, U, V

Colorimetric analysis reveals a trend in the results obtained: samples with the same parametrization show decreasing gloss values as the thickness of the metal film increases. For samples O, P, and Q, this trend is accentuated because a very high deposition current density is used.

Based on what has been said, surface roughness seems to have a primary role in the hydrogen desorption kinetic. Indeed, samples O, P, and Q (4 A/dm^2) show both a higher desorption rate than the other DC samples (at the same thickness, Figure 4.3) and a more matte appearance (Figure 4.9), well visible also to the naked eye. As the gloss values remain consistent even after 24 hours, this aspect cannot be attributed solely to hydrogen removal from the lattice, as might be suggested for samples B and C.

In conclusion, we investigated the influence of electrodeposition parameters, including thickness, current density, and waveform on the formation of α-PdH_x and β-PdH_x using a commercial electroplating bath supplied by Valmet Plating s.r.l. The resulting color maps provide general insights into the hydrogen content of the deposits as a function of time and direct current density. The highest H:Pd ratios were observed in the thickest samples (1 μm) and at the extremes of the

tested current density range: 0.25 and 4 A/dm^2. Samples deposited at 4 A/dm^2 also exhibited the highest desorption rate. Such high current densities, however, resulted in deposits with a dull appearance as confirmed by colorimetric analysis. Notably, samples B and C (0.5 and 1 μm, 0.25 A/dm^2, respectively) yielded significant findings, with the lowest desorption rates and the highest color variations observed, suggesting an actual change in brightness connected to the desorption process. This result opens up the possibility of qualitatively estimating the hydrogen content based on colorimetric analysis.

The behavior of PC and PRC samples differ significantly from that of the DC samples with equal thickness and average current density, confirming the ability of unipolar and bipolar pulsed currents to alter the morphology of deposits and suggesting a correlation between morphology and desorption rate. Sample T was found to have the highest hydrogen content, still largely present even 24 hours after fabrication. This result was attributed not only to the high compactness of the deposit but also to a specific structure of the crystalline grains. However, further investigation is required, particularly regarding potential applications for hydrogen storage.

It is important to note that none of the samples underwent microcracking during the desorption process. This behavior can be attributed to the relatively low hydrogen content (H:Pd never exceeding 0.55) and represents a promising outcome for the use of the specific electroplating bath in decorative applications. Indeed, although the microcracking phenomenon is strictly dependent on the substrate, specifically the crystalline mismatch between two successive layers, this finding represents a good starting point for conducting more in-depth investigations on Pd-Au systems widely used in decorative electroplating.

Finally, treatment of the sample in an oven at 100 °C is sufficient to completely remove the hydrogen from deposits 0.5 μm thick, in 10 minutes.

5 Gold

Gold, one of the most precious metals, is the most malleable and ductile of all metals and is a good conductor of heat and electricity [131]. One of the most important properties of gold from a functional point of view is its resistance against oxidation and the corrosive action of most chemicals. Indeed, gold dissolves only in *aqua regia* (the mixture of concentrated nitric acid and hydrochloric acid in a 1:3 volume ratio), in alkaline solution of cyanide and in mercury, where it forms an amalgam alloy.

Apart from its chemical stability, owing to desirable electrical properties, gold has been accepted as a versatile material in electronic technology, such as microelectronic, optoelectronic and microsystem technologies [132], [133], [134]. Deposits of gold or its alloys are used in various industries, such as in electronics for its anticorrosive and conductive properties [135], or as a final layer combining aesthetics [136], [137] with good mechanical properties and excellent biocompatibility [134]. A pretty wide range of colors of gold alloys can be attained, which is of primary importance for the aesthetics of the final products [138].

Commercial gold electroplating processes are numerous and diversified to meet different application needs [137]. Electroplating of gold and its alloys is carried out mainly starting from alkaline, neutral or acidic cyanide baths, for both technical and decorative uses, and from solutions of either Au(I) or Au(III). In some applications, such as microelectronics or for electroforming, alkaline or neutral sulphite baths are used, being less toxic, less irritating and easier to dispose of than cyanide.

Generally, a layer of gold is electrodeposited on the target substrate using direct currents. However pulsed current comes to our aid in this regard. Modulated currents are used as a research tool to investigate the electrodeposition

mechanism of metals [2], [3], [6], [126]. Through pulse parameters it is possible to modify the properties of deposits [50], [78], [127], [139], [140]; this occurs because pulsed currents affect mass transport, kinetics and electro crystallization phenomena [35], [49], [133], [141], [142].

5.1 Gold-Nickel Alloys - Morphological and Aesthetic Improvement

5.1.1 Introduction

As previously introduced, Au materials fabricated by electroplating have been commonly used as contact materials for high reliability circuit boards , electrical connectors, relays, and micro- and nano-scale electronic components for many decades because of their high electrical conductivity, chemical stability, corrosion resistance, and ductility [143], [144], [145]. Electrodeposition of gold or its alloys is not only used in the electronics industry due to its conductive and anti-corrosive properties, but also as a final layer due to its aesthetic properties [136], [137], good mechanical properties and excellent biocompatibility [134], in fact only 7% of the gold mined each year is used for medical, industrial and technological purposes while the remaining 93% is used in the jewelry industry and banking (e.g. in the production of bars or coins) [146], [147]. Evaluating these data, it is clear how gold is vastly used in a variety of areas, from jewelry to fashion, art, and furniture.

Electrodeposited thin films of gold are generally porous in nature, which may lead to the formation of corrosion products through the pores [132]. Porosity is the amount of discontinuity in the film responsible for corrosion. Pulse electroplating has been reported to be effective in fabricating Au materials with finer grains, higher uniformity, and lower porosity [148]. Although it had long been recognized that in deposits of gold, or its alloys, the best morphology was obtained under pulsed or reverse pulsed current conditions [50], the turning point occurred only in conjunction with the growing importance and value, of gold as a commodity, used in many electronic applications. An illustrative example can be related to Au-Co alloy: whereas due to voids or inclusions the density of DC

plated gold-cobalt (17 g/cm^3) is about 15 per cent less than the theoretical value, the pulse-plated gold cobalt, nearly free of polymer, has a density of 19.2 g/cm^3 which is closer to the theoretical value as determined by the pycnometer method [50], [51]. It is even possible to control the composition and the film thickness by regulating the pulse amplitude and width. Most importantly, an increase in the nuclei density could be achieved to obtain electroplated films with finer grains [149], [150], [151], [152], [153]. By simply adjusting the amplitude and length of the pulses, it is possible to control not only the composition and thickness, in the atomic order, of the deposits, but to improve their characteristics such as grain size, porosity and homogeneity [2], [3], [78], [126], [139]. Only in light of all these considerations pulse plating then emerged as a new technique for the deposition of metals and alloys, seeing a succession of theoretical contributions and industrial applications.

In this study we focused on a cyanide gold-nickel bath, among the most frequently used in the electroplating industry intended for the decorative sector, precisely as the final layer of the entire electroplating process. In this field, the characteristics required by end users focus mainly on the aesthetic evaluation of the deposits, such as deposit brightness (related to the size of the grains and their homogeneity), wear resistance (related to the quality of the deposit and its homogeneity and assessable through different corrosion tests), and above all the possibility of reflecting the quality standards by using the least amount of metal possible.

5.1.2 Experimental

Samples were prepared using a commercial bath of Au-Ni (BLUCLAD 8614 MUP); the solution consists in a full operative bath: 1.0 g/L $KAu(CN)_2$, 1.5 g/L $Ni(SO_3NH_2)_2 \cdot 4H_2O$ and all the necessary proprietary additives (brightening, levelling and complexing agent). This commercial plating bath has a working

range between 0.8 and 1.2 A/dm^2, we choose to use as current density for DC tests, the optimal value of 1 A/dm^2; while for pulsed tests we decide to work with two different values of average current density (J_{AV}): 1 A/dm^2 and 2 A/dm^2. The choice of using an average current density twice as high as the ideal value recommended by the bath producers is related to wanting to take the operating conditions to extremes, to see if pulsed currents allow benefits to be achieved on deposit characteristics even when optimal operating conditions are not respected. The samples used were circular silver plates, having an area of 0.215 dm^2, which were placed centrally inside a polypropylene galvanic tank, measuring 21 x 11 x 11 cm^3, with both faces facing to mixed metal oxides (MMO) anodes. Each deposition was carried out by stirring the solution using magnetic anchor, under controlled temperature conditions of 35 ± 1 °C and a pH range of 3.9 to 4.5, as recommended by the bath data sheet.

A commercial basic degreaser (owned by ITALFIMET) was used for the preliminary preparation of the samples.

The thickness of the deposits was measured by XRF analysis [64], [65], [66], [67], performed with a Bowman B Series XRF spectrometer (Schaumburg, IL, USA) using an acquisition time of 60 s, 50 kV tube voltage, 0.8 mA tube current, and a collimator of 0.6 mm in diameter.

Atomic force microscopy (AFM) measurements were performed in contact mode (0.5 V force set point) with a non-conductive Si_3N_4 triangular cantilever (Veeco, NP-S10, 0.12 N/m force constant) on a Molecular Imaging PicoSPM (10 μm × 10 μm, 512 px × 512 px, 1 lines/s speed) to evaluate the morphology and roughness of the samples.

Scanning electron microscopy (SEM) images and microanalysis were obtained with variable pressure Hitachi SU3800 (Hitachi High-Tech, Tokyo, Japan) equipped with an Oxford Instruments NanoAnalysis Ultim Max 40 silicon drift

EDS detector. The analyses were performed using an accelerating voltage of 5 kV.

Quantitative color comparisons were obtained using the portable spectrophotometer CM-700d (Konica Minolta, Tokyo, Japan) equipped with an integrating sphere controlled by SpectraMagicNX software (Konica Minolta, Tokyo, Japan). Color coordinates were expressed in the CIE-Lab color space: L* = light vs. dark, a* = red vs. green, and b* = yellow vs. blue. In the CIE-Lab color space, the a and b coordinates define the hue (color) and the chroma (vividness/dullness), while the degree of lightness is represented by the L* values. The measurement was obtained from diffuse reflectance spectra according to the CIE's recommendations [68] using a D65 illuminant, an observer at 10°, and maximum aperture with an angle of incidence $\theta = 8°$. The specular component was included (SCI). The measurements were performed using a 11 mm in diameter circular masks (MAV11). The gloss (8°) estimation, the function of luminous directional reflectance of a specimen responsible for its shiny or lustrous appearance, was obtained measuring both the reflectance spectrum of the samples including and excluding the specular component (SCI method and SCE method, respectively) [69], [70]. For both colorimetric and gloss assessment, the results reported are the average of five repeated measurements for each sample.

Damp heat with leather test (UNI EN ISO 4611:2011), salt spray test (ISO 9227:2017) and synthetic sweat test (NFS 80–772:2010) standards were followed to evaluate electroplated items ageing resistance. In particular, an Ascott Sip 120 chamber (Ascott Analytical Equipment Limited, Tamworth, Great Britain) was employed to perform the salt spray test and a Memmert CHP 50 Climatic Chamber (Memmert GmbH, Schwabach, German) was used when requested from standard procedures. Salt spray test was conducted by using a 5 % NaCl

solution whereas synthetic sweat composition was 5 % lactic acid and 10 % NaCl in deionized water.

5.1.3 Results

A preliminary electrochemical study was carried out to choose the parameters to be used for the samples.

Through electrochemical impedance spectroscopy, the capacitance value was derived, resulting in a value of C = 55.4 μF/cm^2.

Through chronopotentiometries we then calculated the overpotential value for different pulse current densities, deriving the lower limits of t_{on} and t_{off}, as shown in Table 5.1.

Table 5.1: Lower operated limits for each current density value

J_p (A/cm^2)	η (V)	t_C (ms)	t_{on} (ms)	t_{off} (ms)
0.01	0.970	5.4	27	38
0.02	1.048	2.9	15	20
0.04	1.156	1.6	8	11
0.06	1.221	1.1	6	8

Through chronoamperometric measurements, the diffusion coefficient and transition time was then estimated relative to the different values of pulse current density, shown in Table 5.2.

Table 5.2: Upper operating limit for each value of pulse current density

J_p (A/cm^2)	D (cm^2/s)	τ (s)
0.01	$3.2 \cdot 10^{-6}$	25.3
0.02	$6.66 \cdot 10^{-6}$	14.9
0.04	$1.56 \cdot 10^{-5}$	8.5
0.06	$1.17 \cdot 10^{-5}$	3.0

Once the upper and lower limits for pulse and pause times (considering mass transport limitations t_{off} has no upper limit) have been established for different values of pulse current density, all that remains is to choose the best parameterization for each type of J_p.

Evaluation was done by analyzing the waveforms, cathodic and discharge, for each J_P value, varying pulse times and t_{on}-t_{off} ratio.

What we expect is that the potential trend is affected by the pulse time, as previously discussed. For pulses that are too short, in fact, the potential suffers from the capacitive effect, never being able to go to steady state, which happens instead when the pulse duration increases; in this case, the deposition process is controlled only by activation kinetics. For pulses that are too long, on the other hand, the potential suffers from depletion by ions in the solution adjacent to the electrode, entering a diffusive regime.

Once the most promising parameters have been selected, silver samples were preliminarily degreased by cathodic degreasing and then immersed in a 5 % acidic H_2SO_4 solution for few seconds. After washing with demineralized water, they were plated using the Au-Ni bath by DC plating and pulsed current deposition methods.

Plating was carried out separately using the same electrolyte and pretreatment, employing a current rectifier capable of providing +2/-6 A.

Samples were prepared through a deposition time of 180 s for both DC and pulsed samples using a average current density of 1 A/dm^2; however, for samples obtained through unipolar pulses having average current density of 2 A/dm^2, the deposition time was reduced by half to 90 s as shown in Table 5.3, in order to maintain the same total amount of deposited charge.

Table 5.3: Samples and their preparation parameters

Name	Current	t_{on} (s)	t_{off} (s)	t_{tot} (s)	J_{AV} (A/dm^2)	J_p (A/dm^2)
A	DC	-	-	180	1	1
B	PC	0.033	0.033	180	1	2
C	PC	0.011	0.011	90	2	4

The assessment we set out to make mainly concerns the use of gold coatings, or its alloys, in electroplating to produce the fashion accessory, where Au is considered a final layer of the entire production process.

Based on this assumption, all the analyses that have been conducted on the samples concern an aesthetic evaluation (such as colorimetric analysis) but also performance evaluation of the production process and the final sample (homogeneity of the deposit, grain size and porosity of the grains).

XRF Thickness Measurement

XRF analysis were used to measure the thickness of the deposit over the entirety of the sample. We define a mapping procedure, that is, we estimate the thickness by sampling 5 spots placed linearly on the diagonal of our sample, so that the dispersion of thicknesses affected by the edge effect can be assessed, as shown in Figure .

The measurement spot has a diameter of 0.6 mm; 30 s sampling time was chosen for the measurement.

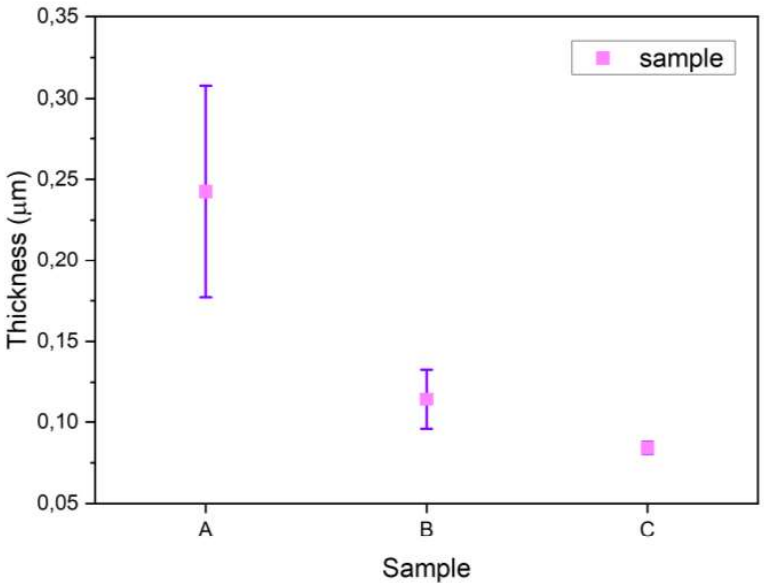

Figure 5.1: Average thickness and its standard deviation of each sample

The first thing one notices is how the thicknesses differ from one sample to another. Although current densities and deposition times were chosen in order to have the same total charge passing for all samples, the amount of metal deposited varied. This may depend on the pulse times used for the samples obtained via unipolar currents. In fact, as the t_{on} decreases, the thickness of metal also undergoes a decrease; this may suggest that too short times do not allow for a complete nucleation phase during the cathodic current pulses. Indeed, particularly in pulse electrolysis with short pulses, adsorption and desorption effects can lead to unexpected trends in current efficiencies. For example, with hydrogen, which tends to desorb during the off-time, a given coulombic charge is consumed at the beginning of a new pulse in building up a new adsorbed layer of hydrogen. If the charge needed for this purpose represents a substantial part of the total charge of the pulse, the current efficiency for metal deposition can show a significant fall. This effect is well known in the case of gold deposition from a typical acid bath containing cobalt as a hardening additive [82], [154].

SEM-EDS Investigation

We investigate the surface morphology of the deposit by scanning electron microscopy, as shown in Figure 5.2. SEM characterization allows to obtain images with micrometer resolution, so that we can visualize the deposition nuclei and the various structures that may have formed in the act of Au(I) reduction.
This evaluation allows us to draw considerations about grain size and consequently on the nucleation and growth process.

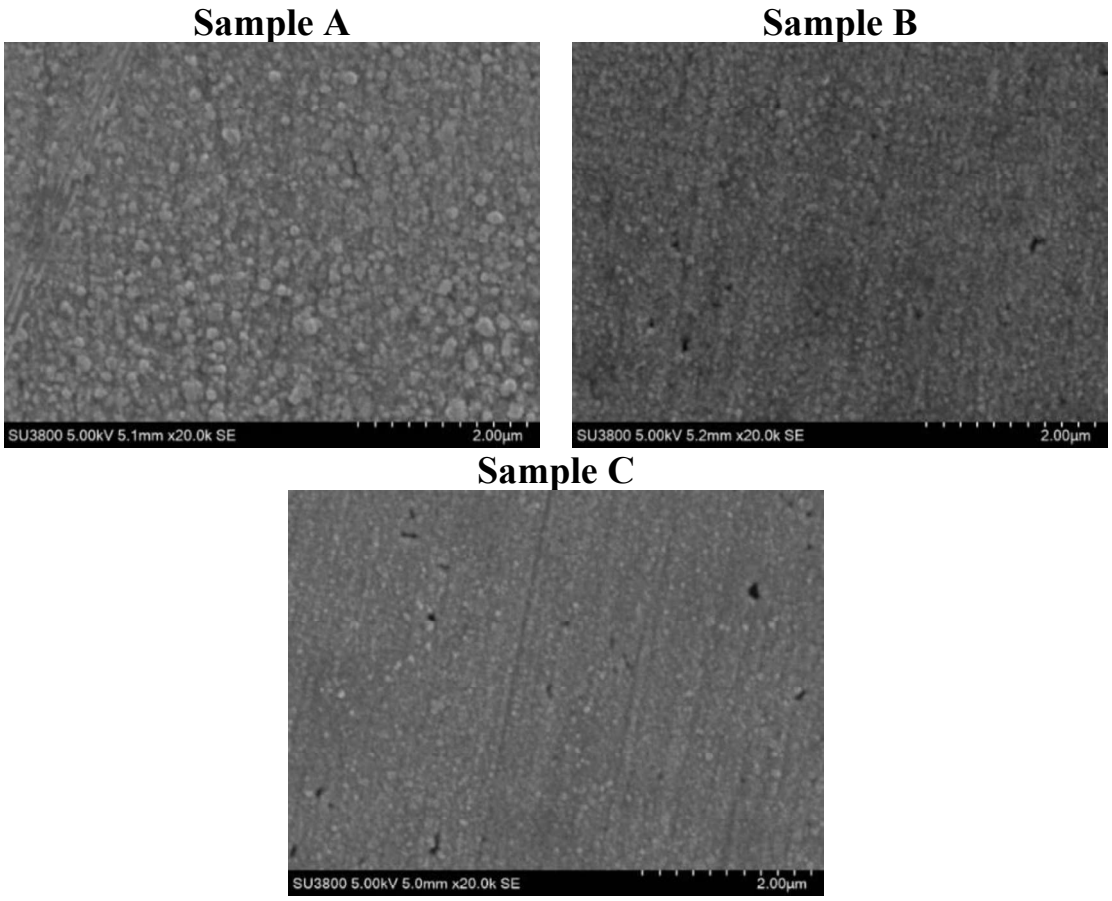

Figure 5.2: SEM images obtained at 20000X magnifications

Further evaluation was also done through ImageJ, a digital image processing computer software, through which we estimated the size of the gold grains in each sample.
In Table 5.4 we report the value of the mean and standard deviation of all metal films.

Table 5.4: Average particle size and its standard deviation

Sample	Grain size (nm)	Standard deviation (nm)
A	85	33
B	63	21
C	54	15

EDS analysis was performed on each sample to investigate possible differences in the composition of the Au-Ni alloy. The EDS spectra show that the relative concentration of the two metals in the electrodeposited layer varied: the percentage of Au was higher in the samples obtained with unipolar currents (99.8 % Au, 0.2 % Ni for sample B; 99.9 % Au, 0.1 % Ni for sample C) than in the sample A produced with direct current (99.3 % Au, 0.7 % Ni).

It is now well known that the use of pulsed currents allows the composition of metal alloys to be modified [78]. By varying the pulse parameters, it is possible to change the percentage composition of the metals that are electroplated in the alloy; by changing their relative concentration, there is also a consequent change in color [148].

Color and Gloss Measurement

Visible light reflectance measurements were performed to measure the colorimetric coordinates and the gloss of the deposits. These parameters are very important for coatings with decorative applications, more over the brightness of a deposit is closely related to its surface morphology. The results are summarized in Table 5.5.

Table 5.5: Colorimetric coordinates for each sample

Sample	Gloss	L*	a*	b*	Pseudo-color
A	769 ± 3	86.53 ± 0.01	5.59 ± 0.01	28.05 ± 0.01	
B	1144 ± 5	88.87 ± 0.01	7.13 ± 0.01	37.42 ± 0.01	
C	1366 ± 6	88.77± 0.01	7.01 ± 0.01	37.66 ± 0.01	

AFM Investigation

Atomic force microscopy (AFM) measurements were performed in contact mode to evaluate the morphology and roughness of the samples, as reported in Figure 5.3.

Table 5.6 shows the two roughness values Sq (mean square roughness and represents the mean square deviation of the profiles from the mean line) and Sa (arithmetic mean roughness is calculated as the average deviation, in absolute value, of the profiles from the mean line) for the individual samples.

Sample A

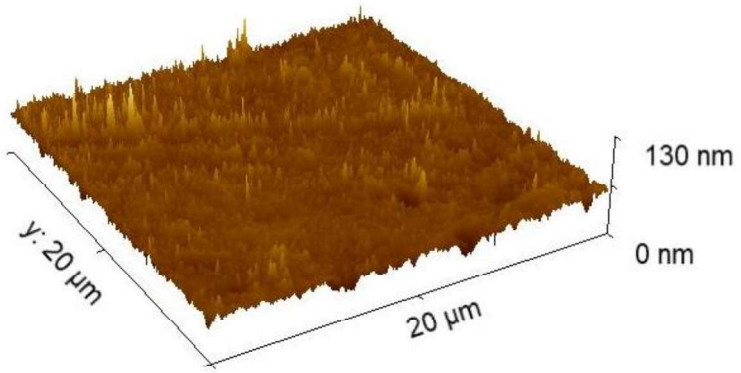

Sample B

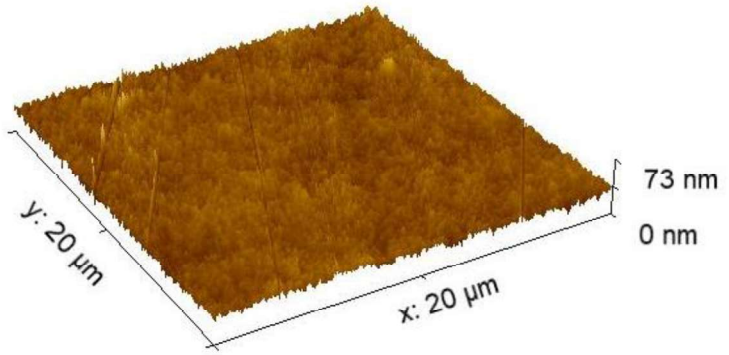

Sample C

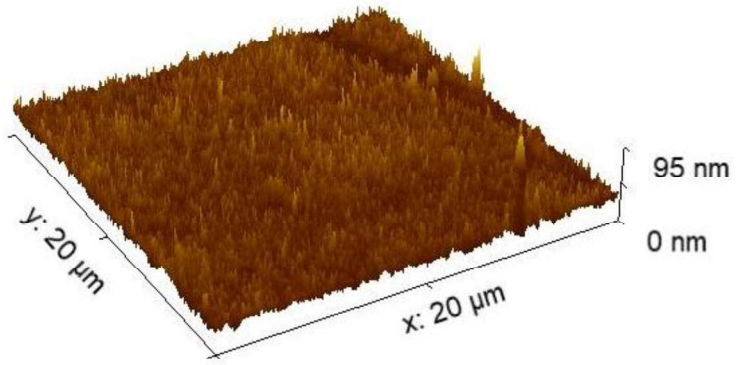

Figure 5.3: Three-dimensional AFM images of each sample

Table 5.6: Roughness parameter values

Sample	Sq (nm)	Sa (nm)
A	5.9 ± 0.2	4.0 ± 0.1
B	4.0 ± 0.1	3.1 ± 0.1
C	5.4 ± 0.2	4.2 ± 0.1

Corrosion tests

In terms of ensuring completeness of research and performance analysis on the use of pulsed currents, preliminary corrosion resistance tests were carried out. In this case, real samples were produced, that is, prototypes replicating potential industrial workpieces, both in shape and in galvanic sequence of metal layers (in

this case brass substrate and in succession copper, bronze, palladium and gold). Chains were then prepared using the same parameters presented above but decreasing the Au thickness of the PC samples by 25 % compared to the sample obtained in DC (0.16 µm Au for sample A; 0.12 µm for samples B and C).
This decrease in thickness is used to test the greater homogeneity but also the refinement of the grains, which appear from previous tests to be smaller and more compact, if obtained by unipolar currents; if the metal layer is indeed homogeneous in thickness over the entire surface, then it means that less metal will be required to be deposited to ensure equal corrosion resistance.
Damp heat test (ISO 4611:2011), salt spray test (ISO 9227:2017) and synthetic sweat test (NFS 80–772:2010) standards (the most used and representative in the fashion-jewelry industry) were performed.

5.1.4 Discussion and Conclusions

In this study, the role of pulsed current in the formation of gold-nickel layers in electroplating destined for fashion accessory and design was investigated.
The XRF analysis shows that unipolar pulses result in more homogeneous coatings from the point of view of electroplated metal thickness. This is extrapolated from the standard deviation values related to the average thickness, which is much lower than that of sample in DC, produced in direct current; relative standard deviation values, compared with the average thickness, are indeed: 26.9 % for sample A, 16.1 % for B and 4.4 % for C.
This result is somewhat surprising and unusual. Normally a greater uniformity of deposition is observed using bipolar currents (such as reverse pulsed currents), where there is a redissolution of deposited metal in areas of higher current density during the anodic pulse phase, resulting in a leveling of deposition. In this case it seems that even through pulsed currents it is possible to mitigate one of the major drawbacks of electroplating, that is, the inhomogeneity of metal thicknesses on

the surface of the workpieces (edge effect); one explanation could be that in areas of higher current density, hydrogen evolution competes with the deposition process and thus there is attenuation of thickness variation.

SEM images show how in sample A the accretion cores are much larger and less uniform in size respect to samples B and C, characteristics that affect not only the chemical and physical properties of the materials but also their aesthetic properties. On the other hand, samples B and C obtained by unipolar pulses are more uniform and have smaller grain size.

The results obtained through ImageJ software confirm the images obtained by scanning electron microscope: the grain size is smaller in the samples produced by unipolar pulses, compared with those of the metal layer produced by direct current.

Another consideration may be the greater homogeneity in size, in fact the standard deviation (to be considered not as a statistical error on grain size but as an estimate of the homogeneity of grain size) of samples B and C (33.97 % and 27.80 % from the mean value) is lower than that of sample A (38.70 %).

The color values allow us to make some observations. The L values confirm what we have seen with SEM analysis, showing the close correlation between the brightness of a sample and its morphology. Samples obtained with pulsed currents, having a smaller grain size and greater uniformity also have a higher L* value than the DC sample.

The change in color occurs not only with respect to the L* coordinate but also with respect to the values of a* and b*, which are higher in the two PC samples than in sample A. This variation is closely related to the different compositions in terms of the relative concentration of Au and Ni in the alloy, as determined by EDS analysis; concentration changes lead to color variation: higher a* and b* values are consistent with a higher percentage of gold in the alloy.

The gloss assessment, again, is consistent with the colorimetric analysis: again, the values are higher for samples in which the gold has been electrodeposited by pulsed current.

Both the AFM images and the mean square roughness values give us an indication of the morphological profiles of the samples. What we can evaluate is the lower roughness of the samples produced by unipolar currents, this is especially true for sample B whose Sq value is 4.0 ± 0.1 nm, compared to sample A obtained using direct currents. These results confirm what we saw through the SEM images, and allow us to make some additional considerations: obtaining more homogeneous and uniform deposits, both in terms of thickness and grain size, is reflected in the possibility of depositing less metal while maintaining constant performance (in terms of aesthetics but especially in terms of corrosion resistance) because there is no need to level out any peaks or holes in the various metal layers of the galvanic sequence.

24 h synthetic sweat led to partial corrosion - pitting - of all the samples tested but to a low extent (< 10 % of the surface). 48 h salt spray test left slight veiling on all samples. 48 h dump heat with leather (40 °C, 93 % RH) did not lead to any visible alterations in samples B and C (both obtained by pulsed currents), while sample A shows brown spots.

Results confirm that the use of pulsed currents allow identical (if not better, in some cases) corrosion resistance to samples obtained with direct current, using smaller thicknesses of precious metal.

The use of modulated currents has proven to be an effective methodology to be able to control and improve the chemical and physical characteristics of metal deposits.

In conclusion, whatever the end use, whether in electronics or simply as a finish in the fashion industry, gold plating is of crucial importance. It is precisely for this reason that the quality of the electrodeposited metal film is very important,

and research is always striving to find new working methods that allow for improved metal films in both aesthetics and performance.

This preliminary study demonstrates how using pulsed currents it is possible to obtain Au-Ni alloys with superior characteristics to those obtained using only direct currents.

Within the electroplating industry intended for the fashion industry, some demands from end users are much more stringent than others, such as aesthetic appearance and especially wear-resistant properties over time, using as little precious as possible.

Deposits obtained by pulsed currents have been shown to have a finer and more compact grain, compared with samples produced by direct current, the roughness is also markedly improved; all characteristics necessary for good corrosion resistance.

Samples produced with the parameters investigated in this study and a gold-nickel thickness decreased by 25 percent compared to a layer produced via DC showed equal, if not better, corrosion resistance to the most used tests in quality control.

The aesthetic aspect is also implemented: indeed, the samples obtained by PC have increased gloss and brightness values.

5.2 Gold-Nickel Alloys – Color Modulation

5.2.1 Introduction

The history of gold closely follows the evolution of human civilization, influencing its extension and development. The rich yellow color of gold has always been attractive, therefore it has been used all over the world, since 3000 BC [155].

Since gold alone is too soft to withstand prolonged use, other metals are alloyed to increase its mechanical properties, such as wear resistance and hardness [156]. However, the addition of metals also causes the color to change, reflecting how the electron configuration changes with composition [157], [158]. Silver and copper are the main metals with which gold is alloyed, but gold can also be alloyed with platinum, nickel, zinc, manganese and palladium, obtaining alloys with different destinations, properties and colors.

The ternary Au-Ag-Cu system is the most widely used to produce elaborate colored 12 to 18 carat gold materials [159]. By changing the percentage composition of the three metals within the alloy, different shades can be obtained, such as yellow green (also called 0N), pale yellow (1N), light yellow (2N), yellow (3N), pink (4N), red (5N) [160], [161].

More color variations, while maintaining a higher carat, can be obtained upon the addition of Ni, Zn, Pd, Cd, Mn or other secondary metals, that produce finishes in green, white [162], purple [155], grey [163], blue [164] or black [165] (containing Co and Ru in the alloy).

The perception of colors occurs when the wavelengths of white light interact with matter causing phenomena such as absorption, diffraction, reflection, refraction and scattering. It can also arise when a non-white light spectrum is emitted by a source [166]. Color perception in metals and their alloys can be explained through band theory [155], [166]. When different colors in white light uniformly

reflected, the resulting perception is white. For gold, however, the reflectivity decreases with increasing energy, particularly in the blue region of the spectrum, resulting in its characteristic yellow and reddish hues due to reduced reflection at higher energies [167].

Nowadays, a variety of colored gold alloys are available, enabling the creation of unique jewelry and decorative pieces. In certain applications, particularly in the fashion and furniture industries, color plays a crucial role. Even slight color differences between similar items can indicate poor quality, which is unacceptable in high-end products [168].

For a long time, in industrial processes, color was evaluated visually by manufacturers, but this approach is no longer suitable, due to the subjectivity of human perception and the empirical nature of the method. For this reason, in the fashion-jewelry industry, an objective method of color measurement is required. This demand for precision has led to the development of several color evaluation systems [155].

The Manufacturing Jewellers & Silversmiths of the America's Committee for Color References brought out a Gold Color Reference Kit, based on the CIE-Lab system [169]. This is an internationally recognized color measurement system that was developed by the CIE (*Commission Internationale de l'Éclairage*), adopted in 1976. This method has the advantage of describing colors mathematically, eliminating human subjectivity. The CIE-Lab method expresses the color in terms of three-dimensional coordinates: L*, a*, and b*. L* indicates brightness, with a value of 0 corresponding to no light reflection and 100 representing total reflection [170]. The a* coordinate measures the intensity of the red (positive) or green (negative) component of the spectrum, while the b* coordinate represents the intensity of the yellow (positive) or blue (negative) component. The color of a sample can be thus defined by plotting these coordinates as a point in the three-dimensional color space L*a*b*.

Among the advantages of using modulated currents, it should also be recalled that in pulsed current deposition processes, in the presence of two or more ion species in solution, the deposition parameters can influence the hierarchy of the reduction reaction according to the nobility of the metals [49], [171], thus allowing alloys with different percentages of metal to be obtained starting from the same electroplating bath.

Although pulse current (PC) electroplating has been explored for improving mechanical properties, wear resistance, and microstructure, there is a notable gap in the literature regarding its potential for precisely tuning color in decorative applications. The ability to systematically control alloy composition and resulting color variations using PC remains underexplored, despite its advantages in mass transport, nucleation, and deposition kinetics.

Despite the wide use of some colored Au alloys, especially in the fields of decoration and fashion, a systematic investigation on the change of color with composition is essential to attain a fundamental understanding of the color-pulse parameters relationship and therefore a better control over these properties [172].

The proposal of this study is to significantly advance the field of electrodeposition in modulated currents by demonstrating that pulse parameters can be exploited to achieve distinct colors from a single gold-nickel plating bath, without altering the bath composition. By establishing correlations between pulse variables, alloy composition, and colorimetric coordinates, this research provides a framework for achieving controlled decorative finishes with greater reproducibility. This new approach reduces dependence on multiple electroplating baths, optimizing production efficiency and cost effectiveness in industries such as jewelry and luxury goods manufacturing.

5.2.2 Experimental

Samples were made using a commercial gold-nickel electroplating bath (BLUCLAD® 8651); the solution contains 1 g/L $KAu(CN)_2$, 1.5 g/L $Ni(SO_3NH_2)_2 \cdot 4H_2O$ and all the necessary additives (brightening, levelling and complexing agent).

The preliminary electrochemical study was conducted using a working circular platinum electrode, of 1.5 mm radius, a mixed metal oxides (MMO) counter electrode and a saturated Ag/AgCl reference electrode (+197 mV vs SHE). Measurements were performed using an Autolab potentiostat/galvanostat PGSTAT101 (Metrohm, Herisau, Switzerland), equipped with NOVA software. The preliminary study aimed to establish the optimal ranges of pulse time and pause time, considering both double-layer electric charge effects and mass transport limitations. Respecting these ranges ensures that the pulsed current electrodeposition process effectively influences the reduction mechanisms. Values of t_{on} and t_{off}, for each P value, were then selected that fell within the previously defined optimal working ranges, as further described in the Results section. The specimens used for the preparation of the final samples were circular brass plates, with an area of 0.27 dm^2, which were placed centrally inside a polypropylene electroplating tank, measuring 21 x 11 x 11 cm^3, with both faces facing to MMO anodes; the system was connected to a rectified (R.C.V., Vicenza, Italy). Each deposition was carried out by stirring the solution using magnetic stirrer, under controlled temperature conditions of 40 ± 1 °C and a pH range of 3.7 to 4.1, as recommended by the bath data sheet. Prior to the plating process, samples were cleaned with a commercial alkaline detergent (ITALFIMET® Decro 885).

X-ray fluorescence analyses were used to determine the thickness of the electrodeposited metal deposits [64], [65], [66], [67]. Measurements were made with a Bowman B Series XRF spectrometer (Schaumburg, IL, USA) with an

acquisition time of 60 seconds, a tube voltage of 50 kV, a tube current of 0.8 mA, and a collimator with a diameter of 0.6 mm.

Compositional analyses were performed with an Hitachi SU3800 scanning electron microscope (Hitachi High-Tech, Tokyo, Japan) equipped with an Oxford Instruments NanoAnalysis Ultim Max 40 silicon drift EDS detector and the software AZtecLive. SEM-EDS measurements were made by setting an accelerating voltage of 5 kV.

Colorimetric measurements were made with a portable spectrophotometer CM-700d (Konica Minolta, Tokyo, Japan) equipped with an integrating sphere controlled by SpectraMagicNX software (Konica Minolta, Tokyo, Japan). Color data were expressed in the CIE-Lab color space: L*, a*, b*. Measurements were based on diffuse reflectance spectra according to the CIE's guidelines [68] using a D65 illuminant, an observation angle of 10° and a maximum aperture with an incidence angle of $\theta = 8°$. The specular component was included (SCI). Every measurement was performed with an 11 mm diameter circular mask (MAV11) and the reported values represent the average of five measurements per sample.

5.2.3 Results

A preliminary electrochemical study was carried out, using the commercial Au-Ni electroplating bath, to investigate the parameters to be varied for the pulse electrodeposition. The purpose of these experiments is to obtain ranges useful in choosing the appropriate settings for pulse plating, taking into consideration the electrochemical limiting factors.

The capacitance value was derived through electrochemical impedance spectroscopy [71], resulting in a value of $C = 41.8\ \mu F/cm^2$.

The commercial Au-Ni plating bath has a working range between 0.5 and 2 A/dm^2, for that we choose to use an average current density value of 1 A/dm^2 for DC and PC tests.

Through chronopotentiometries performed with different current densities (related to each value of P and shown in Figure 5.4), we calculated the overpotential and through Equation 2.10 the value of t_C. Using Equations 2.8 and 2.9 we obtained the lower limits of t_{on}^{min} and t_{off}^{min}, as shown in Table 5.7.

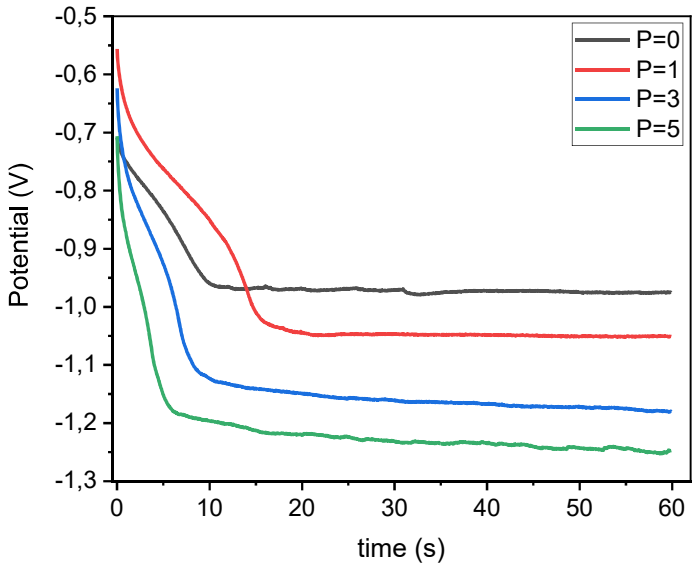

Figure 5.4: Chronopotentiometries acquired at various current densities, corresponding to each P value, used to calculate the overpotential

The diffusion coefficient D and transition time τ were then estimated performing chronoamperometric measurements and using Equations 2.12 and 2.11 respectively. Including these results are displayed in Table 5.7.

The values obtained for t_{on}^{min}, t_{off}^{min} and τ are consistent with those reported in the literature [173], both in terms of the order of magnitude of the results and the overall trend they have (t_{on}^{min}, t_{off}^{min} and τ values tend to decrease as the current density increases).

Table 5.7: Lower operating limit for pulse time and pause time obtained from the experimental value of η and t_C and upper operating limit for pulse time obtained using the values of D, for the chosen P values

P	J_p (A/cm^2)	η (V)	t_C (ms)	t_{on}^{min} (ms)	t_{off}^{min} (ms)	D (cm^2/s)	t_{on}^{max} (s)
DC	0.01	-0.970	4.1	20	28	$3.39 \cdot 10^{-6}$	25.3
1	0.02	-1.048	2.2	11	15	$6.78 \cdot 10^{-6}$	14.9
3	0.04	-1.156	1.2	6	9	$1.36 \cdot 10^{-5}$	8.5
5	0.06	-1.221	8.5	4	6	$2.03 \cdot 10^{-5}$	3.0

Once lower and upper limits have been established, we chose parameterizations within these operational ranges, which are considered optimal, for different values of pulse current density.

A wide range of pulses was evaluated since the purpose of this work is to investigate a correlation between CIE-Lab color coordinates and deposition parameters. Regardless of the parameters chosen, the total through charge was kept constant (since the average current density has been kept constant); this ensures to obtain for each sample, the same deposition thickness of about 100 nm, corresponding to a deposition time of 60 s. Table 5.8 shows the grid of experiments carried out. We also tested some parameterizations that have P value out of the preliminary electrochemical investigation. This choice stems from the need to understand the importance of the upper and lower operating limits of t_{on} and t_{off} and understand if they are stringent values or they only have a purely indicative role. Values of P = 10 were not investigated in the electrochemical study, but despite this we can speculate that the pulse and pause time parameters may be within the optimal ranges (although not estimated). Looking at the lower limit of working time is that as the value of P increases, the minimum acceptable value of t_{on} and t_{off} tend to decrease (see Table 5.7); for P = 5 they are 4 and 6 ms respectively, what is expected is that then for P =10 they are still lower. The same

trend is also found for the upper limit of t_{on}, which tends to decrease as the ratio of pause to pulse increases; what is noticeable, however, is that it always remains in the seconds range for the other values investigated (as shown in Table 5.7). Based on these considerations, it can be said that samples D and G also respect the operational limits. Similar reasoning can be made for the sample H, having P = 0.5, where it is assumed that the chosen on-time and off-time values are reasonably far from the operating limits, although not investigated. Concerning the specimen that falls outside the range considered optimal for pulse and pause values, this is sample B. Although the value of P =1 was studied, we chose t_{on} and t_{off} values below the set limits.

Table 5.8: Selected experiments and parameterizations of sample obtained

Experiments	**P**	**J_p (A/dm^2)**	**t_{on} (ms)**	**t_{off} (ms)**
A	DC	1	/	/
B	1	2	10	10
C	5	6	10	50
D	10	11	10	100
E	1	2	20	20
F	5	6	20	100
G	10	11	20	200
H	0.5	1.5	100	50
I	1	2	100	100

Once the depositions were performed, analyses were carried out to characterize the deposit, in particular, evaluations of percentage compositions, thickness measurement and colorimetric investigation were performed.

Spectroscopic analysis

XRF analyses were used to assess the thickness of the deposit obtained by measuring a central point of each sample, as shown in Table 5.9. It can be seen that there is no evident difference in thickness as the pulse parameters change.

Table 5.9: Thickness measured for each sample

Sample	Thickness (µm)
A	0.12 ± 0.04
B	0.12 ± 0.03
C	0.11 ± 0.03
D	0.11 ± 0.03
E	0.12 ± 0.04
F	0.12 ± 0.03
G	0.11 ± 0.03
H	0.11 ± 0.03
I	0.11 ± 0.03

SEM-EDS analyses were done on each sample to investigate the composition of the Au-Ni alloy, as shown in Table 5.10. Since the purpose of this work is to investigate a possible correspondence between pulse parameters and colorimetric coordinates, it is of primary importance to also associate possible correlations with a change in the percentage composition of the alloying metals.

Table 5.10: Percent composition of gold and nickel present in the alloy of each sample obtained with SEM-EDS analyses.

Sample	%Au	%Ni
A	98.9 ± 0.2	1.0 ± 0.1
B	97.7 ± 0.3	2.3 ± 0.2
C	97.6 ± 0.3	2.4 ± 0.2

D	97.1 ± 0.3	2.9 ± 0.2
E	97.9 ± 0.3	2.1 ± 0.2
F	97.2 ± 0.3	2.8 ± 0.2
G	97.0 ± 0.2	3.0 ± 0.2
H	98.5 ± 0.3	1.5 ± 0.2
I	98.0 ± 0.3	2.0 ± 0.2

Colorimetric coordinates of deposits were determined by performing visible light reflectance measurements, the values of which are given in Table 5.11. The same colorimetric coordinates are also presented through CIE 1931 color space chromaticity diagram, a two-dimensional representation of a specific color space, as shown in Figure 3. In this case the L*a*b* colorimetric coordinates were converted to the CIE-xyY color space. The diagram represents all the chromaticities visible to an average person. These are represented in color, and this region is called the gamut of human vision. The curved edge of the gamut is called the spectral locus and corresponds to monochromatic light (each point represents a pure hue of a single wavelength). The straight edge at the lower part of the gamut is called the violet line. These colors, while at the edge of the gamut, have no counterpart in monochromatic light. Less saturated colors appear within the figure, with white in the center.

Table 5.11: CIE-Lab colorimetric coordinates measured for each sample

Sample	L*(D65)	a*(D65)	b*(D65)
A	85.02 ± 0.01	6.34 ± 0.01	31.48 ± 0.01
B	83.20 ±0.01	6.68 ± 0.01	28.54 ± 0.01
C	84.72 ± 0.01	4.70 ± 0.01	24.53 ± 0.01
D	85.54 ± 0.01	4.19 ± 0.01	22.38 ± 0.01
E	84.40 ± 0.01	4.83 ± 0.01	26.16 ± 0.01
F	85.97 ± 0.01	4.04 ± 0.01	23.02 ± 0.01

G	86.30 ± 0.01	3.83 ± 0.01	22.60 ± 0.01
H	86.94 ± 0.01	4.56 ± 0.01	25.95 ± 0.01
I	87.05 ± 0.01	4.36 ± 0.01	24.97 ± 0.01

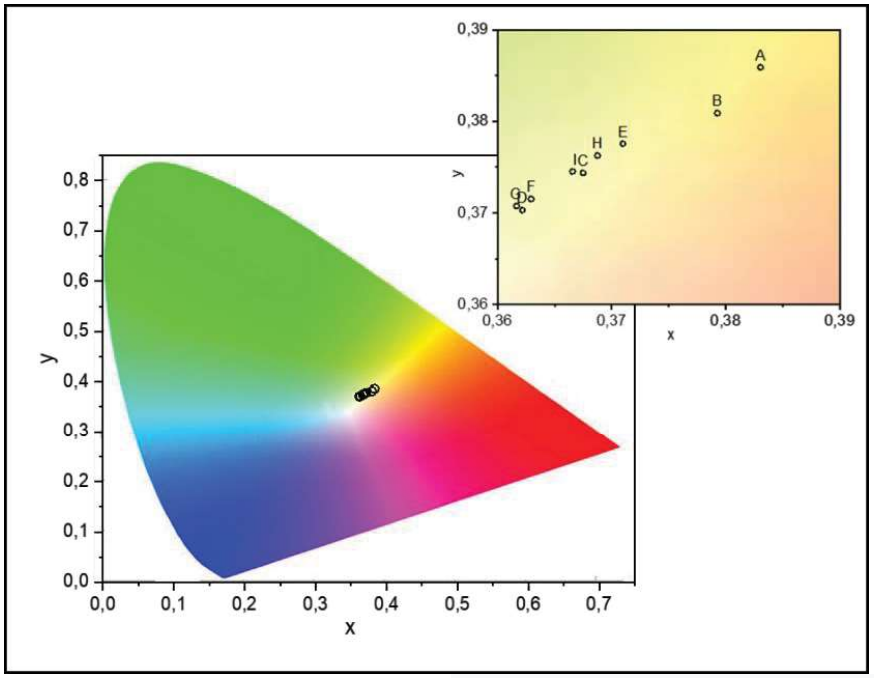

Figure 5.5: Color of each sample within the CIE 1931 color space chromaticity diagram

Applying different pulses results in different color with even substantial variations for individual coordinates.

The color variation was estimated by evaluating ΔE, which is the Euclidean distance between the individual color coordinates of two different samples, which is expressed by the following relationship:

$$\Delta E = \sqrt{(\Delta L^*)^2 + (\Delta a^*)^2 + (\Delta b^*)^2} \tag{5.1}$$

A practical classification of the color perception threshold has been proposed by Schlapfer [174], according to which the difference is perceptible to the human eye if this distance is greater than or equal to 3; in addition, two colors can be

said to be distinctly different when the delta E value is greater than 6. Table 5.12 shows the colorimetric difference between each color.

Table 5.12: ΔE value obtained from each sample and reported by a color scale: green indicates that the color difference is not perceptible ($0 < \Delta E < 3$), yellow indicates that the difference is visible to the naked eye ($3 \leq \Delta E \leq 6$), and orange indicates that the color of the samples is markedly different to the eye ($\Delta E > 6$)

	A	**B**	**C**	**D**	**E**	**F**	**G**	**H**	**I**
A	/	3.5	7.1	9.4	5.6	8.8	9.3	6.1	7.1
B	3.5	/	4.7	7.0	3.2	6.7	7.3	5.0	5.7
C	7.1	4.7	/	2.4	1.7	2.1	2.6	2.6	2.4
D	9.4	7.0	2.4	/	4.0	0.8	0.9	3.9	3.0
E	5.6	3.2	1.7	4.0	/	3.6	4.2	2.6	2.9
F	8.8	6.7	2.1	0.8	3.6	/	0.6	3.1	2.3
G	9.3	7.3	2.6	0.9	4.2	0.6	/	3.5	2.6
H	6.1	5.0	2.6	3.9	2.6	3.1	3.5	/	1.0
I	7.1	5.7	2.4	3.0	2.9	2.3	2.6	1.0	/

A $\Delta E > 3$ was obtained for most of the samples; taking into consideration the sample produced by DC, it can be seen that every other coating (produced by PC) has a recognizably different color from it.

5.2.4 Discussion and Conclusions

As mentioned earlier, color is related to the concentration of metals in the Au-Ni alloy. In this case, with Ni being the minority element, we can say that the color depends on the concentration of the metal in the layer; therefore, a correlation was sought between the percentage of nickel in the deposit and the CIE-Lab colorimetric coordinates.

What can be seen by comparing the pulse parameters and the percentage of nickel present in the samples is that there is a correlation between the two; in fact, for

the same t_{on} value, the amount of nickel in the alloy increases as the P value and thus the pulse current density increases, as shown in Figure 5.6.

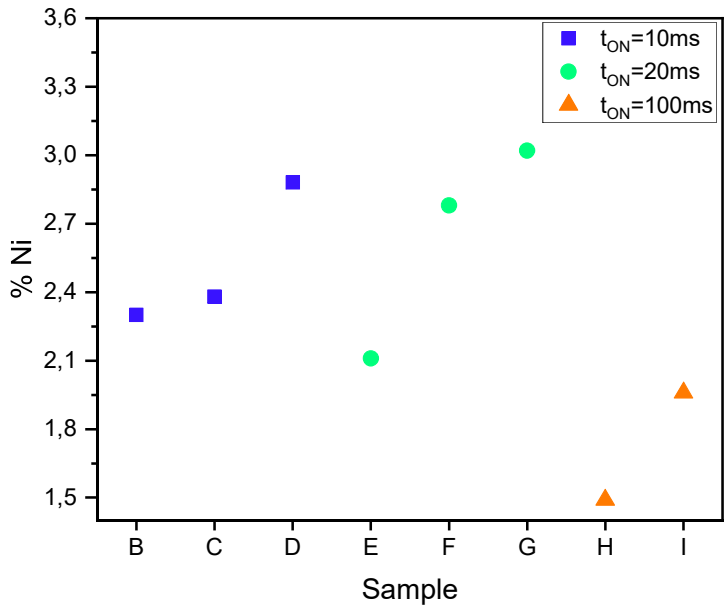

Figure 5.6: Correlation between samples and percentage of nickel in the alloy. Samples are grouped by same t_{ON} (blue square t_{ON} = 10 ms; green circle t_{ON} = 20 ms; orange triangle t_{ON} = 100 ms). Within each group, samples are in ascending order of pulse current density used

If we analyze the results obtained by colorimetric analysis, we observe a correlation between pulse parameters and colorimetric coordinates. What we notice is that for samples having the same t_{on}, the L* coordinate tends to increase as the value of pulse current density rises (consequently as P increases); the a* and b* coordinates, on the other hand, follow an opposite trend, that is, they tend to decrease as the ratio of pause to pulse increases, as shown in Figure 5.7.

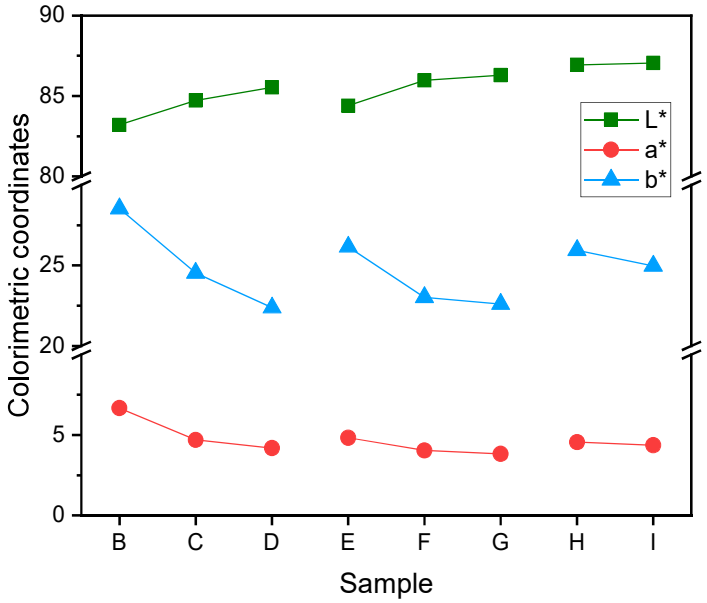

Figure 5.7: Correlation between samples and CIE-Lab colorimetric coordinates for different t_{on} values as P increases: samples B, C, D, t_{on} = 10 ms; samples E, F, G, t_{on} = 20 ms; H, I, t_{on} = 100 ms

In the same way we can highlight a correlation between percentage of nickel present in the alloy and colorimetric coordinates. As shown above, the amount of nickel increases as J_P increases; there is also an increase in L* (brightness) and a decrease in the value of a* and b*, leading to perceptible color shifts. This pattern therefore acquires a logical sense, since samples with a higher percentage of nickel have a color that turns less red (color coordinate a* positive) and yellow (coordinate b* greater than 0).

The results show that all samples follow this trend, even sample B, whose t_{on} and t_{off} parameters did not respect the optimal ranges investigated during the preliminary study. In our opinion, these results do not in any case invalidate the importance of defining optimal parameter intervals for reliable deposition. On the contrary, this indicates that the results obtained in the electrochemical investigation are only approximate and do not set stringent limits on the most suitable range within which to select pulse and pause times, suggesting greater flexibility under certain conditions, which require further investigation.

The ability to correlate deposition parameters with composition and color confirms that pulse plating provides a tunable method for achieving specific finishes, a potentially significant result for various industries, particularly those that rely on metallic coatings where aesthetics and mechanical performance play a key role.

In conclusion, in this work, an electrochemical study of a commercial Au-Ni plating bath was performed using pulsed current. After identifying the ranges of pulse variability using the intrinsic chemical and physical properties of the bath, the aim was to understand whether it is possible to vary the color of a metal deposit as a function of the pulse used and which parameters most influence the colorimetric coordinates.

In conclusion, the results obtained show how it is possible to obtain products with different colors from an electroplating bath with a fixed composition. Using pulsed currents, it is possible to modify the percentage composition of two alloyed metals, in this case gold and nickel, simply by changing the pulse parameters, or better, by changing the cathodic current density.

Of great interest is how PC not only allows the formation of metallic deposits with a brighter appearance than those produced by the classic DC (many samples have a value of L* higher than sample A), but also obtain finishes that differ in color, one from the other, a value of ΔE that in some cases exceeds 9.

The results are particularly relevant to the fashion and jewelry industries, where accurate color control is essential for product quality and customer satisfaction. The ability to precisely adjust the color without altering the bath composition allows manufacturers to create a wider range of gold shades (from warm yellow to cooler tones) using a single electroplating configuration. Since even small variations in color affect the perception of the product, this method would ensure consistency between production batches, reducing defects and returns; in addition, reducing the need for multiple plating baths would simplify operations, decreasing material waste and production costs.

Looking forward, further research could explore the applicability of this technique to other alloy systems besides gold-nickel, investigating whether the correlation between current density and percentage of alloy metals is replicable and shows comparable trends. In addition to decorative applications, this approach could also have implications for functional coatings in other areas, where fine-tuning material properties through electroplating could improve not only aesthetics but also performance. Although aesthetics is the main goal, controlled nickel content also affects conductivity and corrosion resistance, benefiting the electronics industry. In addition, the ability to finely control the composition of an alloy, with the possibility of producing decorative wear-resistant coatings could also have applications in the automotive or aerospace industries.

These results pave the way for adaptive electroplating technologies in which color and material properties can be dynamically adjusted.

6 Sustainable Perspectives in Electroplating Processes

6.1 Introduction

The process of electroplating is vital in many industries that produce modern aerospace materials and electronics, heavy equipment, cars, decoration, and fashion. The increasing focus on sustainability within several areas has also seen a critical re-evaluation of electrodeposition practices within the context of the United Nations' sustainable development goals (SDGs) [175]. The main critical items regarding the plating industry lie within the environmental sector, from production to disposal, and health within the workplace [176], [177]. Electroplating in many instances involves hazardous agents like cyanides, chromium, and nickel, which adversely affect the environment and human beings [178]. Some of the traditional processes consume a lot of energy, thus contributing to the carbon footprint of the industry [179], [180]. Production of galvanized items often involves the extensive use of scarce materials like gold and palladium, which have challenges associated with their mining processes. The issue of manufacturing toxic waste and how to dispose it off is a major environmental concern, which involves high costs and risks.

These are well-known problems that drive research in this area, major themes are finding replacements for toxic compounds with less hazardous alternatives. For instance, using cyanide-free [181] electroplating baths and nickel-free process for reducing of such risks. Others are the use of innovative alloys which minimize on precious materials, solutions seeking to ensure the needed performance whilst employing little quantities of costly metals, and carry out cleaner fabrication, minimizing the production of toxic wastes. Also, encouraging recycling efforts to regain valuable components from electroplating waste. Expansion for

investment into more energy-efficient technology in processes. As discussed above, pulsed, or modulated currents can enhance the deposition efficiency.

The issue is complicated and linked almost exclusively to the ecological problems such as pollution relating to the industry of the electroplating. However, it is important to recall that sustainability is a wider and more complex notion. Economic and social elements frequently remain disregarded as attention is primarily directed at ecological issues. Therefore, corporate strategies embrace green topic that are tied to the communities where the corporations operate and reflect on economic considerations as well. However, only through a single vision that takes into consideration these needs the electro-plating industry and all the others would respond to these challenges equitably and responsibly.

To make the industrial process more sustainable, there is a need to train operators on sustainable practices and environmental awareness with a view that such procedures will take root on the industrial scale. Collaborate with industries and research institutions as part of an effort to set up sustainable guidelines for the electroplating sector as well as share benchmarks. Establish government-backed policies and incentives for promoting cleaner technology, sustainable R&D, etc., within industry. Encourage investors in the development of green technologies as well as research efforts towards sustainability and ultimately, the adoption of greener processes. The successful sustainability of the electroplating industry requires research, innovation, regulation, staff training and cooperation by all stakeholders.

Mathematical models have been developed as well as artificial intelligence methods used to optimize processes and reduce the effect on the environment as part of addressing sustainability problems [182], [183], [184]. Some of them consist in activity like the Pollution prevention (P2) which played an integral role in the development and implementation of technologies designed to prevent the amount of waste generated at a facility. The P2 approach is extended to Profitable

P2 (P3) which seeks economic benefits with environmental reduction [185], and even Cooperative P3 (CP3) for industrial areas, to aid in decision-making toward sustainable development [186].

Song [187] in 2016 explains the prevalent sustainability measurement systems but stresses on the need to generate a specific metrics system for evaluating sustainability performance of the electroplating industry. These comprise of economic sustainability indicators, environmental sustainability indicators, and social sustainability indicators. These indicators focus on issues that include among others profit, value addition, energy, material usage, water consumption, and emissions among many other factors.

In 2015 United Nations stated 17 SDGs for development of the world's agenda on global challenges elimination, improvement of the live standards of people, protection of the planet till 2030. 17 SDGs are a universal call for an end to poverty and a beginning to prosperity, health, and life on earth. The electroplating industry is also based on a thorough critical analysis of the SDGs as a starting point to identify directions for improving sustainability.

Several SDGs are closely related to electrodeposition in a direct perspective. One such example could be on SDG 9 (Industry, Innovation, and Infrastructure) which could advance on efficiency and lessen environmental effects with such technologies of electrodeposition. This is why modern electrodeposition technologies have been adopted as an element of innovations that enhance efficiency and reduce environmental pollution. The development of more sustainable processes through research is key for the industry's growth. New materials and novel electroplating processes can also be utilized to the benefit of the decorative sector, and to a certain extent of technical sector, supplying eco-aesthetic solutions. Simultaneously, attention to responsible utilization of chemical resources which follows SDG 12 becomes vital. Reducing the content of precious metals in electroplating processes is an important contributor to a

more responsible use of resources and answers consumer's demand for more sustainable products. The development of cyanide- and nickel-free electrolytes is one step towards a safer and more sustainable operation process. The strategy can achieve SDG 7 (Clean and accessible energy) due to the implementation of low energy consumption and ambient temperature processes that lead to lower environmental impacts associated with energy consumption; it is related to SDG 13 (Climate Action) as well. When manufacturing galvanized materials, it incorporates low carbon emission processes that assist in climate change mitigation. Water resource management and sustainability in the context of SDG 6 (Clean Water, Sanitation), where efforts are taken for the reduction of water consumption in electroplating. The investment in research and development of the electroplating industry by innovative methods can lead to improved economic growth and skilled jobs according to SDG 8 (Decent work and Economic growth). There are other issues relating to employment and economic development, even in the artisan contexts.

Sustainability of the galvanic system can be regarded as an integration of waste minimization, production enhancement and social sustainability [187]. Environmental impact and health burdens can be effectively reduced by waste reduction. In addition, waste reduction refers to chemical, sludge, water, and energy. Social sustainability involves looking at issues that relate to customer satisfaction, employee satisfaction and local community satisfaction.

The economic globalization has put a strain on the galvanic industry. Most of electroplating companies are usually working in at a loss, as well as using rather obsolete technologies. Nevertheless, the industry is one of the most polluted among the manufacturing industries.

In this paper we will discuss in detail some newly established eco-friendly practices in this industry that may benefit the environment, human being, and society. The aim will be to present a vision for a future in which electrodeposition

does not only respond to the technological requirements but goes further towards a more sustainable environment through case studies and analysis of challenges faced today. Several computations techniques for predicting new formulations without using harmful substances are described specifically. Commercial systems for the better homogeneity and compaction of galvanic deposits to cut down on the amount of material being used will be discussed with some case studies. In the last, treatment and disposal or recovery of wastewater metals for the environmental protection, as well as for the economic benefit of recycling valuable metals, are analysed.

6.2 Deposition systems

Obtaining electrochemical deposits that are as homogeneous as possible is an issue of absolute importance, especially in the field of the high-fashion industry, where precious metals are often used and even a low percentage reduction in consumption leads to a great advantage for the overall process [77].

Having a low standard deviation in the metal deposit allows a smaller amount of material to be used, as the required minimum thickness values can be achieved with less dispersion in the obtained coating, thus operating with reduced costs and less operating time, with clear advantages for the environment sustainability of the entire production process and from an economic and competitive point of view for the manufacturing company. The thickness of the deposits obtained from present galvanic production is very uneven because they are strongly influenced by the shape of the treated objects and the current distribution.

In this work we therefore chose to conduct a study of the distribution of thicknesses in the case of a precious metal finishing, evaluating the effect of different operational set-ups. The thickness distribution of gold deposit within the galvanic frame, obtained using the standard parallel anodes configuration, was taken as the reference. It was compared with two devices operating in direct

current (DC) designed to overcome thickness inhomogeneities and a system operating on pulsed current (PC). The depositions were performed in a typical electroplating tank (Figure 6.1).

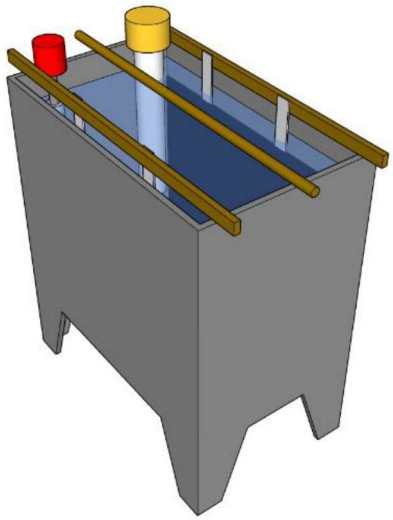

Figure 6.1: 500 L electroplating tank containing: two anode bars, one for each side, to which the MMO anodes are connected; a central cathodic bar, where the frame is attached; a float to control the level and temperature of the solution; a heating element for heating the solution

In all cases, commercial brass plates from Ossian Lagerqvist AB (Jarfalla, Sweden) were used as a substrate: 0.250 mm thickness, 50.0 mm length, 37.5 mm width. The plates were drilled in the center of the short side, at the apical position, the hole has a diameter of 5 mm. The brass surface was kindly electroplated with a thick layer of nickel (>20 μm) by Lotti Srl (Signa, FI, Italy), Gruppo Materia Firenze (Scandicci, FI, Italy) and Eco-Tech Finish Srl (Arezzo, AR, Italy), on their industrial production lines according to internal standard production process. The thickness distribution study was carried out in an area of 24.35 cm X 31.6 cm, 16 plates were placed in each galvanic frame.

The commercial nickel electroplating solution employed presented the following characteristics: nickel (II) sulfate 230 g/L, Nickel (II) chloride 50 g/L, boric acid 48 g/L, brightening additive 11 mL/L, carrier additive 40 ml/L, pH (25 °C) 4.5, working temperature 55 °C, cathodic current 5 A/dm^2.

6.2.1 DC Deposition Systems

The case study carried out on optimization systems operating on DC was performed on a gold deposit, electrodeposited by means of the commercial "Bluclad 8693" galvanic bath. This formulation presents the following characteristics: Au 2.5 g/L, Fe 0.5 g/L, pH (25 °C) 4, working temperature 40 °C, cathodic current 2 A/dm^2. The study was carried out for deposits that present a thickness of about 0.5 μm. Initially, the samples were produced with a classical system operating with common mixed metal oxide (MMO) anodes, the results thus obtained were compared with the results obtained using the commercial systems Italfimet (Monte San Savino, Ar, Italy) RAEP and Luxury Brands Technologies (LBT) (Calenzano, Fi, Italy) HCS, designed to increase the homogeneity of deposited precious metal thicknesses. The thicknesses of each plate were evaluated by XRF analysis at 5 points for each plate: one at the center and four points at all the corners. A Bowman (Schaumburg, IL, USA) BA-100 P series instrument was used.

Italfimet "*Raddrizzatorre Anti Effetto Punta*" (RAEP) aims for the maximum thickness uniformity of precious metal electroplating filling inside the working frame. The principle is based on the supply of a DC, distributed inside the electroplating tanks aimed at minimizing the effect of the presence of areas with high and low current density within the electroplating system, which to date has been inevitable. This is achieved by pre-setting the quantity of continuous current to be distributed in multiple zones within the system itself. In detail, the anodes consist of three anodic elements coated with mixed oxides, which have 3 different anode outputs. Anodes 1 and 3 are the outer ones and have a complementary shape to the inner anode (Figure 6.2 a). The system allows the current of the external anodes to be modulated in the range -999.9 – +100.0, in the upper section of the anode ("high-cut") and in the lower one ("low-cut")

independently. Based on our experience the current is distributed on the three anodes following these rules:

$$i_1 = \frac{i_{tot}(h+1)}{3+h+l}$$
$$i_2 = \frac{i_{tot}}{3+h+l} \quad (6.1)$$
$$i_3 = \frac{i_{tot}(l+1)}{3+h+l}$$

Moreover, $i_1 = 0$ if $h > -1$; $i_3 = 0$ if $l > -1$; $i_1 = i_2 = i_3 = 0$ if $h + l > -3$. Where i_1, i_2, i_3 are respectively the current applied in the upper, center and lower anodes and h and l are respectively the high-cut and the low-cut values. In this work the default parameters provided by the supplier were chosen: high cut of -10.0 and low cut of -30.0. The manufacturing company reports a saving on the cost of the deposition of an average precious metal estimated in the order of 10-15% in addition to a significant reduction in the duration of work cycles related to the deposition of precious metals. This system is applicable to every precious metal deposition system on the market, and it is easily implementable within each galvanic tank [77].

LBT Homogeneous Coating System (HCS) uses a current rectifier "*High Performance System*" (HPS), designed to distribute applied currents according to the different areas of the frame, to be used with a specific system of three anodes associated with three anode outputs (Figure 6.2 b); the central anode has a convex pyramidal shape. The system makes it possible to reduce the differences in current density that can occur between the outer and internal parts of the frame. The current can be modulated for all three electrodes setting the percentages and delays for high, medium and low zones. LBT reports a case study carried out on a palladium bath, in which a reduction of about 11% in mg of metal deposited and a reduction in the standard deviation in measured thicknesses is observed on

minimal thicknesses of 0.8 μm of deposit, evidence of increased homogeneity of the deposit. To confirm the data reported by the suppliers of three-way anode systems, we carried out an empirical validation. In this work the single frame settings given by the supplier [188] were used: percentage high zone 35.0%, percentage medium zone 55.0%, percentage low zone 10.0%, 20 s delay in low area.

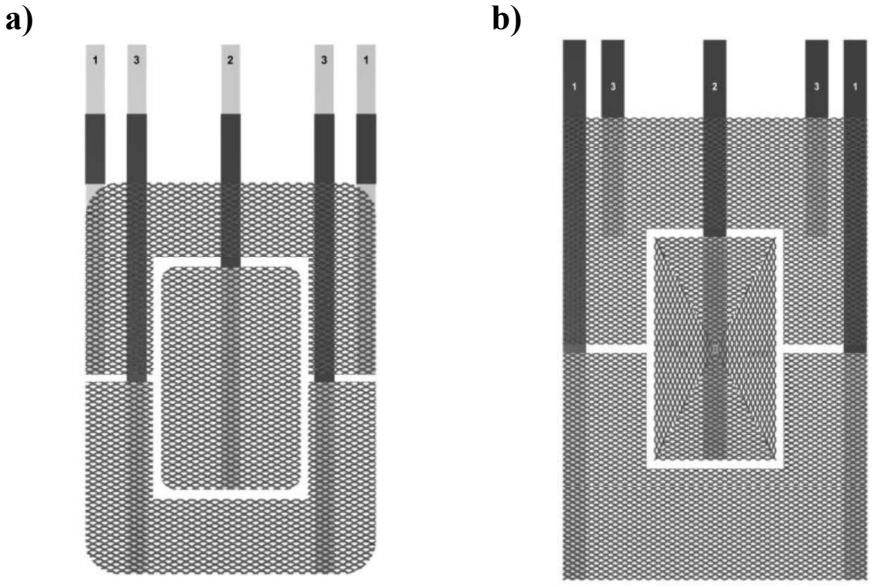

Figure 6.2: Anode schemes of a) Italfimet RAEP system; b) LBT HCS system

The normalized distributions of electrodeposited gold thicknesses are reported in Figure 6.3. As expected, in the centre of each plate there is an area of low deposited thickness, this problem is visibly mitigated in the case of the result obtained by employing the RAEP system.

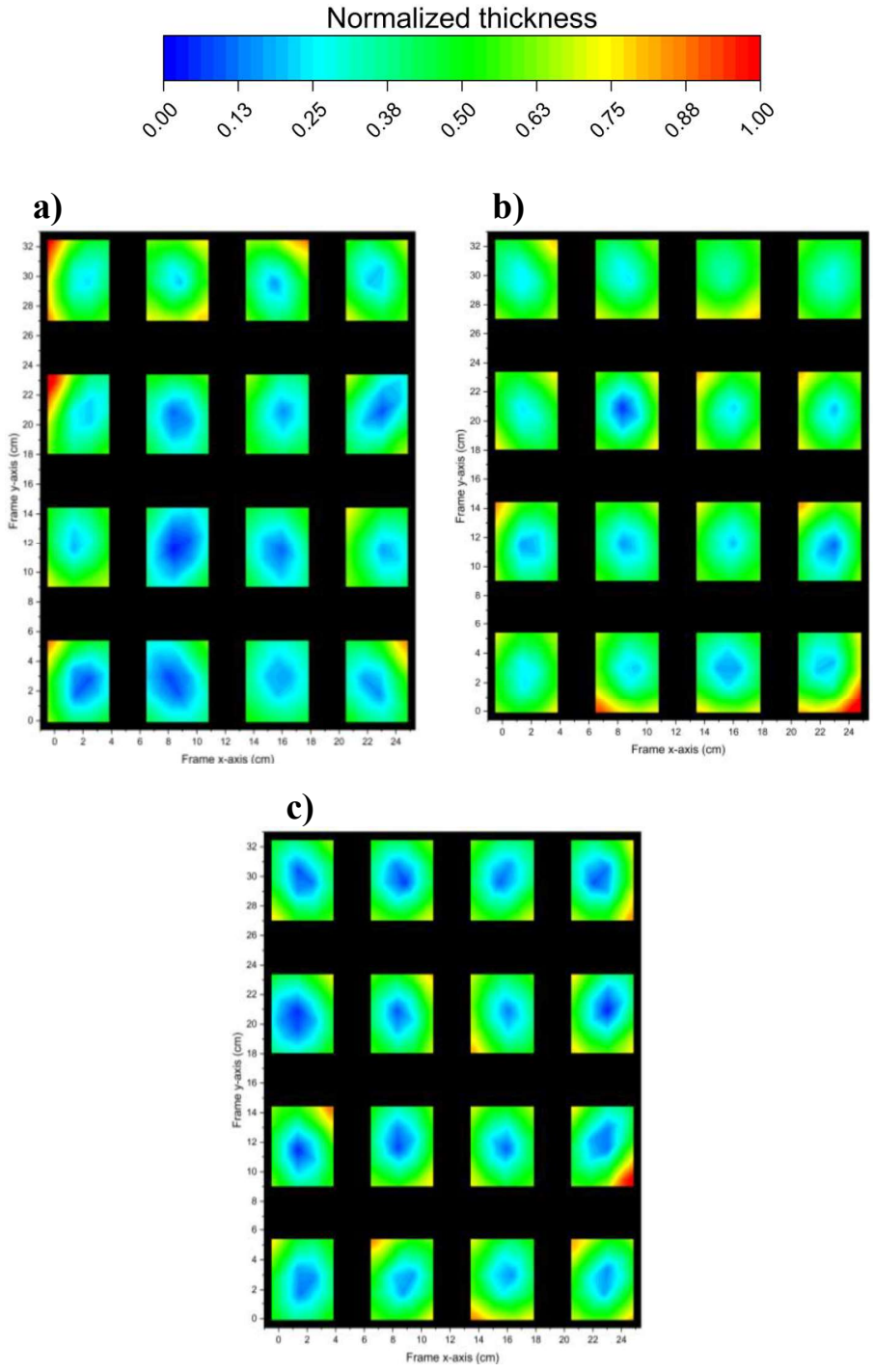

Figure 6.3: Normalized distributions of electrodeposited gold thicknesses relative to the sample obtained a) under standard conditions; b) using the RAEP system; c) using the HCS

These results are confirmed by the standard deviation values obtained on the entire frame (Table 6.1): the RAEP system shows a significant reduction in the standard deviation value, both in terms of absolute and percentage values. The

values obtained in the case of the HCS system are comparable to those obtained in in standard conditions.

Table 6.1: Mean values and standard deviations related to XRF measurements performed on the samples of the entire frame obtained under standard conditions and using the RAEP and HCS systems

	Standard DC1	**RAEP**	**HCS**
Average thickness (µm)	0.57 ± 0.05	0.52 ± 0.05	0.53 ± 0.05
Standard deviation (µm)	0.13	0.09	0.13
Relative Standard deviation %	23.75	18.23	25.46

Further data analysis showed how the RAEP and HCS systems reduce the dispersion of thickness within each plate (Table 6.2).

Table 6.2: Standard deviations of the average thickness of each plate related to XRF measurements made on samples obtained under standard conditions and using the RAEP and HCS systems

	Standard DC1	**RAEP**	**HCS**
Standard deviation of the averages of each plate (µm)	0.05	0.02	0.02
Relative Standard deviation of the averages of each plate (µm)%	9.17	3.03	4.10

Considering this, it can be stated that the RAEP system increases the homogeneity of the deposits throughout the entire frame, allowing to reduce the overall metal used to guarantee the minimum thicknesses required. The HCS system does not decrease the standard deviation relating to all thickness measurements, but reduces the difference observed between the various plates.
To further evaluate the performance of these systems, process capability analyses were carried out. A process capability study predicts whether a manufacturing

process can repeatably produce parts that meet specifications. To make these assessments, the parameters Cp and Cpk were used [189]. Cp (Equation 6.2) measures whether the process spread is narrower than the specification width, hence the potential capacity of the process. While Cpk (Equation 6.3) measures both the centring of the process as well as the spread of the process relative to the specification width, hence actual capacity of the process.

$$C_p = \frac{USL - LSL}{6\sigma} \tag{6.2}$$

$$C_{pk} = Min(\frac{USL - \overline{x}}{3\sigma}; \frac{\overline{x} - LSL}{3\sigma}) \tag{6.3}$$

Where USL and LSL are respectively the customer-defined limits upper and lower process specification customer-defined limits (VOC) and σ is the standard deviation of the process, 0.55 μm was used as the USL and 0.45 μm as the LSL. As observable in Table 6.3, The RAEP system improves the value of Cp over results obtained under standard conditions, while the HCS system returns results comparable to it. The RAEP and HCS systems both allow the improvement of the parameter Cpk (the increase in these parameters is a positive result).

Table 6.3: Evaluation of Cp and Cpk values made on samples obtained under standard conditions and using the RAEP and HCS systems

	Standard DC1	**RAEP**	**HCS**
Cp	0.12	0.18	0.12
Cpk	-0.04	0.11	0.05

6.2.2 Pulsed plating system

The same evaluations performed in the previous section were carried out on the thickness distribution comparing the deposition obtained by operating in DC and PC. To compare the results reported in the literature [127] with the outcomes

shown by three-electrode DC anode systems, we carried out an empirical data validation. The study was performed on a gold deposit, electrodeposited by means of the commercial "Bluclad 8614 MUP" galvanic bath on the previously described plates. This formulation presents the following characteristics: Au 1.1 g/L, Ni 1.6 g/L, In 0.09 g/L, pH (25 °C) 4. The operating conditions were working temperature 36 °C, cathodic current 1 A/dm^2. The depositions were carried out with a duration of 10 minutes. In the case of PC depositions, a pulse current of 2 A/dm^2 was used, with a pulse and pause time equal to 33 ms, maintaining the average current density at 1 A/dm^2. The rectifier used is a commercial rectifier supplied by the company R.C.V. Srl (Altavilla Vicentina, VI, Italy).

Normalized distributions of electrodeposited gold thicknesses are reported in Figure 6.4 6.4. The use of pulsed current improves the overall homogeneity of the thickness of the deposits.

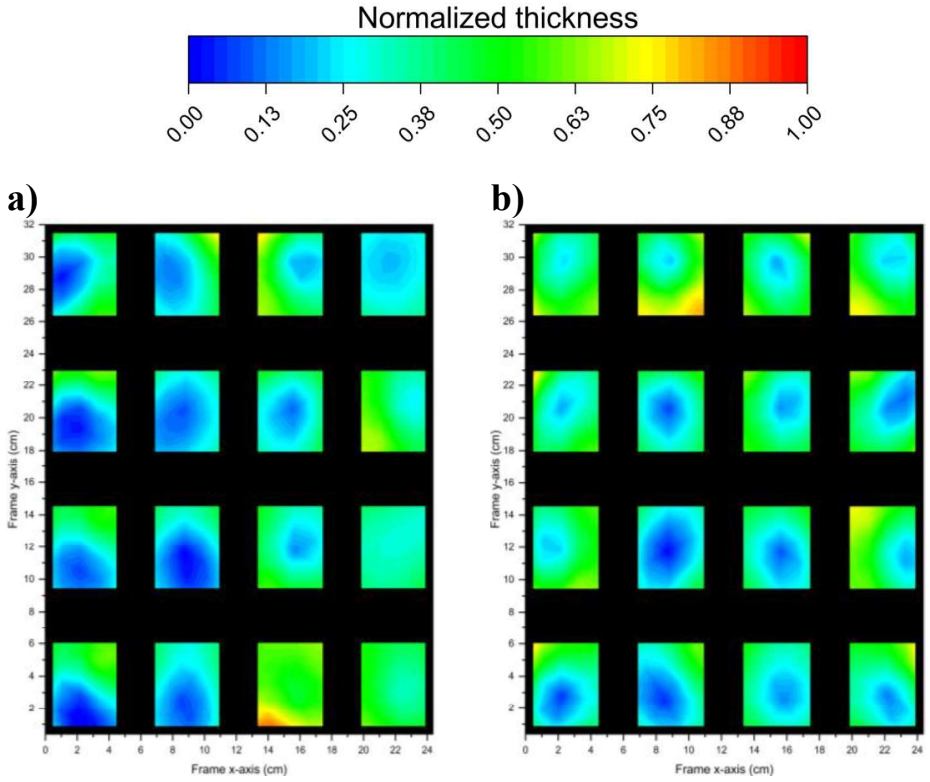

Figure 6.4: Normalized distributions of electrodeposited gold thicknesses relative to the sample obtained a) under standard DC conditions (DC2); b) under PC deposition conditions

As can be assessed from the results shown in Table 6.4, the use of pulsed current reduces the percentage standard deviation.

Table 6.4: Mean values and standard deviations related to XRF measurements made on samples obtained under direct current conditions and under pulsed current conditions

	Standard DC2	**PC**
Average (µm)	0.49 ± 0.05	0.52 ± 0.05
Standard deviation (µm)	0.15	0.15
Relative Standard deviation %	31.66	29.81

It can be stated that the PC system slightly increases the homogeneity of the deposits throughout the entire frame, allowing to reduce the overall metal used to guarantee the minimum thicknesses required.

On the other hand, in Table 6.5 it can be seen how operating in pulsed current in these conditions, slightly increases the standard deviation of the average thickness of each plate.

Table 6.5: Standard deviations of the average thickness of each plate related to XRF measurements made on samples obtained under direct current conditions and under pulsed current conditions

	Standard DC2	**PC**
Standard deviation of the averages of each plate (µm)	0.08	0.09
Relative Standard deviation of the averages of each plate (µm)%	16.36	17.67

An evaluation of the parameters Cp and Cpk was also carried out in this case, the results are shown in Table 6.6.

Table 6.6: Evaluation of Cp and Cpk values made on samples obtained under direct current conditions and under pulsed current conditions

	Standard DC2	**PC**
Cp	0.11	0.11
Cpk	0.08	0.07

The value of Cp improves in the case of PC, while the value Cpk get worse in these conditions, meaning that the PC process still has room for improvement.
Cp and Cpk results, even with improved operating conditions using RAEP, HCS, and PC systems, are still suboptimal. Values of Cp and Cpk equal to 2 should be considered optimal, while values of 1 are considered barely acceptable [189]. However, the distance between optimal values of capability estimators and the results obtained on in-line production processes can be explained how, especially for the high fashion market, customers specifications are made of. Clients only indicate a minimum thickness, not considering the distribution of it and the geometry of the artifact. In the field of high fashion accessories, brands often do not specify the measurement spot causing the approval of the quality control step to be highly influenced by the arbitrariness of the operator. Hence, analytical estimators such as Cp and Cpk, fail to represent the correctness of a process that lacks a profound structuring of demand.
This testifies that the field of electroplating in the high fashion industry shows ample room for improvement, both from an electrochemical-engineering point of view and on the demand side and management of the production process. In the first case working on both anode geometries and current waveforms; and in the second case working on correctly disclosing the issues and physical chemistry behind electrodeposition to line workers.

6.2.3 Corrosion tests

In the literature are present numerous tests to ensure quality control and to verify the performances of the coatings [77], [168]. Among them, neutral salt spray has been chosen to have a benchmark of the systems discussed in this review.

The 4 samples along the diagonal of the galvanic frame were selected, the purpose of this sampling is to evaluate the effects of corrosion as the position in the galvanic frame changes, to correlate the results obtained with those achieved in the previous paragraphs. The samples were tested against neutral salt spray (NSS) test ISO 9227 for 48 h [190]. During this time, the corrosion behaviour of the different coatings was monitored by visual investigation. The samples were visually evaluated by reporting the results with values in the range of 1 to 5, where 5 means no variation occurred on the surface of the sample; 4 slight variation; 3 visible variation; 2 evident variation; 1 considerable variation. This evaluation metric is adopted by major analysis companies in the field of metal accessories of luxury brands [77]. The results are shown in Table 6.7.

Table 6.7: Sample results after NSS test ISO 9227 for 48 h

Standard DC1		**RAEP**		**HCS**	
Sample	**Result**	**Sample**	**Result**	**Sample**	**Result**
DCFE1	4	RAEP1	5	HCS1	3
DCFE2	4	RAEP2	4	HCS2	3
DCFE3	4	RAEP3	5	HCS3	3
DCFE4	5	RAEP4	4	HCS4	3
Average	4.3	**Average**	4.5	**Average**	3

Standard DC2		**Pulsed current**	
Sample	**Result**	**Sample**	**Result**
DC1V	1	PC1	1

DC2V	2	PC2	4
DC3V	2	PC3	3
DC4V	1	PC4	3
Average	1.5	**Average**	2.8

The results obtained using the RAEP system led to an improvement over the one obtained operating under the standard conditions; on the other hand, the use of the HCS system led to a worsening of the results. However, it is important to note that the results obtained using the latter operating conditions resulted in more homogeneous outputs, this agrees with the results obtained during the evaluation of thicknesses. Depositions using pulsed current resulted in a marked increase in corrosion resistance performance.

Given the results observed in the previous paragraph, where we pointed out that the PC system slightly increases the homogeneity of the deposits throughout the entire frame, we can hypothesize that such a marked change in corrosion resistance with respect to a slightly different homogeneity is due to other factors that come into play using pulsed current, such as a change in the chemical-physical structure of the deposit compared with that obtained under direct current conditions. As reported in the literature the use of pulsed current can lead to changes in the morphology of the structure of the deposit [126]. This result is very interesting because it highlights the possibility of obtaining deposits that exhibit greater corrosion resistance for the same amount of precious metal used, with clear advantages both economically and environmentally.

6.3 Computational methods

Despite many attempts by the decorative industry to improve the sustainability [191] of an electroplating plant by optimizing the whole process are accomplished by companies, the R&D process for the optimization of the

numerous variables is still based on a trial-and-error method. In this scenario, *in-silico* procedures are trending as the cut-and-try approach could be translated from the production plant to a chip, or even avoided introducing predictions and systematic studies. Furthermore, *in-silico* approaches are in line with the sustainable model proposed in Agenda 2030 by United Nations [192]. Specifically, three sustainable developments goals (SDG) are achievable: 3 (good health and well-being), 8 (decent work and economic growth) and 10 (reduced inequalities). SDG 3 is related to the reduction and, possibly, the elimination of hazardous in the R&D phase, moreover the prediction and development of new green processes is fundamental to ensure a healthy working environment in production departments. Shifting the workplace from a laboratory to a computer ensures people with motor-related impairments to express their full creative potential, as they are no longer limited by structural barriers, accomplishing SDG 8 and 10. To model an electrochemical process it is helpful to distinguish two different families of simulations depending on the scale: atomistic simulations [193] and multiphysics simulations [194]. The latter are divided further in *ab-initio* and classical approaches, the first one based on quantomechanic calculations and the second one on classical mechanics.

6.3.1 Atomistic simulations

Atomistic simulations are used to design new sustainable additives and to understand the interactions among bath components such as ions and organic molecules [195], [196]. Although promising, they are still mainly applied in academic research due to the need for high-performance computing resources [197] and detailed knowledge of the underlying physicochemical phenomena.
Molecular systems can be treated using Molecular Mechanics (MM), Quantum Mechanics (QM), or hybrid QM/MM frameworks. In MM, molecules are

modeled as atoms linked by springs, following Newtonian mechanics. The total system energy is represented by the Hamiltonian:

$$H_{MM} = K_{MM} + V_{MM} \tag{6.4}$$

With potential energy expressed through "force fields" that define bond stretching, bending, torsional, electrostatic, and van der Waals interactions [198], [199], [200], [201]. MM has low computational cost and is widely used to simulate large systems, including the adsorption of additives and impurities in electroplating baths [202], [203], [204].

Conversely, QM methods describe molecules at the electronic level using the Schrödinger equation [205]:

$$\hat{H}_{QM}\Psi = E\Psi \tag{6.5}$$

These include wavefunction-based methods (Hartree-Fock, post-HF) and Density Functional Theory (DFT) approaches. Although post-HF methods offer higher accuracy [206], they are computationally expensive; hence, DFT and hybrid-DFT are the preferred compromise for electrochemical simulations. Ab-initio studies have elucidated the interaction of additives with Cu(111) surfaces [207] and the performance of novel suppressors in copper baths [208].

To simulate large electrolyte systems, QM/MM hybrid methods can be employed, where a defined active region is treated quantum-mechanically, and the surrounding environment classically [209], [210]. The overall Hamiltonian combines the strengths of both methods:

$$\hat{H}_{QM/MM} = \hat{H}_{QM} + \hat{H}_{MM} + \hat{H}_{QM-MM} \tag{6.6}$$

Although more common in biochemistry [211], QM/MM methodologies can be adapted to electrodeposition, enabling cost-effective yet detailed simulations.

6.3.2 Multiphysics simulations

Multiphysics approaches, based on fluid dynamics simulations, are a reliable tool to understand how the design of manufacts and anodes can influence the thickness distribution due an inhomogeneous current density distribution, even using ordinary computers. In decorative electroplating, where product design often prioritizes aesthetics over manufacturability, sharp edges, cusps, and valleys cause significant current density variations that lead to non-uniform coatings [212].

An example of a complex accessory can be appreciated in Figure 6.5, it was electroplated following the industrial standard for an hypoallergenic cycle (ISO 1811 [213]) - made of Copper/White Bronze/Palladium-Nickel/Gold, where copper is used as leveller and brightener layer [214], white bronze and palladium as anticorrosion [215] and barrier layer against intermetallic diffusion [216] - exhibit thickness variations correlated with geometric features. SEM analysis confirms that morphology strongly influences deposition uniformity.

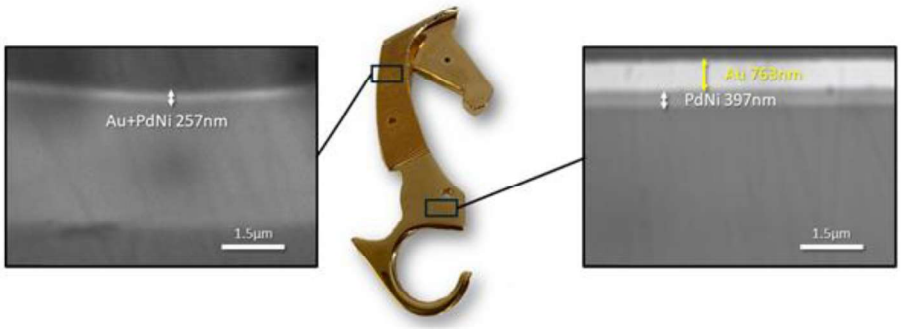

Figure 6.5: Fashion accessories presenting a complex geometry made of many cusps and valleys to represent a horse crest; the difference in deposited thicknesses of precious metals on a plain part and inside a valley observing the cross section of the sample by a scanning electron microscopy (SEM) analysis

CFD-based models describe the electrochemical system using coupled physical equations:

- Continuity and momentum conservation are expressed by the Navier–Stokes equations (Equations 6.7 and 6.8) with velocity (u), dynamic viscosity (μ), density (ρ), and pressure (P) as key parameters [217], [218], [219].

$$\nabla \cdot \boldsymbol{u} = 0 \tag{6.7}$$

$$\frac{\partial \mathbf{u}}{\partial \mathrm{t}} + \nabla \cdot (\mathbf{u} \times \mathbf{u}) - \nabla \cdot (\mu \nabla \mathbf{u}) = -\frac{1}{\rho} \nabla \mathrm{P} + \mathbf{N} \tag{6.8}$$

- Electroneutrality is enforced by Equation 6.9, and ionic transport is modeled through the Nernst–Planck equation (Equation 6.10), accounting for diffusion, migration, and convection [220], [221], [222].

$$\sum \mathrm{n_i c_i} = 0 \tag{6.9}$$

$$\mathbf{J_i} = -\mathrm{D_i} \cdot \nabla \mathrm{c_i} - \frac{\mathrm{D_i n_i F}}{\mathrm{RT}} \mathrm{c_i} \cdot \nabla \phi + \mathrm{c_i} \cdot \mathbf{u} \tag{6.10}$$

- Electrode kinetics are governed by the Butler–Volmer equation (Equation 6.11) [223], while the Faraday law (Equation 6.12) defines the local deposition rate and resulting thickness distribution on the cathode.

$$\mathrm{i} = \mathrm{i_0} \left[\left(\frac{\mathrm{C_0}(0,\mathrm{t})}{\mathrm{C_0^{bulk}}} \right) e^{-\alpha \mathrm{nF} \eta \cdot \frac{1}{\mathrm{T}}} - \left(\frac{\mathrm{C_R}(0,\mathrm{t})}{\mathrm{C_R^{bulk}}} \right) e^{\beta \mathrm{nF} \eta \cdot \frac{1}{\mathrm{T}}} \right] \tag{6.11}$$

$$\frac{\partial \tau}{\partial t} = \mathrm{i} \frac{\mathrm{M_w}}{\rho_\mathrm{m} \mathrm{nF}} \tag{6.12}$$

Solving these coupled differential equations through the Finite Element Method (FEM) [224], [225], [226], [227] allows realistic predictions of current and thickness distributions over complex surfaces. Software such as COMSOL

Multiphysics [228] and OpenFOAM [229] enable direct import of CAD geometries for simulation of decorative or electroforming processes. Kauffman [230] successfully modeled copper electrodeposition with OpenFOAM, while Huang [231] later developed a framework accounting for multiple ionic species, external forces, and magnetic field effects.

By integrating designers, engineers, and chemists within this computational workflow, sustainable manufacturing can be achieved. Designers create optimized geometries; engineers validate mechanical feasibility; and chemists determine and validate electrochemical parameters (exchange current, overpotential, symmetrical factors) through experimental measurements such as (XRF).

Ultimately, multiphysics simulations represent a powerful tool for reducing precious metal waste, production time, and energy consumption, enabling sustainable, data-driven, and collaborative innovation in the electroplating industry [232].

6.4 Recovery of metals

Exponential growth of world's population and limited natural resources are causing new challenges. Pollution prevention, waste minimization and the recycling of end-of-life products (EOL products) have become primary interest topics [67]. Sustainable development in the metallurgical and decorative industries aims to maximize material reuse, minimize energy consumption, and achieve upcycling through efficient management of resources. However, industrialization continues to generate large quantities of solid and liquid waste, particularly in developing countries, leading to severe environmental consequences due to toxic inorganic pollutants and heavy metals [233].

The most significant solid waste materials contain non-ferrous metals such as copper, nickel, gold, molybdenum, zinc, chromium and others, as potential heavy metals.

Heavy metals are elements having atomic weights between 63.5 and 200.6, and a density higher than 5 g/cm^3, characterized by high stability but low levels of biodegradability [68], [69], which lead to bioaccumulation and biomagnification in living organisms, causing long-term damage to ecosystems and human health [236]. According to the United State Environmental Protection Agency (USEPA) standards [237] metals such as cadmium, chromium, and lead have strict maximum contaminant limits (MCLs) in wastewater due to their carcinogenic and toxic effects. Excessive exposure to these metals may result in cancer, organ failure, neurological disorders, and death.

From an industrial perspective, copper, nickel, zinc, and gold represent the most relevant metals both for production and environmental impact. Approximately 75% of copper is used in electronics, communications, and energy applications [238], all crucial sectors in the ecological transition. However, excessive copper intake can cause serious toxicological effects [73].

Zinc, while essential to human health, can be harmful in excess [240]; half of its global production is used for anti-corrosion coatings, while 30% is employed in brass and other alloys [241].

Nickel, mainly used in stainless steel and superalloys [242], is a recognized human carcinogen [234], [243].

Gold, though not limited by EPA regulations, has toxic effects when used therapeutically [244] and is responsible for significant environmental and social issues related to its mining [146]. The mining industry contributes about 19 million tons of sulfur dioxide annually (13% of global emissions), driving acid rain and air pollution [245]. Precious metal extraction consumes 7–10% of the world's annual energy and generates massive waste: 6 billion tons in 2010 alone,

mainly from gold, iron, and copper mining [246]. Consequently, recycling has become a strategic pillar of sustainability, enabling energy savings, CO_2 reduction, and resource conservation [247].

For example, producing one ton of usable gold results in 300,000 tons of waste, meaning a single wedding ring generates roughly 3 tons of mine tailings and uses 50–150 g of mercury [248]. Mercury's persistence in the environment causes bioaccumulation and severe health effects in nearby populations. Additionally, gold mining often leads to illegal land appropriation, child labor, and unsafe working conditions, affecting over 10 million miners, including 1 million children [236]

In response, Fairtrade certification promotes ethical gold mining, emphasizing legal operations, fair wages, gender equality, and environmentally responsible practices that align with the UN Sustainable Development Goals (SDGs)—specifically SDGs 1, 3, 5, 8, 10, 12, 13, and 15 [249]. Ethical gold mining minimizes mercury use and prioritizes the protection of local communities. As Lezak (Oxford University) notes, global gold demand could be fully met through recycling, which would reduce air emissions and ecosystem impact by 99%, with the remaining 1% attributed only to transport and processing [250].

Optimizing recovery solutions indeed opens up new paths in research field, considering growing demand, resources depletion and global need of development. Precious metals resulted after the recovery processes have the same properties, even after multiple life cycles, therefore recycling allows:

- recovery of the valuable material without quality loss
- energy saving in comparison with primary production
- reducing resulted emissions and reducing greenhouse gas emissions
- reduction of mining activities
- reducing waste

Industrialized countries are therefore shifting toward long-term sustainable policies emphasizing innovation, cleaner technologies, and environmental protection. These strategies directly support SDGs 9 (Industry, Innovation and Infrastructure), 11 (Sustainable Cities and Communities), and 12 (Responsible Consumption and Production).

Among the most polluting sectors, the electroplating industry is recognized as one of the most hazardous due to the discharge of metal-contaminated wastewater [251].

Rinsing operations in plating plants generate effluents containing up to 20% of the chemicals used in baths [252], [253], [254]. These effluents often exceed the USEPA Industrial Effluent Guidelines [255] and must therefore be treated before release [251]. However, in precious-metal plating (e.g., Ag, Au, Pt), the wastewater contains recoverable quantities of valuable metals, making combined treatment and recovery systems both environmentally and economically desirable [253].

A wide range of wastewater treatment technologies has been developed, including chemical precipitation, coagulation–flocculation, flotation, ion exchange, and membrane filtration. Each offers distinct advantages and limitations.

Electrochemical methods, such as electrodialysis [256], membrane electrolysis [257] and electrochemical precipitation [258] provide high metal removal efficiency and low sludge generation but remain costly due to energy requirements.

In general, physicochemical treatments are fast, flexible, and space-efficient, accommodating variable waste compositions. However, they suffer from high operational and chemical costs and sludge management challenges. Efforts to employ low-cost adsorbents and sludge minimization techniques have improved their viability for inorganic effluents [236]. Electrochemical treatments stand out

for their precision, reduced reagent use, and minimal sludge production, though high capital and energy costs currently limit industrial adoption [234].

Table 6.8 summarizes the main advantages and disadvantages of the various treatments for electroplating wastewater.

Table 6.8: Different treatment techniques for wastewater and their advantages and disadvantages

Type of treatment	Advantages	Disadvantages
Chemical precipitation	Low capital cost, simple operation	Sludge generation, extra operational cost for sludge disposal
Coagulation–flocculation	Shorter time to settle out suspended solids, improved sludge settling	Sludge production, extra operational cost for sludge disposal
Dissolved air flotation	Low cost, shorter hydraulic retention time	Subsequent treatments are required to improve the removal efficiency of heavy metal
Ultrafiltration	Smaller space requirement	High operational cost, prone to membrane fouling
Nanofiltration	Low pressure than RO (7-30 bar)	Costly, prone to membrane fouling
Reverse osmosis	High rejection rate, able to withstand high temperature	High energy consumption due to high pressure required (20–100 bar), susceptible to membrane fouling
Ion exchange	No sludge generation, less time consuming	Not all ion exchange resin is suitable for metal removal, high capital cost
Adsorption	Low-cost, easy operating conditions, having wide pH range, high metal binding capacities	Low selectivity, production of waste products
Electrodialysis	High separation selectivity	High separation operational cost due to membrane fouling and energy consumption
Membrane electrolysis	Use over a wide range of metal concentrations	High energy consumption
Electrochemical precipitation	Fewer chemicals, acidic or basic conditions	Sludge production
Photocatalysis	Removal of metals and organic pollutants	Long duration time, limited applications

simultaneously, less harmful by-products

Among the treatments presented in the table, no single technology provides a universal solution. Therefore, selecting an appropriate treatment depends on metal concentration, economic feasibility, environmental impact, and plant reliability. Ultimately, the most effective wastewater management system must balance technical applicability, simplicity, and cost-effectiveness to meet both environmental regulations and sustainability goals.

6.5 Conclusions

For over two decades, sustainability in the plating industry has been one of the key concerns of the industry. This makes it critical for the industry to assess the entire sustainability of virtually every plating facilities and then come up with both short-term and long-term approaches for improving sustainability performance. In this article, we discussed three different but complementary lines of actions to improve sustainability in Agenda 2030 SDGs optic of the electroplating industry, especially in non-mandatory fields such as the decorative one. Either different plating techniques, in-silico simulations and the metal recovery are linked to each other in minimizing the material usage and, consequently, metal extraction. The principal SDGs addressed by all of them are the SDG 8 (decent work and economic growth), SDG 10 (reduce inequalities), SDG 12 (responsible consumption and production), SDG 13 (climate action). Despite that, to reach good sustainability standards there is a lot of work to be done. It is fundamental to fashion designers to take care of the whole production processes, thinking out of the schemes for new sustainable geometries and for industries to embrace simulations to test them. Hence, deposition techniques should improve by trying to merge AC properties with three ways rectifiers engineering and calibrate the deposition parameters with analytical techniques

such as spectroscopies. Furthermore, electroplating facilities are needed to dedicate forces to select and optimize recovery methods according to their specific internal needs.

7 Final Remarks

The research presented in this doctoral thesis aimed to deepen the understanding of pulsed current electrodeposition applied to metallic coatings used in decorative electroplating for fashion and luxury goods sector. Through a systematic and multidisciplinary approach that combines electrochemistry, materials science and process engineering, this study explored both the scientific foundations and the industrial implications of current modulation in electrodeposition processes.

The work focused on four metallic systems that represent the backbone of decorative electroplating: alkaline copper, acid copper, palladium and gold. Each of these metals was examined under both direct current and pulsed current conditions in order to determine how waveform parameters - such as amplitude, frequency, and duty cycle - affect the resulting deposit in terms of morphology, composition and physical properties. Despite the different electrochemical behaviors of these metals, the results reveal a consistent trend: pulsed current electrodeposition provides tangible improvements in coating quality when properly optimized.

For copper, both in its alkaline and acid formulations, the adoption of current modulation led to deposits characterized by enhanced compactness, reduced nodularity and more uniform grain size. The improved control over nucleation and growth processes resulted in smoother and brighter surfaces, with better leveling and reduced internal stress compared to direct current deposition. Palladium, often employed as an intermediate layer or as a nickel substitute, exhibited a significant reduction in porosity and an improvement in corrosion resistance when deposited under pulsed current conditions. By carefully adjusting the duty cycle and frequency, it was possible to tailor its microstructure and surface texture, allowing a decrease in the amount of precious metal required while maintaining high aesthetic and functional performance.

Finally, for gold, which represents the most valuable and visually critical coating in the decorative industry, current modulation proved to be an effective means to enhance brightness, reflectivity and mechanical stability. The optimized pulsed current parameters enabled the deposition of thinner yet more compact layers, contributing to material and economic sustainability without compromising aesthetic appeal.

From an industrial perspective, this work demonstrates that, although direct current remains the prevailing standard in decorative electroplating, pulsed current represents a viable and forward-looking evolution of the process. Its implementation at a larger scale has traditionally been hindered by the complexity of power control systems, the difficulty of optimizing parameters for different baths and the need to ensure process reproducibility. However, recent developments in digital rectifiers, advanced process control and automated monitoring systems are progressively removing these limitations, paving the way for a wider adoption of current modulation in decorative applications.

Another key contribution of this research lies in bridging the gap between empirical practice and scientific understanding. By combining electrochemical analysis with surface characterization techniques such as SEM, XRD and colorimetric evaluation, it was possible to establish direct correlations between electrical parameters and deposit properties. This approach transforms what has long been a craft-based process into a data-driven and knowledge-based methodology, enhancing predictability and reproducibility.

Equally significant is the contribution of this work to sustainability in the electroplating industry. The results demonstrate that the optimization of pulsed current parameters can effectively reduce the consumption of precious metals such as gold and palladium while maintaining or even improving coating performance. The use of thinner yet more compact layers lead to reduced waste

and lower environmental impact, aligning with the broader objectives of green chemistry, resource efficiency and circular manufacturing.

In conclusion, this doctoral research provides a comprehensive framework for understanding and optimizing pulsed current electrodeposition in the decorative sector. By uniting theoretical modeling, experimental validation and industrial application, it offers new insights into how process parameters influence the chemical, physical and aesthetic properties of metallic coatings. The findings not only contribute to the scientific advancement of electrochemical deposition but also offer practical guidelines for improving sustainability and efficiency in industrial galvanic production.

Looking ahead, the integration of real-time monitoring, artificial intelligence and predictive control algorithms may further enhance the precision and adaptability of pulsed electroplating processes, extending their application to new materials and substrates. The outcomes of this thesis thus represent a significant step toward a more technologically advanced, economically efficient and environmentally responsible decorative electroplating industry.

8 References

[1] Y. D. Gamburg and G. Zangari, *Theory and Practice of Metal Electrodeposition*. 2011. doi: 10.1007/978-1-4419-9669-5.

[2] M. S. Chandrasekar and M. Pushpavanam, "Pulse and pulse reverse plating-Conceptual, advantages and applications," *Electrochim. Acta*, vol. 53, no. 8, pp. 3313–3322, 2008, doi: 10.1016/j.electacta.2007.11.054.

[3] N. V. Mandich, "Pulse and pulse-reverse electroplating," *Metal Finishing*, vol. 97, no. 1, pp. 382–387, 2002, doi: 10.1016/s0026-0576(99)80039-7.

[4] P. Kurzweil, "Electrochemical Double-layer Capacitors," in *Electrochemical Energy Storage for Renewable Sources and Grid Balancing*, Elsevier, 2015, pp. 345–407. doi: 10.1016/B978-0-444-62616-5.00019-X.

[5] Mordechay Schlesinger and Milan Paunovic, *Modern Electroplating*. Wiley, 2010. doi: 10.1002/9780470602638.

[6] J.-C. Puippe and F. Leaman, *Theory and Practice of Pulse Plating*. Orlando, 2022.

[7] J. Cl. Puippe and N. Ibl, "Influence of charge and discharge of electric double layer in pulse plating," *J. Appl. Electrochem.*, vol. 10, no. 6, pp. 775–784, Nov. 1980, doi: 10.1007/BF00611281.

[8] J.-C. Puippe, "Guidelines for setting the useful range of pulse plating parameters," *Transactions of the IMF*, vol. 96, no. 5, pp. 244–252, Sep. 2018, doi: 10.1080/00202967.2018.1501907.

[9] J. E. Greene, "Tracing the 5000-year recorded history of inorganic thin films from ~3000 BC to the early 1900s AD," *Appl. Phys. Rev.*, vol. 1, no. 4, p. 041302, Dec. 2014, doi: 10.1063/1.4902760.

[10] C. Raub, "The history of electroplating," in *Metal Plating and Patination*, Elsevier, 1993, pp. 284–290. doi: 10.1016/B978-0-7506-1611-9.50027-3.

[11] L. B. Hunt, "The early history of gold plating," *Gold Bull.*, vol. 6, no. 1, pp. 16–27, Mar. 1973, doi: 10.1007/BF03215178.

[12] M. Innocenti, W. Giurlani, M. Passaponti, A. De Luca, and E. Salvietti, "Electrodeposition and innovative characterization of precious metal alloys for the Galvanic and Jewel industry," in *Substantia*, vol. 3, 2019, pp. 29–37.

[13] G. Elkington and H. Elkington, "Improvements in Coating, Covering, or Plating certain Metals," 8447, 1840

[14] B. Abner and E. R. Grace, “Nickel plating by chemical reduction ,” 2532283, 1950

[15] D. Antuña-Jiménez, G. Díaz-Díaz, M. C. Blanco-López, M. J. Lobo-Castañón, A. J. Miranda-Ordieres, and P. Tuñón-Blanco, “Molecularly Imprinted Electrochemical Sensors,” in *Molecularly Imprinted Sensors*, Elsevier, 2012, pp. 1–34. doi: 10.1016/B978-0-444-56331-6.00001-3.

[16] C. P. Horwitz, N. Y. Suhu, and G. C. Dailey, “Synthesis, characterization and electropolymerization of ferrocene monomers with aniline and phenol substituents,” *Journal of Electroanalytical Chemistry*, vol. 324, no. 1–2, pp. 79–91, Feb. 1992, doi: 10.1016/0022-0728(92)80037-5.

[17] P. S. Sharma, A. Pietrzyk-Le, F. D’Souza, and W. Kutner, “Electrochemically synthesized polymers in molecular imprinting for chemical sensing,” *Anal. Bioanal. Chem.*, vol. 402, no. 10, pp. 3177–3204, Apr. 2012, doi: 10.1007/s00216-011-5696-6.

[18] T. Yoshida *et al.*, “Electrodeposition of Inorganic/Organic Hybrid Thin Films,” *Adv. Funct. Mater.*, vol. 19, no. 1, pp. 17–43, Jan. 2009, doi: 10.1002/adfm.200700188.

[19] A. P. Abbott, F. Endres, and D. R. Macfarlane, “Why Use Ionic Liquids for Electrodeposition?,” in *Electrodeposition from Ionic Liquids*, Wiley, 2017, pp. 1–15. doi: 10.1002/9783527682706.ch1.

[20] Q. Zhang, Q. Wang, S. Zhang, X. Lu, and X. Zhang, “Electrodeposition in Ionic Liquids,” *ChemPhysChem*, vol. 17, no. 3, pp. 335–351, Feb. 2016, doi: 10.1002/cphc.201500713.

[21] M. Armand, F. Endres, D. R. MacFarlane, H. Ohno, and B. Scrosati, “Ionic-liquid materials for the electrochemical challenges of the future,” *Nat. Mater.*, vol. 8, no. 8, pp. 621–629, Aug. 2009, doi: 10.1038/nmat2448.

[22] D. Tench and J. White, “Enhanced tensile strength for electrodeposited nickel-copper multilayer composites,” *Metallurgical Transactions A*, vol. 15, no. 11, pp. 2039–2040, Nov. 1984, doi: 10.1007/BF02646838.

[23] J. Yahalom and O. Zadok, “Formation of composition-modulated alloys by electrodeposition,” *J. Mater. Sci.*, vol. 22, no. 2, pp. 499–503, Feb. 1987, doi: 10.1007/BF01160760.

[24] H. S. Kang *et al.*, “Smart manufacturing: Past research, present findings, and future directions,” *International Journal of Precision Engineering and*

Manufacturing-Green Technology, vol. 3, no. 1, pp. 111–128, Jan. 2016, doi: 10.1007/s40684-016-0015-5.

[25] M. I. Marcus and et all, "Recovery of galvanic sludge by physicochemical mechanisms," *Journal of Environmental Protection and Ecology*, vol. 18, pp. 1117–1126, 2017.

[26] E. Bertorelle, *Trattato di galvanotecnica*. 1960.

[27] P.paracchini, *Manuale di trattamenti e finiture*. 2003.

[28] C. L. Siu, H. C. Man, and C. H. Yeung, "Electrodeposition of Co–Mo–P barrier coatings for Cu/Au coated systems," *Surf. Coat. Technol.*, vol. 200, no. 7, pp. 2223–2227, Dec. 2005, doi: 10.1016/j.surfcoat.2004.07.125.

[29] J. J. López-García, J. Horno, and C. Grosse, "Poisson–Boltzmann Description of the Electrical Double Layer Including Ion Size Effects," *Langmuir*, vol. 27, no. 23, pp. 13970–13974, Dec. 2011, doi: 10.1021/la2025445.

[30] F.-Y. Shen, W.-P. Dow, A.-H. Liu, J.-Y. Lin, P.-H. Chang, and S.-M. Huang, "Periodic Pulse Reverse Cu Plating for Through-Hole Filling," *ECS Electrochemistry Letters*, vol. 2, no. 5, pp. D23–D25, 2013, doi: 10.1149/2.003305eel.

[31] N. Ibl, "Some theoretical aspects of pulse electrolysis," *Surface Technology*, vol. 10, no. 2, pp. 81–104, Feb. 1980, doi: 10.1016/0376-4583(80)90056-4.

[32] CG Zoski, *Handbook of electrochemistry*. 2006.

[33] J. W. Dini and D. D. Snyder, "Electrodeposition of Copper," in *Modern Electroplating*, Hoboken, NJ, USA: John Wiley & Sons, Inc., 2011, pp. 33–78. doi: 10.1002/9780470602638.ch2.

[34] A. Ibañez and E. Fatás, "Mechanical and structural properties of electrodeposited copper and their relation with the electrodeposition parameters," *Surf. Coat. Technol.*, vol. 191, no. 1, pp. 7–16, Feb. 2005, doi: 10.1016/j.surfcoat.2004.05.001.

[35] T. A. Green and S. Roy, "Application of a duplex diffusion layer model to pulse reverse plating," *Transactions of the Institute of Metal Finishing*, vol. 95, no. 1, pp. 46–51, 2017, doi: 10.1080/00202967.2016.1214354.

[36] M. Vizza *et al.*, "Electrodeposition of Cu on PEDOT for a Hybrid Solid-State Electronic Device," *Surfaces*, vol. 4, no. 2, pp. 157–168, May 2021, doi: 10.3390/surfaces4020015.

[37] W. Giurlani, M. Vizza, A. A. Leonardi, M. J. Lo Faro, A. Irrera, and M. Innocenti, “Optimization and Characterization of Electrodeposited Cadmium Selenide on Monocrystalline Silicon,” *Nanomaterials*, vol. 12, no. 4, p. 610, Feb. 2022, doi: 10.3390/nano12040610.

[38] W. Giurlani *et al.*, “Electrodeposition of Nanoparticles and Continuous Film of CdSe on n-Si (100),” *Nanomaterials*, vol. 9, no. 10, p. 1504, Oct. 2019, doi: 10.3390/nano9101504.

[39] C. Kaiser and W. Fleischer, “Reverse pulse plating for decorative copper plating,” *Galvanotechnik*, no. 4, pp. 851–860, 2007.

[40] E. M. Dela Pena and S. Roy, “Electrodeposited copper using direct and pulse currents from electrolytes containing low concentration of additives,” *Surf. Coat. Technol.*, vol. 339, pp. 101–110, Apr. 2018, doi: 10.1016/j.surfcoat.2018.01.067.

[41] K. I. Popov, M. D. Maksimović, B. M. Ocokoljić, and B. J. Lazarević, “Fundamental aspects of pulsating current metal electrodeposition I: The effect of the pulsating current on the surface roughness and the porosity of metal deposits,” *Surface Technology*, vol. 11, no. 2, pp. 99–109, Aug. 1980, doi: 10.1016/0376-4583(80)90024-2.

[42] T. A. Green, X. Su, and S. Roy, “Pulse Electrodeposition of Copper in the Presence of a Corrosion Reaction,” *J. Electrochem. Soc.*, vol. 168, no. 6, p. 062515, Jun. 2021, doi: 10.1149/1945-7111/ac0a21.

[43] B.-C. Huang, C.-H. Yang, C.-Y. Lee, Y.-L. Hu, C.-C. Hsu, and C.-E. Ho, “Effect of pulse-reverse plating on copper: Thermal mechanical properties and microstructure relationship,” *Microelectronics Reliability*, vol. 96, pp. 71–77, May 2019, doi: 10.1016/j.microrel.2019.04.004.

[44] C. Shanthi, S. Barathan, R. Jaiswal, R. M. Arunachalam, and S. Mohan, “The effect of pulse parameters in electro deposition of silver alloy,” *Mater. Lett.*, vol. 62, no. 30, pp. 4519–4521, Dec. 2008, doi: 10.1016/j.matlet.2008.08.032.

[45] M. J. Kim, S. K. Cho, H.-C. Koo, T. Lim, K. J. Park, and J. J. Kim, “Pulse Electrodeposition for Improving Electrical Properties of Cu Thin Film,” *J. Electrochem. Soc.*, vol. 157, no. 11, p. D564, 2010, doi: 10.1149/1.3481564.

[46] C. Ma, H. He, F. Xia, and M. Cao, “Effect of Pulse Electrodeposition Mode on Microstructures and Properties of Ni-TiN Composite Coatings,”

Coatings, vol. 14, no. 11, p. 1384, Oct. 2024, doi: 10.3390/coatings14111384.

[47] S. J. MacHardy and L. J. J. Janssen, "The diffusion coefficient of Cu(II) ions in sulfuric acid–aqueous and methanesulfonic acid–methanol solutions," *J. Appl. Electrochem.*, vol. 34, no. 2, pp. 169–174, Feb. 2004, doi: 10.1023/B:JACH.0000009956.75577.ef.

[48] J. Bauer and M. Moats, "Effective Copper Diffusion Coefficients in CuSO4–H2SO4 Electrowinning Electrolytes," 2020, pp. 1237–1247. doi: 10.1007/978-3-030-36296-6_114.

[49] W. E. G. Hansal, S. Roy, P. Leisner, T. Green, and A. Reichenbach, *Pulse Plating*, First Edit. Eugen G. Leuze Verlag KG, 2012.

[50] Ch. J. Raub and A. Knödler, "The electrodeposition of gold by pulse plating," *Gold Bull.*, vol. 10, no. 2, pp. 38–44, Jun. 1977, doi: 10.1007/BF03215426.

[51] H. Karami and H. Babaei, "Electroplating Nanostructured Hard Gold through the Pulse Galvanostatic Method," *Int. J. Electrochem. Sci.*, vol. 7, no. 1, pp. 601–614, Jan. 2012, doi: 10.1016/S1452-3981(23)13362-1.

[52] M. J. Kim, T. Lim, K. J. Park, S. K. Cho, S.-K. Kim, and J. J. Kim, "Characteristics of Pulse-Reverse Electrodeposited Cu Thin Films," *J. Electrochem. Soc.*, vol. 159, no. 9, pp. D538–D543, Jan. 2012, doi: 10.1149/2.045209jes.

[53] N. D. Nikolić, G. Branković, V. M. Maksimović, M. G. Pavlović, and K. I. Popov, "Application of pulsating overpotential regime on the formation of copper deposits in the range of hydrogen co-deposition," *Journal of Solid State Electrochemistry*, vol. 14, no. 2, pp. 331–338, Feb. 2010, doi: 10.1007/s10008-009-0842-1.

[54] N. Tantavichet and M. D. Pritzker, "Effect of plating mode, thiourea and chloride on the morphology of copper deposits produced in acidic sulphate solutions," *Electrochim. Acta*, vol. 50, no. 9, pp. 1849–1861, Mar. 2005, doi: 10.1016/j.electacta.2004.08.045.

[55] G. Devaraj, S. Guruviah, and S. K. Seshadri, "Pulse plating," *Mater. Chem. Phys.*, vol. 25, no. 5, pp. 439–461, 1990, doi: 10.1016/0254-0584(90)90111-M.

[56] J. R. Macdonald, "Impedance spectroscopy," *Ann. Biomed. Eng.*, vol. 20, no. 3, pp. 289–305, May 1992, doi: 10.1007/BF02368532.

[57] S. Roy, “Mass transfer considerations during pulse plating,” *Transactions of the IMF*, vol. 86, no. 2, pp. 87–91, Mar. 2008, doi: 10.1179/174591908X272942.
[58] D. Landolt, “Mass Transport in Pulse Plating,” in *Theory and Practice of Pulse Plating*, 1986, pp. 55–71.
[59] M. Datta and D. Landolt, “Experimental investigation of mass transport in pulse plating,” *Surface Technology*, vol. 25, no. 2, pp. 97–110, Jun. 1985, doi: 10.1016/0376-4583(85)90022-6.
[60] K. B. Oldham, “Edge effects in semiinfinite diffusion,” *J. Electroanal. Chem. Interfacial Electrochem.*, vol. 122, pp. 1–17, May 1981, doi: 10.1016/S0022-0728(81)80136-2.
[61] C. N. Tharamani, B. N. Maruthi, and S. M. Mayanna, “Development of a Non- cyanide Alkaline Bath for Industrial Copper Plating,” *Transactions of the IMF*, vol. 80, no. 2, pp. 37–39, Jan. 2002, doi: 10.1080/00202967.2002.11871427.
[62] M. LI, G. WEI, J. WANG, M. LI, X. ZHAO, and Y. BAI, “COPPER PLATING FROM NON-CYANIDE ALKALINE BATHS,” *Surface Review and Letters*, vol. 21, no. 01, p. 1450009, Feb. 2014, doi: 10.1142/S0218625X14500097.
[63] M. A. M. Ibrahim and R. S. Bakdash, “New non-cyanide acidic copper electroplating bath based on glutamate complexing agent,” *Surf. Coat. Technol.*, vol. 282, pp. 139–148, Nov. 2015, doi: 10.1016/j.surfcoat.2015.10.024.
[64] W. Giurlani, E. Berretti, A. Lavacchi, and M. Innocenti, “Thickness determination of metal multilayers by ED-XRF multivariate analysis using Monte Carlo simulated standards,” *Anal. Chim. Acta*, vol. 1130, pp. 72–79, Sep. 2020, doi: 10.1016/j.aca.2020.07.047.
[65] W. Giurlani, E. Berretti, M. Innocenti, and A. Lavacchi, “Measuring the Thickness of Metal Coatings: A Review of the Methods,” *Coatings*, vol. 10, no. 12, p. 1211, Dec. 2020, doi: 10.3390/coatings10121211.
[66] W. Giurlani, E. Berretti, A. Lavacchi, and M. Innocenti, “Thickness determination of metal multilayers by ED-XRF multivariate analysis using Monte Carlo simulated standards,” *Anal. Chim. Acta*, vol. 1130, pp. 72–79, Sep. 2020, doi: 10.1016/j.aca.2020.07.047.
[67] W. Giurlani, E. Berretti, M. Innocenti, and A. Lavacchi, “Coating Thickness Determination Using X-ray Fluorescence Spectroscopy: Monte

Carlo Simulations as an Alternative to the Use of Standards," *Coatings*, vol. 9, no. 2, p. 79, Jan. 2019, doi: 10.3390/coatings9020079.

[68] M. D. Fairchild, "CIE 015:2018 Colorimetry, 4th Edition. The International Commission on Illumination, Vienna, Austria," *Color Res. Appl.*, vol. 44, no. 4, pp. 674–675, Aug. 2019, doi: 10.1002/col.22387.

[69] Harry K., Hammond III, and Isadore Nimeroff, "Measurement of Sixty-Degree Specular Gloss," *Journal of Research N.B.S.*, vol. 44, pp. 585–598, Jun. 1950.

[70] K. Yuan, H. Yan, and S. Jin, "The design of color spectrophotometer based on diffuse illumination and compatible SCE/SCI geometric condition," H.-Y. Tam, K. Xu, H. Xiao, J. Zhu, and C.-L. Zhao, Eds., Dec. 2013, p. 90460V. doi: 10.1117/12.2036508.

[71] B.-Y. Chang, "Conversion of a Constant Phase Element to an Equivalent Capacitor," *Journal of Electrochemical Science and Technology*, vol. 11, no. 3, pp. 318–321, Aug. 2020, doi: 10.33961/jecst.2020.00815.

[72] Serguei N. Lvov, *Introduction to Electrochemical Science and Engineering*, 2nd ed. Boca Raton: CRC Press, 2021. doi: https://doi.org/10.1201/b21893.

[73] S. A. Watson, "The Throwing Power of Nickel and Other Plating Solutions," *Transactions of the IMF*, vol. 37, no. 1, pp. 28–39, Jan. 1960, doi: 10.1080/00202967.1960.11869799.

[74] H. E. Haring and W. Blum, "The electrodeposition of lead-tin alloys," *Trans. Am. Electrochem. Soc 40*, pp. 287–304, 1921.

[75] G. S. Pawley, "Unit-cell refinement from powder diffraction scans," *J. Appl. Crystallogr.*, vol. 14, no. 6, pp. 357–361, Dec. 1981, doi: 10.1107/S0021889881009618.

[76] P. Leisner, M. Fredenberg, and I. Belov, "Pulse and pulse reverse plating of copper from acid sulphate solutions," *Transactions of the IMF*, vol. 88, no. 5, pp. 243–247, 2010, doi: 10.1179/002029610x12791981507721.

[77] W. Giurlani *et al.*, "Electroplating for Decorative Applications: Recent Trends in Research and Development," *Coatings*, vol. 8, no. 8, Jul. 2018, doi: 10.3390/coatings8080260.

[78] D. Landolt and A. Marlot, "Microstructure and composition of pulse-plated metals and alloys," *Surf. Coat. Technol.*, vol. 169–170, pp. 8–13, Jun. 2003, doi: 10.1016/S0257-8972(03)00042-2.

[79] W.-C. Tsai, C.-C. Wan, and Y.-Y. Wang, “Frequency Effect of Pulse Plating on the Uniformity of Copper Deposition in Plated Through Holes,” *J. Electrochem. Soc.*, vol. 150, no. 5, p. C267, 2003, doi: 10.1149/1.1560942.

[80] E. Broitman, “Indentation Hardness Measurements at Macro-, Micro-, and Nanoscale: A Critical Overview,” *Tribol. Lett.*, vol. 65, no. 1, Mar. 2017, doi: 10.1007/s11249-016-0805-5.

[81] M. D. Maksimović and Z. S. Dimitrijević, “Fundamental aspects of pulsating current metal electrodeposition V: The determination of the optimal frequency range,” *Surface Technology*, vol. 17, no. 1, pp. 3–9, Sep. 1982, doi: 10.1016/0376-4583(82)90055-3.

[82] N. Ibl, J. Cl. Puippe, and H. Angerer, “Electrocrystallization in pulse electrolysis,” *Surface Technology*, vol. 6, no. 4, pp. 287–300, Mar. 1978, doi: 10.1016/0376-4583(78)90044-4.

[83] T. A. Green and S. Roy, “Application of a duplex diffusion layer model to pulse reverse plating,” *Transactions of the IMF*, vol. 95, no. 1, pp. 46–51, Jan. 2017, doi: 10.1080/00202967.2016.1214354.

[84] K. I. Popov and N. D. Nikolić, “General Theory of Disperse Metal Electrodeposits Formation,” vol. 54, no. November, S. S. Djokić, Ed., in Modern Aspects of Electrochemistry, vol. 54. , Boston, MA: Springer US, 2012, pp. 1–62. doi: 10.1007/978-1-4614-2380-5_1.

[85] K. I. Popov, N. V. Krstajić, and S. R. Popov, “The morphology of cadmium deposits obtained on foreign substrates at high overpotentials,” *J. Appl. Electrochem.*, vol. 15, no. 1, pp. 151–154, Jan. 1985, doi: 10.1007/BF00617753.

[86] K. I. Popov, M. D. Maksimović, and D. Ć. Totovski, “Fundamental aspects of pulsating current metal electrodeposition VI: The comparison of electrode surface roughening in pulsating current and periodic reverse current electrodeposition of metals,” *Surface Technology*, vol. 17, no. 2, pp. 125–129, Oct. 1982, doi: 10.1016/0376-4583(82)90014-0.

[87] K. I. Popov, D. Ć. Totovski, and M. D. Maksimović, “Fundamental aspects of pulsating current metal electrodeposition VII: The comparison of current density distributions in pulsating current and periodic reverse current electrodeposition of metals,” *Surface Technology*, vol. 19, no. 2, pp. 181–185, Jun. 1983, doi: 10.1016/0376-4583(83)90068-7.

[88] “Yu. Ya. Vene and S. A. Nikolayeva, Zh. Prikl. Khim., 24 (1955) 811.”.

[89] I. J. Beyerlein, X. Zhang, and A. Misra, “Growth Twins and Deformation Twins in Metals,” *Annu. Rev. Mater. Res.*, vol. 44, no. 1, pp. 329–363, Jul. 2014, doi: 10.1146/annurev-matsci-070813-113304.

[90] L. Lu, M. L. Sui, and K. Lu, “Superplastic Extensibility of Nanocrystalline Copper at Room Temperature,” *Science (1979).*, vol. 287, no. 5457, pp. 1463–1466, Feb. 2000, doi: 10.1126/science.287.5457.1463.

[91] C.-L. Lu *et al.*, “Extremely anisotropic single-crystal growth in nanotwinned copper,” *NPG Asia Mater.*, vol. 6, no. 10, pp. e135–e135, Oct. 2014, doi: 10.1038/am.2014.90.

[92] K. M. Chow, W. Y. Ng, and L. K. Yeung, “Barrier properties of Ni, Pd and Pd-Fe for Cu diffusion,” *Surf. Coat. Technol.*, vol. 105, no. 1–2, pp. 56–64, 1998, doi: 10.1016/S0257-8972(98)00442-3.

[93] R. H. Atkinson and A. R. Raper, “The Electrodeposition of Palladium,” *Transactions of the IMF*, vol. 8, no. 1, pp. 10.1-10.24, 1932, doi: 10.1080/00202967.1932.11871599.

[94] F. Biffoli *et al.*, “Tailoring barrier layers design for haute couture through X-ray microanalysis: Insights and guidelines,” *Heliyon*, vol. 10, no. 11, p. e32147, 2024, doi: 10.1016/j.heliyon.2024.e32147.

[95] M. Pushpavanam, “Electrodeposition of palladium-nickel alloy,” 1990.

[96] S. E. Nam and K. H. Lee, “A study on the palladium/nickel composite membrane by vacuum electrodeposition,” *J. Memb. Sci.*, vol. 170, no. 1, pp. 91–99, 2000, doi: 10.1016/S0376-7388(99)00359-2.

[97] M. E. Baumgärtner and D. R. Gabe, “Palladium-Iron Alloy Electrodeposition. Part I Single Metal Systems,” *Transactions of the IMF*, vol. 78, no. 1, pp. 11–16, Jan. 2000, doi: 10.1080/00202967.2000.11871297.

[98] K. Hubkowska, M. Pająk, and A. Czerwiński, “Hydrogen electrosorption properties of electrodeposited Pd-Ir alloys,” *Journal of Solid State Electrochemistry*, vol. 26, no. 1, pp. 103–109, 2022, doi: 10.1007/s10008-021-04973-3.

[99] V. V. Bhat, C. I. Contescu, and N. C. Gallego, “The role of destabilization of palladium hydride in the hydrogen uptake of Pd-containing activated carbons,” *Nanotechnology*, vol. 20, no. 20, 2009, doi: 10.1088/0957-4484/20/20/204011.

[100] R. Gremaud *et al.*, "Hydrogenography of PdHx thin films: Influence of H-induced stress relaxation processes," *Acta Mater.*, vol. 57, no. 4, pp. 1209–1219, 2009, doi: 10.1016/j.actamat.2008.11.016.

[101] J. E. Worsham, M. K. Wilkinson, and C. G. Shull, "Neutron-diffraction observations on the palladium-hydrogen and palladium-deuterium systems," *Journal of Physics and Chemistry of Solids*, vol. 3, no. 3–4, pp. 303–310, 1957, doi: 10.1016/0022-3697(57)90033-1.

[102] V. O. Lume, "P-PdH,,and P-PdD,,with," *Phys. Rev. B*, vol. 12, no. 1, pp. 117–118, 1975.

[103] A. M. Abdellah *et al.*, "Impact of palladium/palladium hydride conversion on electrochemical CO2 reduction via in-situ transmission electron microscopy and diffraction," *Nat. Commun.*, vol. 15, no. 1, pp. 1–15, 2024, doi: 10.1038/s41467-024-45096-3.

[104] L. E. Isaeva, D. I. Bazhanov, E. I. Isaev, S. V. Eremeev, S. E. Kulkova, and I. A. Abrikosov, "Dynamic stability of palladium hydride: An ab initio study," *Int. J. Hydrogen Energy*, vol. 36, no. 1, pp. 1254–1258, 2011, doi: 10.1016/j.ijhydene.2010.06.130.

[105] Y. Wang, S. N. Sun, and M. Chou, "Total-energy study of hydrogen ordering in PdH x(0⩽x⩽1)," *Phys. Rev. B Condens. Matter Mater. Phys.*, vol. 53, no. 1, pp. 1–4, 1996, doi: 10.1103/PhysRevB.53.1.

[106] J. M. P. F.D. Manchester, A. San-Martin, "The H-Pd (Hydrogen-Palladium) S y s t e m," *Phase diagram evaluations: Section II*, vol. 15, no. 1, pp. 62–83, 1994.

[107] I. Wei and J. Brewer, "Desorption of Hydrogen from Palladium Plating," *AMP Journal of Technology*, vol. 5, pp. 49–53, 1996.

[108] H. Akiba *et al.*, "Nanometer-Size Effect on Hydrogen Sites in Palladium Lattice," *J. Am. Chem. Soc.*, vol. 138, no. 32, pp. 10238–10243, 2016, doi: 10.1021/jacs.6b04970.

[109] S. Wang *et al.*, "Uniform PdH 0.33 nanodendrites with a high oxygen reduction activity tuned by lattice H," *Electrochem. commun.*, vol. 102, no. April, pp. 67–71, 2019, doi: 10.1016/j.elecom.2019.04.002.

[110] "Angew Chem Int Ed - 2020 - Xu - Nanoporous Palladium Hydride for Electrocatalytic N2 Reduction under Ambient Conditions.pdf."

[111] E. Guan *et al.*, "New Role of Pd Hydride as a Sensor of Surface Pd Distributions in Pd−Au Catalysts," *ChemCatChem*, vol. 12, no. 3, pp. 717–721, 2020, doi: 10.1002/cctc.201901847.

[112] T. Kawae, Y. Inagaki, S. Wen, S. Hirota, D. Itou, and T. Kimura, “Superconductivity in Palladium Hydride Systems,” *J. Physical Soc. Japan*, vol. 89, no. 5, p. 051004, May 2020, doi: 10.7566/JPSJ.89.051004.
[113] Z. Zhao *et al.*, “Synthesis of Stable Shape-Controlled Catalytically Active β-Palladium Hydride,” *J. Am. Chem. Soc.*, vol. 137, no. 50, pp. 15672–15675, 2015, doi: 10.1021/jacs.5b11543.
[114] J. D. Benck, A. Jackson, D. Young, D. Rettenwander, and Y.-M. Chiang, “Producing High Concentrations of Hydrogen in Palladium via Electrochemical Insertion from Aqueous and Solid Electrolytes,” *Chemistry of Materials*, vol. 31, no. 11, pp. 4234–4245, Jun. 2019, doi: 10.1021/acs.chemmater.9b01243.
[115] A. Schneemann *et al.*, “Nanostructured Metal Hydrides for Hydrogen Storage,” *Chem. Rev.*, vol. 118, no. 22, pp. 10775–10839, 2018, doi: 10.1021/acs.chemrev.8b00313.
[116] M. Yamauchi, R. Ikeda, H. Kitagawa, and M. Takata, “Nanosize effects on hydrogen storage in palladium,” *Journal of Physical Chemistry C*, vol. 112, no. 9, pp. 3294–3299, 2008, doi: 10.1021/jp710447j.
[117] G. Abbondanza *et al.*, “Hydride formation and dynamic phase changes during template-assisted Pd electrodeposition,” *Nanotechnology*, vol. 34, no. 50, 2023, doi: 10.1088/1361-6528/acf66e.
[118] M. Suleiman *et al.*, “Phase transition and lattice expansion during hydrogen loading of nanometer sized palladium clusters,” *J. Alloys Compd.*, vol. 356–357, pp. 644–648, 2003, doi: 10.1016/S0925-8388(02)01286-0.
[119] R. Felici, L. Bertalot, A. DeNinno, A. LaBarbera, and V. Violante, “In situ measurement of the deuterium (hydrogen) charging of a palladium electrode during electrolysis by energy dispersive x-ray diffraction,” *Review of Scientific Instruments*, vol. 66, no. 5, pp. 3344–3348, 1995, doi: 10.1063/1.1145505.
[120] H. Karami and H. Babaei, “Electroplating nanostructured hard gold through the pulse galvanostatic method,” *Int. J. Electrochem. Sci.*, vol. 7, no. 1, pp. 601–614, 2012, doi: 10.1016/s1452-3981(23)13362-1.
[121] Y. J. Chiu, C. Y. Shen, H. W. Chang, and S. R. Jian, “Characteristics of Iron-Palladium alloy thin films deposited by magnetron sputtering,” *Results Phys.*, vol. 9, pp. 17–22, 2018, doi: 10.1016/j.rinp.2018.02.024.

[122] S. N. Kabekkodu, A. Dosen, and T. N. Blanton, “PDF-5+: A comprehensive powder diffraction file™ for materials characterization,” *Powder Diffr.*, pp. 1–13, 2024, doi: 10.1017/S0885715624000150.
[123] M. Wojdyr, “Fityk: A general-purpose peak fitting program,” *J. Appl. Crystallogr.*, vol. 43, no. 5 PART 1, pp. 1126–1128, 2010, doi: 10.1107/S0021889810030499.
[124] C. A. Schneider, W. S. Rasband, and K. W. Eliceiri, “NIH Image to ImageJ: 25 years of image analysis,” *Nat. Methods*, vol. 9, no. 7, pp. 671–675, 2012, doi: 10.1038/nmeth.2089.
[125] H. Abrams, “Grain size measurement by the intercept method,” *Metallography*, vol. 4, no. 1, pp. 59–78, 1971, doi: 10.1016/0026-0800(71)90005-X.
[126] E. Mariani, W. Giurlani, M. Bonechi, V. Dell’Aquila, and M. Innocenti, “A systematic study of pulse and pulse reverse plating on acid copper bath for decorative and functional applications,” *Sci. Rep.*, vol. 12, no. 1, p. 18175, Oct. 2022, doi: 10.1038/s41598-022-22650-x.
[127] E. Mariani, W. Giurlani, M. Verrucchi, V. dell’Aquila, P. Lo Nostro, and M. Innocenti, “Pulse Electroplating of Gold-Nickel Alloys: Morphological and Aesthetic Improvement Compared to DC,” *J. Electrochem. Soc.*, vol. 171, no. 1, p. 012504, Jan. 2024, doi: 10.1149/1945-7111/ad1d97.
[128] J. H. L. Voncken and T. W. Verkroost, “Powder diffraction of cubic oα-brass,” *Powder Diffr.*, vol. 12, no. 4, pp. 228–229, 1997, doi: 10.1017/s0885715600009787.
[129] G. Peleggi, D. Rossi, and P. Zanola, “Il Palladio,” *La Chimica e l’Industria*, vol. 88, no. 10, p. 92, 2006.
[130] A. Sohrabi, A. Dolati, M. Ghorbani, M. R. Barati, and P. Stroeve, “Elucidation of the structural texture of electrodeposited Ni/SiC nanocomposite coatings,” *Journal of Physical Chemistry C*, vol. 116, no. 6, pp. 4105–4118, 2012, doi: 10.1021/jp2095714.
[131] T. Kizuka, “Atomic configuration and mechanical and electrical properties of stable gold wires of single-atom width,” *Phys. Rev. B*, vol. 77, no. 15, p. 155401, Apr. 2008, doi: 10.1103/PhysRevB.77.155401.
[132] S. Mohan and V. Raj, “A comparative study of DC and pulse gold electrodeposits,” *Transactions of the IMF*, vol. 83, no. 2, pp. 72–76, Apr. 2005, doi: 10.1179/002029605X29393.

[133] P. L. Cavallotti, P. Cojocaru, and L. Magagnin, “Soft gold coatings: influence of additives and pulse plating,” *Transactions of the IMF*, vol. 90, no. 5, pp. 246–251, Sep. 2012, doi: 10.1179/0020296712Z.00000000048.

[134] T. A. Green, “Gold electrodeposition for microelectronic, optoelectronic and microsystem applications,” *Gold Bull.*, vol. 40, no. 2, pp. 105–114, Jun. 2007, doi: 10.1007/BF03215566.

[135] A. Vicenzo and P. L. Cavallotti, “Gold Electroplating,” in *Gold: Science and Applications*, I., C. Corti and R. Holliday, Eds., CRC Press, 2009.

[136] H. Renner *et al.*, “Gold, Gold Alloys, and Gold Compounds,” in *Ullmann’s Encyclopedia of Industrial Chemistry*, Weinheim, Germany: Wiley, 2000. doi: 10.1002/14356007.a12_499.

[137] E. Drost and J. Haußelt, “Uses of Gold in Jewellery,” *Interdisciplinary Science Reviews*, vol. 17, no. 3, pp. 271–280, Sep. 1992, doi: 10.1179/030801892791925448.

[138] E. Piciollo *et al.*, “Electrodeposition and Characterization of Thin Film of Black-Gold,” *ECS Meeting Abstracts*, vol. MA2017-02, no. 16, pp. 921–921, Sep. 2017, doi: 10.1149/MA2017-02/16/921.

[139] G. Devaraj, S. Guruviah, and S. K. Seshadri, “Pulse plating,” *Mater. Chem. Phys.*, vol. 25, no. 5, pp. 439–461, 1990, doi: 10.1016/0254-0584(90)90111-M.

[140] S. Yu *et al.*, “Effect of pulse current density on creep ageing behavior of 2195 Al-Li alloy,” *Materials Science and Engineering: A*, vol. 909, p. 146814, Sep. 2024, doi: 10.1016/j.msea.2024.146814.

[141] W. Giurlani *et al.*, “What Is the Current State of Sustainability in the Decorative Electroplating Industry? A Close Look at New Practices and Advances,” *Sustainability*, vol. 16, no. 13, p. 5821, Jul. 2024, doi: 10.3390/su16135821.

[142] X. Guo *et al.*, “Effect of Pulse Current on Interface Microstructure and Bonding Properties of TA1/304 Double-Layer Clad plates,” *Chinese Journal of Mechanical Engineering*, vol. 37, no. 1, p. 116, Oct. 2024, doi: 10.1186/s10033-024-01097-3.

[143] C.-Y. Chen *et al.*, “Pulse electroplating of ultra-fine grained Au films with high compressive strength,” *Electrochem. commun.*, vol. 67, pp. 51–54, Jun. 2016, doi: 10.1016/j.elecom.2016.03.017.

[144] T. Yokoshima, A. Takanaka, T. Hachisu, A. Sugiyama, Y. Okinaka, and T. Osaka, “Mechanical and Electrical Properties of Au-Ni-C Alloy Films Produced by Pulsed Current Electrodeposition,” *J. Electrochem. Soc.*, vol. 160, no. 11, pp. D513–D518, Sep. 2013, doi: 10.1149/2.012311jes.

[145] M. Viswanathan and Ch. J. Raub, “Pulse plating of nickel-gold alloys,” *Surface Technology*, vol. 4, no. 4, pp. 339–342, Jul. 1976, doi: 10.1016/0376-4583(76)90004-2.

[146] “Quanto male fa al pianeta l’estrazione dell’oro?” [Online]. Available: https://www.wired.it/article/estrazione-oro-danni-ambiente-inquinamento/

[147] “Gold and precious metals.” [Online]. Available: https://www.fairtrade.net/product/gold

[148] A. Ruffoni and D. Landolt, “Pulse-plating of Au□Cu□Cd alloys—II. Theoretical modelling of alloy composition,” *Electrochim. Acta*, vol. 33, no. 10, pp. 1281–1289, Oct. 1988, doi: 10.1016/0013-4686(88)80116-6.

[149] A. M. Alfantazi, J. Page, and U. Erb, “Pulse plating of Zn-Ni alloy coatings,” *J. Appl. Electrochem.*, vol. 26, no. 12, Dec. 1996, doi: 10.1007/BF00249924.

[150] A. M. El-Sherik, U. Erb, and J. Page, “Microstructural evolution in pulse plated nickel electrodeposits,” *Surf. Coat. Technol.*, vol. 88, no. 1–3, pp. 70–78, Jan. 1997, doi: 10.1016/S0257-8972(96)02928-3.

[151] K. C. Chan, N. S. Qu, and D. Zhu, “Quantitative texture analysis in pulse reverse current electroforming of nickel,” *Surf. Coat. Technol.*, vol. 99, no. 1–2, pp. 69–73, Feb. 1998, doi: 10.1016/S0257-8972(97)00523-9.

[152] M. Saitou, W. Oshikawa, M. Mori, and A. Makabe, “Surface Roughening in the Growth of Direct Current or Pulse Current Electrodeposited Nickel Thin Films,” *J. Electrochem. Soc.*, vol. 148, no. 12, p. C780, 2001, doi: 10.1149/1.1415548.

[153] N. S. Qu, D. Zhu, K. C. Chan, and W. N. Lei, “Pulse electrodeposition of nanocrystalline nickel using ultra narrow pulse width and high peak current density,” *Surf. Coat. Technol.*, vol. 168, no. 2–3, pp. 123–128, May 2003, doi: 10.1016/S0257-8972(03)00014-8.

[154] K. ; A. N. ; P. J. C. ; I. N. Hosokawa, “ Pulse-Plated Deposits of Gold and Rhenium,” *Plating and surfacing finishing*, vol. 67, pp. 68–72, 1980.

[155] C. Cretu and E. van der Lingen, “Coloured gold alloys,” *Gold Bull.*, vol. 32, no. 4, pp. 115–126, Dec. 1999, doi: 10.1007/BF03214796.

[156] I.-L. Bolunduț, “Gold: Properties, Minerals, Alloys, Uses and Recycling,” *Mining Revue*, vol. 28, no. 2, pp. 42–48, Jun. 2022, doi: 10.2478/minrv-2022-0013.

[157] J. Liu *et al.*, “Combinatorial exploration of color in gold-based alloys,” *Gold Bull.*, vol. 48, no. 3–4, pp. 111–118, Dec. 2015, doi: 10.1007/s13404-015-0167-z.

[158] D. J. Arrowsmith and G. Brown, “The Colour of Gold and Gold Alloy Electrodeposits,” *Transactions of the IMF*, vol. 61, no. 1, pp. 1–8, Jan. 1983, doi: 10.1080/00202967.1983.11870627.

[159] A. Serin, M. Bourlion, F. Diologent, R. Ziegenhagen, and V. Germain, “New deeply coloured 18-K gold materials built by nanotechnologies,” *Gold Bull.*, vol. 48, no. 1–2, pp. 13–20, Aug. 2015, doi: 10.1007/s13404-014-0154-9.

[160] W. S. Rapson, “The metallurgy of the coloured carat gold alloys,” *Gold Bull.*, vol. 23, no. 4, pp. 125–133, Dec. 1990, doi: 10.1007/BF03214713.

[161] A. S. McDonald and G. H. Sistare, “The metallurgy of some carat gold jewellery alloys,” *Gold Bull.*, vol. 11, no. 3, pp. 66–73, Sep. 1978, doi: 10.1007/BF03215089.

[162] I. B. MacCormack and J. E. Bowers, “New white gold alloys,” *Gold Bull.*, vol. 14, no. 1, pp. 19–24, Mar. 1981, doi: 10.1007/BF03216555.

[163] W. Corti Chris and E. Van der Lingen, “Special colors of precious-metal jewelry: present and future,” in *Proceedings of the Santa Fe Symposium on Jewelry Manufacturing Technology*, May 2016, pp. 165–197.

[164] J. Fischer-Bühner, A. Basso, and M. Poliero, “Metallurgy and processing of coloured gold intermetallics — Part II: Investment casting and related alloy design,” *Gold Bull.*, vol. 43, no. 1, pp. 11–20, Mar. 2010, doi: 10.1007/BF03214962.

[165] W. Corti Chris, “Blue, black and purple! The special colours of gold,” in *The Santa Fe Symposium*, Albuquerque: Met-Chem Research, May 2004, pp. 121–133.

[166] K. Nassau, “The fifteen causes of color: The physics and chemistry of color,” *Color Res. Appl.*, vol. 12, no. 1, pp. 4–26, Feb. 1987, doi: 10.1002/col.5080120105.

[167] K. E. Saeger and J. Rodies, “The colour of gold and its alloys,” *Gold Bull.*, vol. 10, no. 1, pp. 10–14, Mar. 1977, doi: 10.1007/BF03216519.

[168] M. Vorobyova *et al.*, “PVD for Decorative Applications: A Review,” *Materials*, vol. 16, no. 14, p. 4919, Jul. 2023, doi: 10.3390/ma16144919.
[169] D. P. Agarwal and G. Raykhtsaum, “Color technology for Jewelry alloy applications,” *The Santa Fe Symposium on Jewelry Manufacturing*, pp. 229–244, 1988.
[170] R. D. Overheim and D. L. Wagner, *Light and Color*, 1st Edition. John Wiley & Sons, 1982.
[171] Z. Shojaei, G. R. Khayati, and E. Darezereshki, “Study of the Effect of Current Density on the Metallurgical Properties of AlFeCrNiTi High Entropy Alloy Coating Produced by Pulse Plating,” *Metals and Materials International*, vol. 31, no. 2, pp. 442–454, Feb. 2025, doi: 10.1007/s12540-024-01767-w.
[172] W. Giurlani, F. Gambinossi, E. Salvietti, M. Passaponti, and M. Innocenti, “Color Measurements in Electroplating Industry: Implications for Product Quality Control,” *ECS Trans.*, vol. 80, no. 10, pp. 757–766, Oct. 2017, doi: 10.1149/08010.0757ecst.
[173] J.-C. Puippe, “Guidelines for setting the useful range of pulse plating parameters,” *Transactions of the IMF*, vol. 96, no. 5, pp. 244–252, Sep. 2018, doi: 10.1080/00202967.2018.1501907.
[174] K. Schlapfer, *Farbmeytik in der Reproduktionstechnik und im Mehrfarbendruck*, 2nd ed. Gallen, Switzerland: UGRA, 1993.
[175] United Nations, “Sustainable Development Goals.” Accessed: Mar. 19, 2024. [Online]. Available: https://sdgs.un.org/goals
[176] S. Jeyamala, A. K. Kumaraguru, and N. Nagarani, “Occupational health effects due to nickel and chromium exposure in electroplating workers,” *Toxicol. Environ. Chem.*, vol. 94, no. 8, pp. 1583–1590, Sep. 2012, doi: 10.1080/02772248.2012.715382.
[177] B. Moura, E. Papaioannou, A. Grigoropoulos, A. Zoikis-Karathanasis, and H. Monteiro, “Sustainability of Spent Nickel-Based Electroplating Baths: An Innovative Valorisation Process,” *Sustainability*, vol. 15, no. 21, p. 15366, Oct. 2023, doi: 10.3390/su152115366.
[178] P. Xu *et al.*, “Insights into the health status of the general population living near an electroplating industry zone: metal elevations and renal impairment,” *Environmental Science and Pollution Research*, vol. 30, no. 11, pp. 31905–31915, Dec. 2022, doi: 10.1007/s11356-022-24411-9.

[179] Y. Yu, Y. Xie, L. Ji, J. Zhang, Y. Cai, and Z. Yang, "Water management for industrial development, energy conservation, and subjective attitudes: a comprehensive risk-oriented model to explore the tolerance of unbalanced allocation problem," *Journal of Water and Climate Change*, vol. 13, no. 1, pp. 139–157, Jan. 2022, doi: 10.2166/wcc.2021.377.

[180] T. Li *et al.*, "Comparative study of electroplating sludge reutilization in China: environmental and economic performances," *Environmental Science and Pollution Research*, vol. 30, no. 48, pp. 106598–106610, Sep. 2023, doi: 10.1007/s11356-023-29849-z.

[181] F. Pizzetti, E. Salvietti, W. Giurlani, R. Emanuele, C. Fontanesi, and M. Innocenti, "Cyanide-free silver electrodeposition with polyethyleneimine and 5,5-dimethylhydantoin as organic additives for an environmentally friendly formulation," *Journal of Electroanalytical Chemistry*, vol. 911, p. 116196, Apr. 2022, doi: 10.1016/j.jelechem.2022.116196.

[182] R. Bandinelli, V. Fani, and B. Bindi, "Electroplating and pvd finishing technologies in the fashion industry: Perspectives and scenarios," *Sustainability (Switzerland)*, vol. 13, no. 8, 2021, doi: 10.3390/su13084453.

[183] A. Siddiqui, R. Potoff, and Y. Huang, "Sustainability metrics and technical solution derivation for performance improvement of electroplating facilities," *Clean Technol. Environ. Policy*, no. 0123456789, Dec. 2023, doi: 10.1007/s10098-023-02696-9.

[184] E. A. Iñigo and L. Albareda, "Understanding sustainable innovation as a complex adaptive system: a systemic approach to the firm," *J. Clean. Prod.*, vol. 126, pp. 1–20, Jul. 2016, doi: 10.1016/j.jclepro.2016.03.036.

[185] J. Xiao and Y. Huang, "Technology Integration for Sustainable Manufacturing: An Applied Study on Integrated Profitable Pollution Prevention in Surface Finishing Systems," *Ind. Eng. Chem. Res.*, vol. 51, no. 35, pp. 11434–11444, Sep. 2012, doi: 10.1021/ie300154n.

[186] C. Piluso and Y. Huang, "Collaborative profitable pollution prevention: an approach for the sustainable development of complex industrial zones under uncertain information," *Clean Technol. Environ. Policy*, vol. 11, no. 3, pp. 307–322, Sep. 2009, doi: 10.1007/s10098-008-0187-y.

[187] H. Song, N. Bhadbhade, and Y. Huang, "Sustainability Assessment and Performance Improvement of Electroplating Process Systems," in *Sustainability in the Design, Synthesis and Analysis of Chemical*

Engineering Processes, Elsevier, 2016, pp. 227–248. doi: 10.1016/B978-0-12-802032-6.00010-4.

[188] Luxury Brands Technologies, "HCS: Homogeneous Coating System." Accessed: Mar. 19, 2024. [Online]. Available: https://luxurybrandstechnologies.it/hcs-homogeneous-coating-system/

[189] M. Chen, M. Wu, and C. Lin, "Application of Indices Cp and Cpk to Improve Quality Control Capability in Clinical Biochemistry Laboratories," vol. 57, no. 5, pp. 63–68, 2014, doi: 10.4077/CJP.2014.BAB170.

[190] *ISO 9227:2017 Corrosion tests in artificial atmospheres -- Salt spray tests*. Geneva, Switzerland: International Organization for Standardization, 2017.

[191] B. V. Todeschini, M. N. Cortimiglia, D. Callegaro-de-Menezes, and A. Ghezzi, "Innovative and sustainable business models in the fashion industry: Entrepreneurial drivers, opportunities, and challenges," *Bus. Horiz.*, vol. 60, no. 6, pp. 759–770, Nov. 2017, doi: 10.1016/j.bushor.2017.07.003.

[192] United Nations (UN), *Transforming our World: The 2030 Agenda for Sustainable Development*. New York, USA: United Nations (UN), 2015.

[193] B. Wu *et al.*, "Experimental and DFT study of the effect of mercaptosuccinic acid on cyanide-free immersion gold deposition," *RSC Adv.*, vol. 10, no. 17, pp. 9768–9776, 2020, doi: 10.1039/d0ra00925c.

[194] G. Pinto, F. Silva, J. Porteiro, J. Míguez, and A. Baptista, "Numerical simulation applied to PVD reactors: An overview," *Coatings*, vol. 8, no. 11, pp. 1–21, 2018, doi: 10.3390/COATINGS8110410.

[195] W. Giurlani *et al.*, "Specific ion effects on copper electroplating," *Colloids Surf. B Biointerfaces*, vol. 225, p. 113287, May 2023, doi: 10.1016/j.colsurfb.2023.113287.

[196] Z. Lai *et al.*, "A comparison of typical additives for copper electroplating based on theoretical computation," *Comput. Mater. Sci.*, vol. 147, pp. 95–102, May 2018, doi: 10.1016/j.commatsci.2017.11.049.

[197] P. Maris, M. Sosonkina, J. P. Vary, E. Ng, and C. Yang, "Scaling of ab-initio nuclear physics calculations on multicore computer architectures," *Procedia Comput. Sci.*, vol. 1, no. 1, pp. 97–106, May 2010, doi: 10.1016/j.procs.2010.04.012.

[198] N. L. Allinger, X. Zhou, and J. Bergsma, “Molecular mechanics parameters,” *Journal of Molecular Structure: THEOCHEM*, vol. 312, no. 1, pp. 69–83, Jan. 1994, doi: 10.1016/S0166-1280(09)80008-0.

[199] J. Wang, R. M. Wolf, J. W. Caldwell, P. A. Kollman, and D. A. Case, “Development and testing of a general amber force field,” *J. Comput. Chem.*, vol. 25, no. 9, pp. 1157–1174, Jul. 2004, doi: 10.1002/jcc.20035.

[200] K. G. Sprenger, V. W. Jaeger, and J. Pfaendtner, “The General AMBER Force Field (GAFF) Can Accurately Predict Thermodynamic and Transport Properties of Many Ionic Liquids,” *J. Phys. Chem. B*, vol. 119, no. 18, pp. 5882–5895, May 2015, doi: 10.1021/acs.jpcb.5b00689.

[201] S. Di Grande, I. Ciofini, C. Adamo, M. Pagliai, and G. Cardini, “Absorption Spectra of Flexible Fluorescent Probes by a Combined Computational Approach: Molecular Dynamics Simulations and Time-Dependent Density Functional Theory,” *J. Phys. Chem. A*, vol. 126, no. 47, pp. 8809–8817, Dec. 2022, doi: 10.1021/acs.jpca.2c04637.

[202] H. Daneshmand, M. Araghchi, M. Asgary, M. Karimi, and M. Torab-Mostaedi, “New insight into adsorption mechanism of nickel–ammonium complex on the growth of nickel surfaces with hierarchical nano/microstructure,” *Results in Surfaces and Interfaces*, vol. 3, p. 100014, May 2021, doi: 10.1016/j.rsurfi.2021.100014.

[203] V. A. Pérez Jiménez, V. Hernández-Montoya, L. A. Ramírez-Montoya, F. Castillo-Borja, R. Tovar-Gómez, and M. A. Montes-Morán, “Adsorption of impurities from nickel-plating baths using commercial sorbents to reduce wastewater discharges,” *J. Environ. Manage.*, vol. 284, p. 112024, Apr. 2021, doi: 10.1016/j.jenvman.2021.112024.

[204] Q. Li, J. Hu, J. Zhang, P. Yang, Y. Hu, and M. An, “Screening of electroplating additive for improving throwing power of copper pyrophosphate bath via molecular dynamics simulation,” *Chem. Phys. Lett.*, vol. 757, p. 137848, Oct. 2020, doi: 10.1016/j.cplett.2020.137848.

[205] I. N. Levine, *Quantum Chemistry*. 2013.

[206] S. Di Grande, M. Kállay, and V. Barone, “Accurate thermochemistry at affordable cost by means of an improved version of the JunChS-F12 model chemistry,” *J. Comput. Chem.*, vol. 44, no. 27, pp. 2149–2157, Oct. 2023, doi: 10.1002/jcc.27187.

[207] A. Dianat, H. Yang, M. Bobeth, and G. Cuniberti, “DFT study of interaction of additives with Cu(111) surface relevant to Cu

electrodeposition," *J. Appl. Electrochem.*, vol. 48, no. 2, pp. 211–219, Feb. 2018, doi: 10.1007/s10800-018-1150-1.

[208] Y. Li *et al.*, "The influence of leveler Brilliant Green on copper superconformal electroplating based on electrochemical and theoretical study," *Journal of Industrial and Engineering Chemistry*, vol. 118, pp. 78–90, Feb. 2023, doi: 10.1016/j.jiec.2022.10.047.

[209] J. I. Mendieta-Moreno, I. Marcos-Alcalde, D. G. Trabada, P. Gómez-Puertas, J. Ortega, and J. Mendieta, "A Practical Quantum Mechanics Molecular Mechanics Method for the Dynamical Study of Reactions in Biomolecules," 2015, pp. 67–88. doi: 10.1016/bs.apcsb.2015.06.003.

[210] G. Hou, X. Zhu, M. Elstner, and Q. Cui, "A Modified QM/MM Hamiltonian with the Self-Consistent-Charge Density-Functional-Tight-Binding Theory for Highly Charged QM Regions," *J. Chem. Theory Comput.*, vol. 8, no. 11, pp. 4293–4304, Nov. 2012, doi: 10.1021/ct300649f.

[211] C. E. Tzeliou, M. A. Mermigki, and D. Tzeli, "Review on the QM/MM Methodologies and Their Application to Metalloproteins," *Molecules*, vol. 27, no. 9, p. 2660, Apr. 2022, doi: 10.3390/molecules27092660.

[212] T. M. Braun, D. Josell, J. John, and T. P. Moffat, "Editors' Choice—Simulation of Copper Electrodeposition in Through-Hole Vias," *J. Electrochem. Soc.*, vol. 167, no. 1, p. 013510, Oct. 2020, doi: 10.1149/2.0102001JES.

[213] European Committee for Standardization, *EN 1811:2011+A1:2015 Reference Test Method for Release of Nickel from All Post Assemblies Which Are Inserted into Pierced Parts of the Human Body and Articles Intended to Come into Direct and Prolonged Contact with the Skin*. Brussels, Belgium, 2015.

[214] L. Fabbri *et al.*, "Optimisation of Thiourea Concentration in a Decorative Copper Plating Acid Bath Based on Methanesulfonic Electrolyte," *Coatings*, vol. 12, no. 3, pp. 1–11, 2022, doi: 10.3390/coatings12030376.

[215] E. Berretti *et al.*, "Electrodeposited white bronzes on brass: Corrosion in 3.5 % sodium chloride solution," *Corros. Sci.*, vol. 175, p. 108898, Oct. 2020, doi: 10.1016/j.corsci.2020.108898.

[216] W. Giurlani *et al.*, "Analytic procedure for the evaluation of copper intermetallic diffusion in electroplated gold coatings with energy

dispersive X-ray microanalysis," *Anal. Chim. Acta*, vol. 1269, p. 341428, Aug. 2023, doi: 10.1016/j.aca.2023.341428.

[217] M. M. Rahman, W. Liu, M. Lv, and H. Pan, "Exploring SIMPLE algorithm for all speeds," *Ain Shams Engineering Journal*, vol. 14, no. 2, p. 101854, Mar. 2023, doi: 10.1016/j.asej.2022.101854.

[218] R. I. Issa, A. D. Gosman, and A. P. Watkins, "The computation of compressible and incompressible recirculating flows by a non-iterative implicit scheme," *J. Comput. Phys.*, vol. 62, no. 1, pp. 66–82, Jan. 1986, doi: 10.1016/0021-9991(86)90100-2.

[219] R. Payri, S. Ruiz, J. Gimeno, and P. Martí-Aldaraví, "Verification of a new CFD compressible segregated and multi-phase solver with different flux updates-equations sequences," *Appl. Math. Model.*, vol. 39, no. 2, pp. 851–861, Jan. 2015, doi: 10.1016/j.apm.2014.07.011.

[220] S. Li, "Introduction to Electrochemical Reaction Engineering," in *Chemical Reaction Engineering*, Elsevier, 2017, pp. 599–651. doi: 10.1016/B978-0-12-410416-7.00013-6.

[221] Y. Nishiki, K. Aoki, K. Tokuda, and H. Matsuda, "Secondary current distribution in a two-dimensional model cell composed of an electrode with an open part," *J. Appl. Electrochem.*, vol. 16, no. 2, pp. 291–303, Mar. 1986, doi: 10.1007/BF01093363.

[222] A. N. Colli and J. M. Bisang, "Tertiary Current and Potential Distribution Including Laminar/Turbulent Convection, Diffusion, and Migration by the Finite Volume Method Using OpenFOAM," *Ind. Eng. Chem. Res.*, vol. 60, no. 32, pp. 11927–11941, Aug. 2021, doi: 10.1021/acs.iecr.1c01884.

[223] E. J. F. Dickinson and A. J. Wain, "The Butler-Volmer equation in electrochemical theory: Origins, value, and practical application," *Journal of Electroanalytical Chemistry*, vol. 872, p. 114145, Sep. 2020, doi: 10.1016/j.jelechem.2020.114145.

[224] A. C. Ngandjong *et al.*, "Investigating electrode calendering and its impact on electrochemical performance by means of a new discrete element method model: Towards a digital twin of Li-Ion battery manufacturing," *J. Power Sources*, vol. 485, p. 229320, Feb. 2021, doi: 10.1016/j.jpowsour.2020.229320.

[225] T. Chandrupatla and A. Belegundu, *Introduction to Finite Elements in Engineering*. Cambridge University Press, 2021. doi: 10.1017/9781108882293.

[226] L. Sabat and C. K. Kundu, “History of Finite Element Method: A Review,” 2021, pp. 395–404. doi: 10.1007/978-981-15-4577-1_32.
[227] D. Tsige, M. Korita, and A. Beyene, “Deformation analysis of cement modified soft clay soil using finite element method (FEM),” *Heliyon*, vol. 8, no. 6, p. e09613, Jun. 2022, doi: 10.1016/j.heliyon.2022.e09613.
[228] V. Goel and K. Thornton, “Enabling the electrochemical simulation of Li-ion battery electrodes with anisotropic tortuosity in COMSOL Multiphysics®,” *MethodsX*, vol. 8, p. 101425, 2021, doi: 10.1016/j.mex.2021.101425.
[229] H. Jasak, “OpenFOAM: Open source CFD in research and industry,” *International Journal of Naval Architecture and Ocean Engineering*, vol. 1, no. 2, pp. 89–94, Dec. 2009, doi: 10.2478/IJNAOE-2013-0011.
[230] J. Kauffman, J. Gilbert, and E. Paterson, “Multi-Physics Modeling of Electrochemical Deposition,” *Fluids*, vol. 5, no. 4, p. 240, Dec. 2020, doi: 10.3390/fluids5040240.
[231] M. Huang, N. Weber, and G. Mutschke, “A Simulation Framework for Electrochemical Processes with Electrolyte Flow,” *J. Electrochem. Soc.*, vol. 170, no. 7, p. 073502, Jul. 2023, doi: 10.1149/1945-7111/ace333.
[232] S. Martinuzzi *et al.*, “A robust and cost-effective protocol to fabricate calibration standards for the thickness determination of metal coatings by XRF,” *Spectrochim. Acta Part B At. Spectrosc.*, vol. 182, p. 106255, Aug. 2021, doi: 10.1016/j.sab.2021.106255.
[233] L. Canda, T. Heput, and E. Ardelean, “Methods for recovering precious metals from industrial waste,” *IOP Conf. Ser. Mater. Sci. Eng.*, vol. 106, p. 012020, Feb. 2016, doi: 10.1088/1757-899X/106/1/012020.
[234] F. Fu and Q. Wang, “Removal of heavy metal ions from wastewaters: A review,” *J. Environ. Manage.*, vol. 92, no. 3, pp. 407–418, Mar. 2011, doi: 10.1016/j.jenvman.2010.11.011.
[235] J. U. Ani, K. G. Akpomie, U. C. Okoro, L. E. Aneke, O. D. Onukwuli, and O. T. Ujam, “Potentials of activated carbon produced from biomass materials for sequestration of dyes, heavy metals, and crude oil components from aqueous environment,” *Appl. Water Sci.*, vol. 10, no. 2, p. 69, Feb. 2020, doi: 10.1007/s13201-020-1149-8.
[236] M. A. Barakat, “New trends in removing heavy metals from industrial wastewater,” *Arabian Journal of Chemistry*, vol. 4, no. 4, pp. 361–377, Oct. 2011, doi: 10.1016/j.arabjc.2010.07.019.

[237] S. Babel, “Low-cost adsorbents for heavy metals uptake from contaminated water: a review,” *J. Hazard. Mater.*, vol. 97, no. 1–3, pp. 219–243, Feb. 2003, doi: 10.1016/S0304-3894(02)00263-7.
[238] M. Bragagni and L. Xhaferraj, “Copper and our sustainable future,” *Esharelife Foundation*, 2021, doi: 10.13140/RG.2.2.26384.53762.
[239] A. T. Paulino, F. A. S. Minasse, M. R. Guilherme, A. V. Reis, E. C. Muniz, and J. Nozaki, “Novel adsorbent based on silkworm chrysalides for removal of heavy metals from wastewaters,” *J. Colloid Interface Sci.*, vol. 301, no. 2, pp. 479–487, Sep. 2006, doi: 10.1016/j.jcis.2006.05.032.
[240] N. J. O. M. E. G. E. Oyaro, “The contents of Pb, Cu, Zn and Cd in meat in nairobi, Kenya,” *International journal of food, agriculture and environment* , vol. 5, no. 3–4, pp. 119–121, 2007.
[241] H. Kania and M. Saternus, “Evaluation and Current State of Primary and Secondary Zinc Production—A Review,” *Applied Sciences*, vol. 13, no. 3, p. 2003, Feb. 2023, doi: 10.3390/app13032003.
[242] Cleanmetals SA, “Nickel.” Accessed: Mar. 19, 2024. [Online]. Available: http://www.elsametal.com/metals/nickel/
[243] C. E. Borba, R. Guirardello, E. A. Silva, M. T. Veit, and C. R. G. Tavares, “Removal of nickel(II) ions from aqueous solution by biosorption in a fixed bed column: Experimental and theoretical breakthrough curves,” *Biochem. Eng. J.*, vol. 30, no. 2, pp. 184–191, Jun. 2006, doi: 10.1016/j.bej.2006.04.001.
[244] H. Tomioka, T. E. King, and A. Schnabel, “Gold-induced pulmonary disease: Clinical features, outcomes, and differentiation from rheumatoid lung disease.,” *Pneumologie*, vol. 51, no. 9, p. 921, 1997.
[245] E. A. Ripley *et al.*, *Environmental Effects of Mining*. Routledge, 2018. doi: 10.1201/9780203757147.
[246] Earthworks and Oxfam America, “Dirty Metals - Mining, Communities and the Environment.”
[247] J. Cui and E. Forssberg, “Mechanical recycling of waste electric and electronic equipment: a review,” *J. Hazard. Mater.*, vol. 99, no. 3, pp. 243–263, May 2003, doi: 10.1016/S0304-3894(03)00061-X.
[248] Fairtrade, “Oro etico: un passo avanti verso un futuro sostenibile.” [Online]. Available: https://www.fairtrade.it/blog/fairtrade/oro-etico-un-passo-avanti-verso-un-futuro-sostenibile/

[249] Fairtrade, “Gold and precious metals.” Accessed: Mar. 19, 2024. [Online]. Available: https://www.fairtrade.net/product/gold
[250] S. Lezak, C. Wilson, A. Ansar, and M. Bazilian, “The case against gold mining,” *Environmental Research Letters*, vol. 18, no. 1, p. 011001, Jan. 2023, doi: 10.1088/1748-9326/ac9f26.
[251] T. A. Kurniawan, G. Y. S. Chan, W.-H. Lo, and S. Babel, “Physico–chemical treatment techniques for wastewater laden with heavy metals,” *Chemical Engineering Journal*, vol. 118, no. 1–2, pp. 83–98, May 2006, doi: 10.1016/j.cej.2006.01.015.
[252] B. R. BABU, S. U. BHANU, and K. S. MEERA, “Waste Minimization in Electroplating Industries: A Review,” *Journal of Environmental Science and Health, Part C*, vol. 27, no. 3, pp. 155–177, Aug. 2009, doi: 10.1080/10590500903124158.
[253] A. A. Azmi, J. Jai, N. A. Zamanhuri, and A. Yahya, “Precious Metals Recovery from Electroplating Wastewater: A Review,” *IOP Conf. Ser. Mater. Sci. Eng.*, vol. 358, p. 012024, May 2018, doi: 10.1088/1757-899X/358/1/012024.
[254] K. Upadhyay, “Solution for wastewater problem related to electroplating industry: an overview.,” *Journal of Industrial Pollution Control*, vol. 22, no. 1, pp. 59–66, 2006.
[255] N. ADHOUM, L. MONSER, N. BELLAKHAL, and J. BELGAIED, “Treatment of electroplating wastewater containing Cu2+, Zn2+ and Cr(VI) by electrocoagulation,” *J. Hazard. Mater.*, vol. 112, no. 3, pp. 207–213, Aug. 2004, doi: 10.1016/j.jhazmat.2004.04.018.
[256] A. J. Pedersen, “Characterization and electrodialytic treatment of wood combustion fly ash for the removal of cadmium,” *Biomass Bioenergy*, vol. 25, no. 4, pp. 447–458, Oct. 2003, doi: 10.1016/S0961-9534(03)00051-5.
[257] L. Janssen, “The role of electrochemistry and electrochemical technology in environmental protection,” *Chemical Engineering Journal*, vol. 85, no. 2–3, pp. 137–146, Jan. 2002, doi: 10.1016/S1385-8947(01)00218-2.
[258] N. Kongsricharoern and C. Polprasert, “Electrochemical precipitation of chromium (Cr) from an electroplating wastewater,” *Water Science and Technology*, vol. 31, no. 9, 1995, doi: 10.1016/0273-1223(95)00412-G.